POLITECNICO DI MILANO

School of Industrial and Information Engineering

Master of Science in Materials Engineering and Nanotechnology

Chemistry, Materials and Chemical Engineering department "Giulio Natta"

SIGNAL ENHANCEMENT OF MICROFLUIDIC PAPER-BASED ANALYTICAL DEVICES

Supervisor: Prof. Chiara Bertarelli

Co-supervisor: Prof. Daniel Citterio

Master Degree Thesis

Percassi Valeria

M. 782667

Academic year 2012/2013

The experimental part of the present work has been performed at the
Analytical Chemistry Laboratory
Dept. of Applied Chemistry
of Keio University, Yokohama, Japan,
under the supervision of Prof. Daniel Citterio

Fall seven times,
stand up eight.
(Japanese Proverb)

INDEX

LIST OF FIGURES

LIST OF SCHEMES

LIST OF TABLES

ABSTRACT

The demand for easy-to-use and low-cost analytical devices is increasing, as they are, for example, introduced in developing countries or as a mean of point-of-care testing. In both these applications, there is the need for a simple device that allows for a profitable use by non-specialized users. The most attractive features of such a device are a simple and quick readout, any or limited need for power sources and resistant materials.

Microfluidic paper-based analytical devices (μPADs) represent a valid solution to many existing sensors, as they combine both the advantages of a microfluidic system (small amount of sample, multi-sensing and miniaturized dimension) and the paper substrate (low cost, light weight, great availability and disposability). The other great advantage of μPADs is that they can be entirely produced via ink-jet printing, with several others benefits: high reproducibility, drop-on-demand, small reagents loss, low-cost and the possibility of mass-production. In particular, the combination of microfluidic technology and the visualization of chemical/biological phenomena by fluorophores (a well-established practice) is gaining increasing interest in the scientific community.

One of the major overcomes in such type of microfluidic devices is represented by the brightness of the output signal, that is often insufficiently clear.

The chemical device developed in this work is a microfluidic paper-based chemical sensor realized via ink-jet printing, and it uses a common fluorescent dye (Rose Bengal) for the visualization of the analyzed phenomena. It does not have a specific purpose yet, but the sensing area contains easily functionalizable $Ag@SiO_2$ core@shell structures, that could be modified to make them a specific sensitive assay. The fluorescent signal from the dye is amplified thanks to the presence of the nanoparticles: it is known, in fact, that metallic nanostructures are able to modify the fluorescence of fluorophores, through an effect called “Metal enhanced fluorescence (MEF)”. MEF is a relatively new field and, at present moment, it is the first time that it is applied on paper surface for the improvement of a microfluidic ink-jet printed analytical device.

The experimental activity of the present work can be summarized in the following points:

1. Production and characterization of silver nanoparticles
2. Surface modification of nanoparticles via silica coating and optimization of thickness and morphology
3. Investigation of optimized conditions to achieve MEF from paper substrate
4. Design and fabrication of a prototype microfluidic device

ESTRATTO IN LINGUA ITALIANA

La domanda di sensori chimici e biochimici di semplice utilizzo e costo ridotto è significativamente cresciuta negli ultimi anni, a fronte dell'introduzione degli stessi, per esempio, in paesi in via di sviluppo o come mezzi di diagnosi "point-of-care", ossia strumenti di diagnostici di prima necessità, che possano essere usati dai pazienti nelle proprie abitazioni. In entrambe queste applicazioni, si crea, appunto, la necessità di avere dei dispositivi che siano semplici da usare anche da parte di personale non qualificato. Le caratteristiche distintive di tali dispositivi sono: la possibilità di una lettura del risultato chiara e non ambigua, nessuna o limitata necessità di fonti energetiche per il funzionamento e materiali robusti.

I dispositivi analitici microfluidici realizzati su substrati cellulosici (Microfluidic Paper-based Analytical Devices, µPADs) rappresentano una valida alternativa a molti sensori, già esistenti, dalla struttura più complessa. Questo tipo di dispositivi unisce sia i vantaggi della microfluidica (piccole quantità di reagenti, analisi multipla e ridotte dimensioni) a quelli della carta (basso costo, leggerezza, grande disponibilità e facile smaltimento). Un ulteriore grande vantaggio dei µPADs è che possono essere fabbricati interamente mediante una stampante a getto d'inchiostro, con numerosi altri benefici: alta riproducibilità, produzione personalizzata, limitata perdita di reagenti, basso prezzo del dispositivo finito, limitato investimento economico per la costruzione dell'impianto produttivo. In modo particolare, la combinazione della tecnologia microfluidica con un sistema di visualizzazione dei fenomeni chimici o biologici oggetto di studio mediante l'uso di pigmenti fluorescenti (una prassi ormai comune) sta riscontrando sempre maggiore interesse da parte della comunità scientifica.

Uno dei principali ostacoli da superare per la messa in produzione di questo tipo di strumenti di analisi è rappresentato dalla brillantezza del segnale fluorescente, spesso scarsa e inefficace a una chiara visualizzazione dei fenomeni in esame.

Il dispositivo chimico oggetto del presente lavoro è un µPAD realizzato mediante stampa a getto d'inchiostro, che usa un pigmento fluorescente di uso comune (rosa bengala) per la visualizzazione dei fenomeni in esame. Il dispositivo non ha, al momento, uno scopo definito, ma contiene, stampate, nanoparticelle di tipo "core@shell", costituite da un nucleo d'argento e un rivestimento di silice, che sono facilmente funzionalizzabili per renderle substrato adatto ad un'analisi selettiva. Il segnale luminescente del rosa bengala viene amplificato grazie alla presenza delle nanoparticelle: è noto, infatti, che nanostrutture metalliche sono in grado di modificare la fluorescenza dei fluorofori, tramite un effetto chiamato "Metal enhanced of fluorescence (MEF)". L'applicazione della MEF è un campo ancora relativamente nuovo e, al momento, il presente lavoro è il primo che propone la combinazione di MEF e sensori microfluidici ottenuti mediante stampa a getto d'inchiostro su carta.

L'attività sperimentale del presente lavoro può essere riepilogata nei seguenti punti:

1. Produzione e caratterizzazione di nanoparticelle d'argento
2. Modifica superficiale tramite coating di silice e ottimizzazione di morfologia e spessore
3. Studio e ottimizzazione delle condizioni per avere MEF su carta
4. Design e fabbricazione di un prototipo di µPAD

INTRODUCTION

Concept

The aim of the present work consists in the development of a method to enhance the luminescent signal of fluorophores, suitable to be applied to ink-jet printed microfluidic paper-based analytical devices (μPADs).

Signal enhancement is a highly desirable feature in the fields of chemical sensing or imaging and bioimaging, enabling a more intense analytical response and, in turn, increasing sensitivity. A brighter signal is effective, for example, in the visualization of phenomena involving very small structures, like DNA, or very limited amounts of analytes, thus allowing early diagnosis, detection of pollutants or toxic substances. As a general statement, three strategies can be performed, alone or in combination, to enhance the sensitivity of an analytical device:

1. Improve the signal-to-noise ratio, by using materials that are able to exploit fluorescence only in presence of specific interactions
2. Increase the concentration of the fluorescent moiety, by trapping it into the sensing area of the device
3. Use the "MEF (metal-enhanced fluorescence)" effect

The present work focuses on the exploitation of the third strategy, gaining enhancement as a consequence of the interaction between silver nanoparticles and a fluorescent dye (Rose Bengal).

Metal nanoparticles, due to their peculiar electronic structure, are able, as a consequence of the interaction with an electromagnetical wave, to enhance the electrical field of the wave itself, due to the excitation of collective vibrations of the electrons in the outermost shell of the metal atoms constituting the nanoparticle. These oscillations are called "surface plasmons", and they oscillate in resonance with the electrical field at a specific frequency. Further details of this mechanism are provided in chapter 1. When a fluorescent molecule (fluorophore) is placed in close proximity to a metal nanostructure, a particular effect occurs, that is called "Metal-Enhanced Fluorescence, MEF". The physics of the interaction between the nanoparticle and the fluorophore is complex, and it will be discussed in chapter 2. Briefly, it can be stated that, due to the enhancement of the local electrical field, a higher fraction of electrons of the fluorophore can be excited from the ground state to excited states, from which it can decay radiatively, thus emitting photons (fluorescence emission). Additionally, there is a secondary effect in MEF, that is the reduced lifetime of the excited state. It means that excited electrons spend less time, on average, in an excited state and, consequently, it is less likely that they undergo deactivation due to processes other than photon emission.

Although it is a relatively new field, MEF has been proved to be effective from various substrates, including glass[1,2,3], copper[4] and plastics[5,6]. However, just one work dealing with MEF on paper substrate has been reported in the literature[7]. Paper is an ideal substrate for the fabrication of simple sensors, and it has been used effectively for the fabrication of microfluidic analytical devices (μPADs). Microfluidics refers to the manipulation of small amounts of fluids inside tiny channels (from mm to μm in width and length). These channels can be fabricated in a substrate by means of various techniques; in the case of paper, cutting, drawing, dip-coating, wax-printing, *via* photolitography and by ink-jet printing. Among all these techniques, ink-jet printing offers the advantages to be user-friendly and to require the most limited investment, being based on conventional desktop printers. Furthermore, ink-jet printing allows not only to draw the channels but, also, to deposit sensing particles and reagents. Details about the state of the art in microfluidics, the potential of paper as sensing substrate and the main features of paper patterning are given in chapter 3. In the present work, a prototype μPAD has been entirely fabricated (channel design and functionalization with silver particles) via ink-jet printing, as described in the experimental section of chapter 3.

The main objective of this research was to demonstrate MEF from paper substrate and the retaining of such capability when printing the nanoparticles and the fluorescent dye on paper. The application of the fabricated μPAD to a specific function is beyond the scope of this thesis work. Nevertheless, it is believed that a selective sensing capability can be easily achieved by combining the discussed MEF strategy, together with the improvement of signal-to noise ratio. That is the reason why, in the present work, silica coated silver nanoparticles have been fabricated (see the experimental part of chapters 1 and 2 for details regarding the synthesis of silver particles and the coating process, respectively). It is not trivial, that the enhancing effect of silver nanoparticles could be retained when they are coated with silica.

---

[1] Aslan, Kadir, Joseph R. Lakowicz, and Chris D. Geddes. "Rapid deposition of triangular silver nanoplates on planar surfaces: application to metal-enhanced fluorescence." *The Journal of Physical Chemistry B* 109.13 (2005): 6247-6251.

[2] Aslan, Kadir, et al. "Fast and slow deposition of silver nanorods on planar surfaces: application to metal-enhanced fluorescence." *The Journal of Physical Chemistry B* 109.8 (2005): 3157-3162.

[3] Geddes, Chris D., et al. "Metal-enhanced fluorescence (MEF) due to silver colloids on a planar surface: Potential applications of indocyanine green to in vivo imaging." *The Journal of Physical Chemistry A* 107.18 (2003): 3443-3449.

[4] Zhang, Yongxia, et al. "Metal-enhanced fluorescence from copper substrates." *Applied physics letters* 90.17 (2007): 173116.

[5] Aslan, Kadir, et al. "Metal-enhanced fluorescence from plastic substrates." *Journal of fluorescence* 15.2 (2005): 99-104.

[6] Aslan, Kadir, Patrick Holley, and Chris D. Geddes. "Metal-enhanced fluorescence from silver nanoparticle-deposited polycarbonate substrates." *Journal of Materials Chemistry* 16.27 (2006): 2846-2852.

[7] Zhang, Yongxia, et al. "Metal-enhanced fluorescence from paper substrates: Modified spectral properties of dyes for potential high-throughput surface analysis and assays and as an anti-counterfeiting technology." *Dyes and Pigments* 77.3 (2008): 545-549.

A typical sensing assay is given by silica (SiO_2) nanoparticles that are surface-engineered with functional groups able to bind selectively only a specific analyte. Hence, when exposed to a multi-components sampling solution, only some specific constituents will be anchored to the particles surface. The analyte was labeled, in the pristine state, to a non-activated fluorophore, that lights up after the binding due to energy transfer while a donor-acceptor system is created. This concept is explained in the picture below.

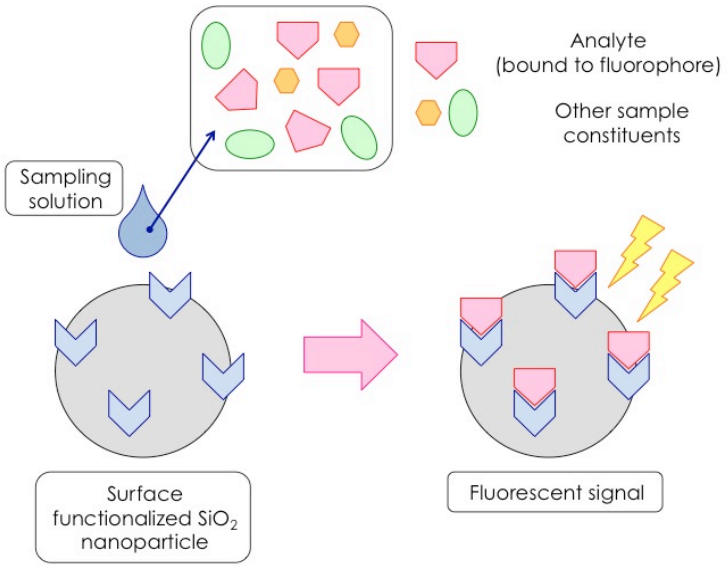

Scheme 1 Representation of a silica nanoparticle-based sensing assay for specific analyte detection

This is, for example, the principle immunoassays are based on. The signal of these systems is often insufficiently bright. In the following picture, a plausible application of the concept developed in the present work is represented: due to the presence of the metallic core the luminescent output of the sensing assay is brighter.

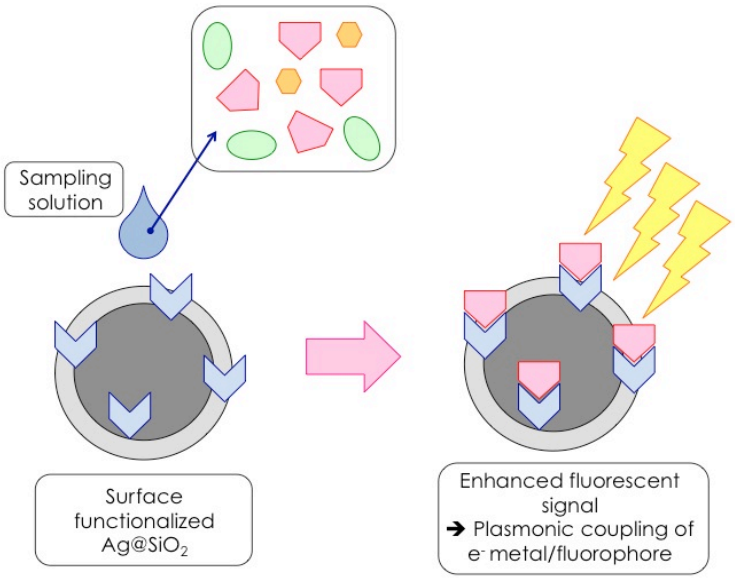

Scheme 2 Representation of a core@shell-based sensing assay. The metal core enables enhanced fluorescent signal

Research outline, goals and main features

Summarizing, the concept of this work can be presented as follows:

- Fabricate silica-coated silver nanoparticles and optimize the coating process to obtain a stable, thin and uniform shell
- Investigate the possibility to detect fluorescence enhancement (MEF) from paper functionalized with $Ag@SiO_2$ nanoparticles, and define the influencing variables
- Design and fabricate a prototype µPAD, with both channels fabrication and reagents deposition entirely achieved via ink-jet printing

For an easier approach for the reader of the present work, the three points above are developed in three separate chapters, including both the state-of-the-art and the experimental section.

The final research goal combines known methods and available materials (core@shell particles, paper, microfluidics, ink-jet prinitng) for the developement of a new, simple, easy reproducible and inexpensive strategy for signal enhancement of ink-jet printed µPADs, through the exploitation of a complex and interesting physical phenomenon, that is MEF.
The principal features of the materials and the techniques used are the following:

SILVER@SILICA NANOPARTICLES

- ✓ Absorption spectra in the visible
- ✓ Easy surface functionalization
- ✓ Relatively low cost, if compared with other metals for plasmonic applications

PAPER SUBSTRATE

- ✓ Cheap
- ✓ Great availability
- ✓ Disposable
- ✓ Light and robust
- ✗ New substrate for the investigation of MEF (limited literature)

INK-JET PRINTING

- ✓ Inexpensive printing apparatus (desktop printers) and software
- ✓ Simple and intuitive mechanism
- ✓ Simple implementation for mass-scale production

1. ONE-DIMENSIONAL NANOSTRUCTURES: CORE@SHELL

1.1 State of the art

1.1.1 Nanotechnology and nanostructured materials: an overview

In the year 2000, the Interagency Working Group on Nanoscience, Engineering and Technology gave a presentation at the Congress of the United States of America about the future plans on investments about research on nanotechnology. They defined nanotechnology as being "concerned with materials and systems whose structures and components exhibit novel and significantly improved physical, chemical and biological properties, phenomena and processes due to their nanoscale size. The aim (of nanotechnology, ndr) is to exploit these properties by gaining control of structures and devices at atomic, molecular and supramolecular levels and to learn to efficiently manufacture and use these devices"[1].

Nanotechnology deals with materials or structures with dimensions ranging from subnanometers to several hundreds nanometers: at this small scale, the properties of a material may be very different from the ones of bulk, and peculiar effects, such as size confinement, predominance of interfacial phenomena and quantum mechanics become observable. One of the main goals of nanotechnology is to identify such properties and develop new applications based on them. Furthermore, nanotechnology is also the science of miniaturization of existing structures and devices, to increase the number of possible applications, from computer science, to medicine, to energy storage, mentioning just a few[2-7]. Nanotechnology, though, is a wide world, which can hardly be univocally defined, precisely because it covers a broad range of applications as well as many different disciplines. Nanotechnology, as it is intended nowadays, was born with the goal to decrease the size of components in the semiconductor industry. As predicted in 1965 by the famous Moore's law[8], the shrinkage of the dimensions of semiconductor devices has followed a trend by a factor 2 every 18 months since 1950. The law is illustrated in fig.1.

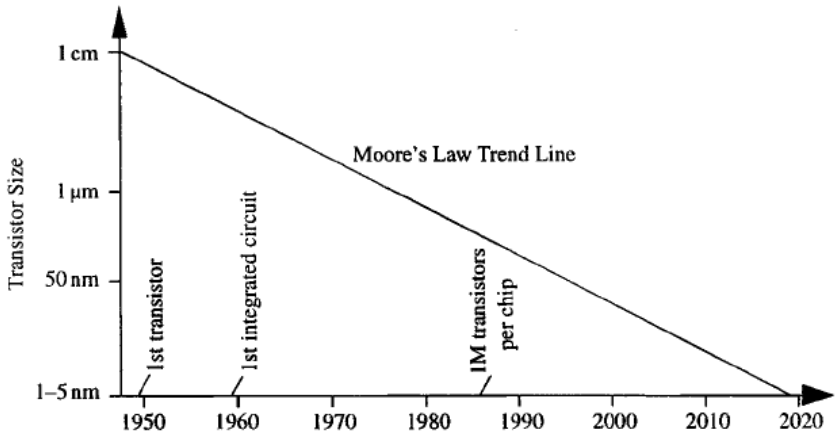

Fig. 1 Moore's plot of transistor size vs year[9]

It may look like nanotechnology is a relatively new field, but some nanostructured materials have been known from centuries by mankind: colloidal dispersions of metal nanoparticles in glass, exhibiting unique optical properties, were used to make precious glassware able to change color, depending on the type of illumination shining on them. The most famous example is the roman "Lycurgus cup", shown in fig.2, that dates back to the IV sec.. It contains tiny gold and silver particles in a glass matrix, and it appears red, when illuminated by transmitted light, or green, if illuminated by reflected light.

Fig. 2: Lycurgus cup, British Museum, London[10]

What has changed from the past, is the ability to see and manipulate systems at the nanometers scale. Examples of nanostructured materials, which, by definition, have at least one dimension at the nanometric scale, include nanoparticles, quantum dots, nanowires, thin films and, also, bulky materials built up by the connection of nanostructured blocks, like carbon fullerenes[11], carbon nanotubes[12] (fig.3) and ordered mesoporous materials[13].

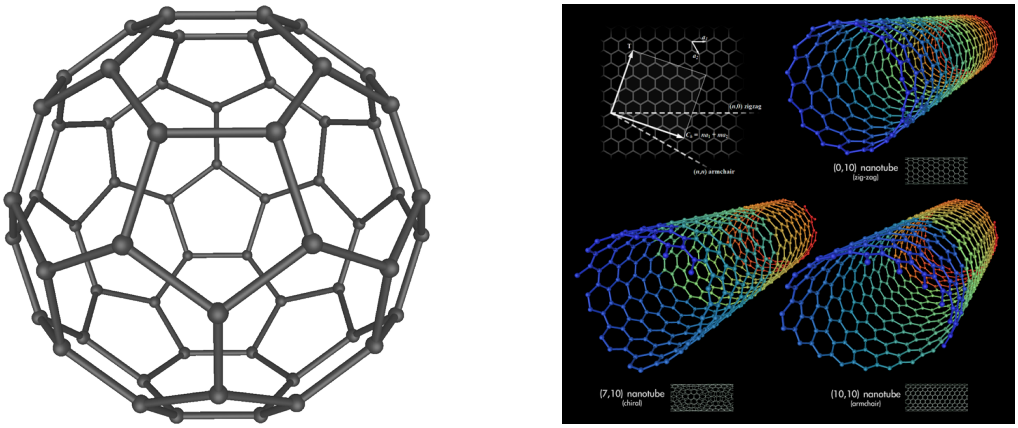

Fig. 3-a,b a)Fullerene C60; b)carbon nanotubes[14]

Clearly, new challenges in fabrication and integration of new nanomaterials or nanostructures into existing technologies arise. Major problems in fabrication and processing are:

1. Overcome the huge surface energy, resulting from the enormous surface-to-volume ratio
2. Ensure all nanomaterials with the desired size, size distribution, morphology, cristallinity, chemical composition and microstructure that altogether result in the desired properties
3. Prevent coarsening via Ostwald ripening or agglomeration as time evolves, that naturally occurs because materials tend to reduce their level of free energy[15]

Observation of phenomena at the nanometer scale is also non trivial, and advances in measuring technologies developed in parallel with the arising nanoscience; characterization of nanomaterials has improved since the invention of scanning tunnelling microscope (STM), scanning probe microscopy (SPM) like atomic force microscopy (AFM), in combination with other well-established techniques as transmission electron microscopy (TEM).

1.1.2 Zero-dimensional structures: from nanoparticles to core-shells

Among all types of nanostructured materials, nanoparticles are particularly interesting due to the facile tailoring of properties by tuning their sizes or functionalizing their surfaces. They are considered “zero-dimensional” nanostructures.

1.1.2.1 General approaches to the fabrication of nanoparticles

Nanoparticles (NPs) may derive from a variety of materials, such as metals, polymers or ceramics. There are two routes for the preparation of nanoparticles. The first one is a *“top-down”* approach: particles originate from mechanical milling or attrition of bulky materials or from lithographic techniques. Top-down approaches lead to the preparation of particles of various sizes, from a few to hundreds of nanometers in diameter, but they generate a wide size distribution and may induce internal stresses, cause the formation of defects, or add impurities, that inevitably affect the material properties. *“Bottom-up”* techniques are mostly used and many different routes have

been developed. Broadly speaking, it is possible to distinguish two main routes to achieve bottom-up fabrications:

- A *thermodinamic equilibrium* approach, which is by far the most popular, and consists of some consequential steps.
  I. Generation of supersaturation conditions, by reducing the temperature of a mixture at equilibrium or via chemical reactions
  II. Nucleation
  III. Growth
- A *kinetic* approach, either limiting the amount of precursor or the space available for the process to occur.

The mechanism of nucleation and growth has been proposed by LaMer and co-workers[16] in the early 50's (see fig.4).

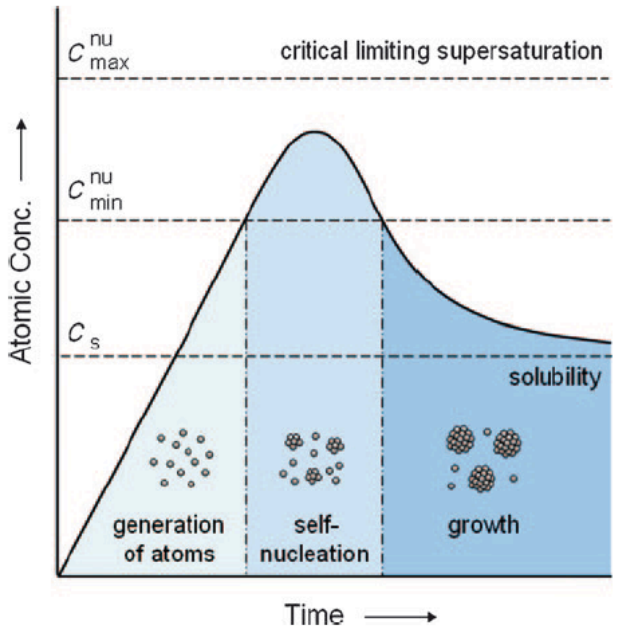

Fig. 4 Generation of supersaturation conditions, nucleation and growth process as described by LaMer and co-workers[17]

Nanoparticles can be synthesized either by homogeneous or heterogeneous nucleation. Homogeneous nucleation can be obtained, basically with the same fundamentals, in solid, liquid or gaseous environment. It requires the establishment of supersaturation conditions, from which seeds of the growing species may start form spontaneously. Heterogeneous nucleation occurs at the interface with another material, and it is generally easier than homogeneous nucleation, because the contact angle between the growing species and the substrate is often less than 180°, value at which the barrier energy for both mechanism is the same. When some wetting conditions are established, which means that the contact angle is less than 180°, then the barrier for heterogeneous nucleation is lower than for homogeneous nucleation. In both cases, anyway, the formation of a new phase decreases the Gibbs free energy of the system but increases the total

surface energy. For the nucleation process to start, a critical radius value and a critical Gibbs energy value must be overcome.

For the development of the ink-jet printed device, which is the aim of the present work, silver nanoparticles have been produced via homogeneous nucleation; hence, the next dissertation will only focus on metal nanoparticles in general and silver nanoparticles in particular.

1.1.2.2 Synthesis of metal nanoparticles

Colloidal metals can be defined as isolable particles with a size ranging from 1 to 50 nm, dispersed in water ("hydrosols") or in organic solvents ("organosols"). Metallic sols are known from centuries, as they were used as pigments for glass or ceramics. They combine unique electronic properties and extremely large surface area, which accounts for an increasing number of potential applications. A chemical wet route *via* reduction of metal salts, electrochemical techniques and the controlled decomposition of metastable organometallic compounds are the possible ways to synthesize metal nanoparticles. To control the growth rate, stabilizers, as polymers, surfactants and donor ligands, are widely used; such compounds also prevent agglomeration of the newly formed particles. They act by hindering the diffusion of growing species onto the already grown surfaces, so that the diffusion process is the limiting step in the whole process.

Back in 1857, Michael Faraday for the first time rigorously described a colloidal hydrosol of gold synthesized *via* reduction of metal salts, reporting his observation about the interaction of gold with light in his famous "Bakerian Lecture"[18]. The colloidal gold prepared by Faraday was stable for nearly one century before being destroyed during the Second World War. The most famous method to produce colloidal gold in a reproducible way is the "Turkevich method", from the name of his discoverer in 1951[19]. He was able to synthesize 20 nm gold colloids by reduction of $[AuCl_4]^-$ with sodium citrate. He also proposed the essential mechanism of cluster formation, which passes through the steps of nucleation, growth and agglomeration. In the early stage of the colloid formation, the formation of zero-valent metal atoms occurs due to the reaction with the reducing agent. Then, such atoms may collide with other ions, atoms or clusters to originate stable metal nuclei, whose size can be even below 1 nm, depending on the strength of the metal-metal bonds and the difference between the redox potential of the metal and the reducing agent. Several reducing agents may be used to obtain different kinds of nanoparticles: a summary is provided in table 1. Experimentally, $AgNO_3$ is the most commonly used precursor for the preparation of Ag nanostructures *via* reduction, because of its good solubility in polar solvents.

Precursors	*Formula*
Metal anode	Pd, Ni, Co
Palladium chloride	$PdCl_2$
Hydrogen hexachloroplatinate IV	H_2PtCl_6
Hydrogen hexachloroplatinate II	K_2PtCl_4
Silver nitrate	$AgNO_3$
Silver tetraoxylchlorate	$AgClO_4$
Chloroauric acid	$HauCl_4$
Rhodium chloride	$RhCl_3$
Reduction Reagents	
Hydrogen	H
Sodium citrate	$Na_3C_6H_5O_7$
Hydroxylamine hydrochloride	$NH_4OH + HCl$
Citric acid	$C_6H_8O_7$
Carbon monoxide	CO
Phosphorus in ether	P
Methanol	CH_3OH
Hydrogen peroxide	H_2O_2
Sodium carbonate	Na_2CO_3
Sodium hydroxide	NaOH
Formaldehyde	HCHO
Sodium tetrahydroborate	$NaBH_4$
Ammonium ions	NH_4^-

Polymer Stabilizers
Poly(vinylpirrolydone), PVP
Polyvinylalcohol, PVA
Polyethyleneimine
Sodium polyphosphate
Sodium polyacrilate
Tetraalkylammonium halogenides

Table 1 Summary of precursors, reduction agents and stabilizers (adapted)[20]

The reduction of metal salts in liquid environment presents the advantages to be easily reproducible and allows for a narrower size distribution. Colloids are considered “monodisperse” when the particle size deviates less than 15% from the average size, or exhibiting a “narrow size distribution” when the deviation is about 20%[21].

To stabilize the colloid, two ways are possible:

- *Electrostatic stabilization*, based on the Coulombic repulsions between the particles, which originates from the electrical double layer formed by ions adsorbed on the particle surface (for example, sodium citrate). This is the case of $[AuCl_4]^-$ sol. (Scheme 3)
- *Steric stabilization,* due to the interference between organic molecules adsorbed onto the metallic particle surface. These are for example polymers or block copolymers, solvents, long alkyl chains or surfactants. (Scheme 4)

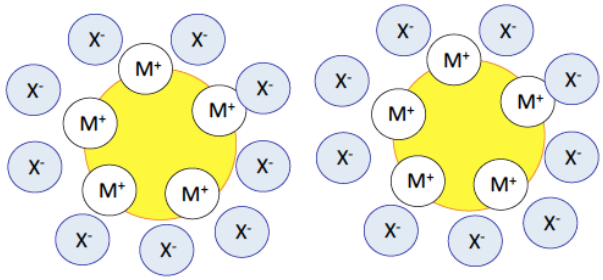

Scheme 3: Electrostatic stabilization of colloidal particles

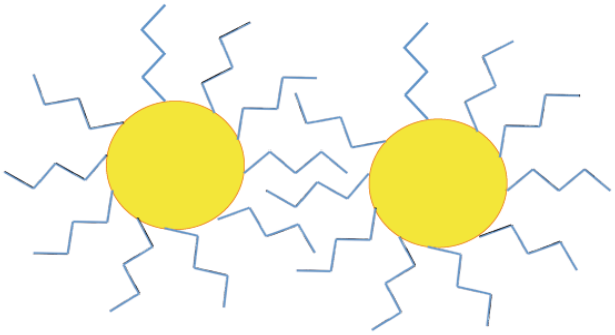

Scheme 4: Steric stabilization of colloidal particles

Metal nanoparticles can be produced also via electrochemical methods, as demonstrated for the first time in 1994 by Reetz et al.[22]. Scheme 5 represents the electrochemical synthesis, which consists of six elementary steps:

1. Oxidative dissolution of the sacrificial bulk metal, M_{bulk}
2. Migration of M^{n+} ions to the cathode
3. Formation of zerovalent metal atoms at the cathode
4. Nucleation and growth of metal particles
5. Arrest of the growth and particle stabilization via protective agents, for ex. tetraalkylammonium ions
6. Precipitation of the as-prepared metal colloid

Anode: $M_{bulk} \rightarrow M^{n+} + ne^-$

Cathode: $M^{n+} + ne^- + stabilizer \rightarrow M_{coll}/stabilizer$

TOT: $M_{bulk} + stabilizer \rightarrow M_{coll}/stabilizer$

Scheme 5 Electrochemical formation of metal NPs

This method allows for uncontaminated, size-selective particle formation, these also easily isolated from the precipitate. Platinum, Palladium, Rhenium, Ruthenium and Osmium are commonly prepared by this method.

The action of heat, light or ultrasound may generate zero-valent metal ions from organometallic complexes or organic derivatives of transition metals, which are subsequently stabilized by protective agents: thermolysis is commonly used, and recently it has been demonstrated that it can be performed with a common household microwave oven[23-25]. Decomposition of metal complexes may occur due to the addition of CO or H_2 in presence of appropriate stabilizers[26-28], or due to photochemical process activated by light (that is the case of silver, where Ag_3^+ or Ag_3 clusters may easily form in solid $AgNO_3$)[29]. Finally, nanoparticles have been synthesized in micelles, reverse micelles and by encapsulation[30-32].

Nevertheless, the chemical route results to be the easiest and the most used so far; for this method, the effect of the reducing agent is of primary importance for the success of the synthesis. In fact, the size and the size distribution of the final colloid strongly depend on the relative rates of nucleation and growth, which in turn depend on the type of reaction agent. The stronger the reagent, the faster the reaction rate, limiting the growth of big particles. On the other hand, if the reaction speed is slow, bigger particles are formed, either with a narrow or wide size distribution. A narrow distribution is achieved when no secondary nucleation occurs, and the growth of nuclei is determined by the availability of zero-valent atoms[33,34]. Other factors also come into play, like the solvent, the concentration of the initial species, the quantity and nature of polymer stabilizers, temperature and pressure.

Summarizing, the fundamentals to achieve monodispersed metal nanoparticles are:

1. The nucleation stage has to be very fast, and it can be achieved either by supersaturation or by introducing in the reactive environment seeds for heterogeneous nucleation
2. Diffusion-limited growth of nuclei, achieved either by using a barrier (polymeric protective layers) or limiting the concentration of the growing species
3. Carefully control the amount of reducing agent and the pH of the medium, as well as other operational factors
4. Control the synthesis parameters to avoid coarsening
5. After the synthesis, size-selective precipitation may be performed to separate aggregates by size

1.1.2.3 Optical properties of metal nanoparticles

Metal nanoparticles, as previously stated, are particularly interesting for their potential applications[35]. They can be used in catalysis, both for homogeneous and heterogeneous reactions, in fuel cells, and in material science. They have specific physical properties, including magnetic, optical, melting point, specific heat and surface reactivity, which are all size-dependent. Arranged in one dimension, they can build up semiconducting nanopaths[36], while if arranged in two-dimensional arrays, like Langmuir-Blodgett films, they could be used as substrate for data-storage[37]. Nanoparticles may also be used as reinforcement of other materials, and there are new strategies that aim at building bio-metallic nanotechnological devices by connecting particles to DNA fragments[38]. Optical properties of metal nanoparticles constitute one of the major features. These optical properties, as already pointed out, are known by centuries, but it is only in recent times that the fundamentals of such properties have been understood and, consequently, profit by such knowledge.

Faraday's work has already been cited[39]. A step ahead was made in 1908 by Gustav Mie[40], who gave a mathematical formulation of the observations made by Faraday as well as other scientists. He started from the Maxwell equation, deriving the analytical expression of the extinction, scattering and absorption cross sections for gold, showing the dependence on the particle size. Before introducing the specific properties of metal nanoparticles, some considerations about metals in general are worth to be discussed.

Metals can be considered as made by positive ions, consisting of nuclei and fixed core electrons, surrounded by a "cloud" of electrons, which are free and mobile, that are responsible, for example, of the their high conductivity. Generally, the positive charge of the ions and the negative charge of the electron plasma are in equilibrium, hence the material as a whole is neutral. If some external stimulus is applied, the electrons of the electron cloud may be disturbed and start moving, creating regions in which the electron density increases. An example of stimulus is electromagnetical irradiation. If the density of electrons increases, electrons are brought closer but, as they have negative charge, they repel each other, and tend to move back to their original position, thus gaining kinetic energy, which causes them to locally oscillate back and forth instead of staying at rest. All electrons oscillate at the same frequency, and the plasma of oscillating electron is called "*plasmon*". A plasmon is hence characterized by its typical frequency, precisely called "plasma frequency" (eq.1).

$$\omega_p = \sqrt{\frac{N_E e^2}{m\varepsilon_0}}$$

Eq. 1 Plasma frequency. N_E represents the number of electrons, e and m, respectively the charge and the mass of the electron, ε_0 is the dielectric constant in vacuum

Actually, this model should be corrected for real metals, because the striking electromagnetic wave is partially shielded by highly localized electrons of *d* orbitals. These oscillations cause the rise of an absorption band in the visible, accounting for the color of some metals (like copper red).

The described entity is actually a "*volume plasmon*", because a slightly different entity, called "*surface plasmon*" originates at the interface between a metal and a dielectric medium, like air. To excite a volume plasmon, a longitudinally polarized electron beam is needed, while for surface plasmon a monochromatic electron beam must be used; alternatively, a prism can be used to generate a condition of total internal reflection in proximity of the metal surface, since surface plasmons are not excited by a propagating wave, rather by an evanescent wave (a wave penetrating for a very limited distance inside the metal, thus exciting only very superficial electrons). The value of the surface plasmon frequency is provided in eq.2.

$$\omega_{sp} = \frac{\omega_p}{\sqrt{1+\varepsilon_d}}$$

Eq. 2 Surface plasmon frequency. ω_p is the plasma frequency (from eq.1), ε_d the dielectric constant of the medium at the interface

It is interesting to point out that the dispersion relation for plasmons and the one for surface plasmons lie, respectively, above and below the dispersion relation of light in vacuum (Fig.5). This means that for value of frequencies between ω_p and ω_{sp}, light cannot propagate inside the metal: this originates a waveguide, which may have a number of potential applications[41-43].

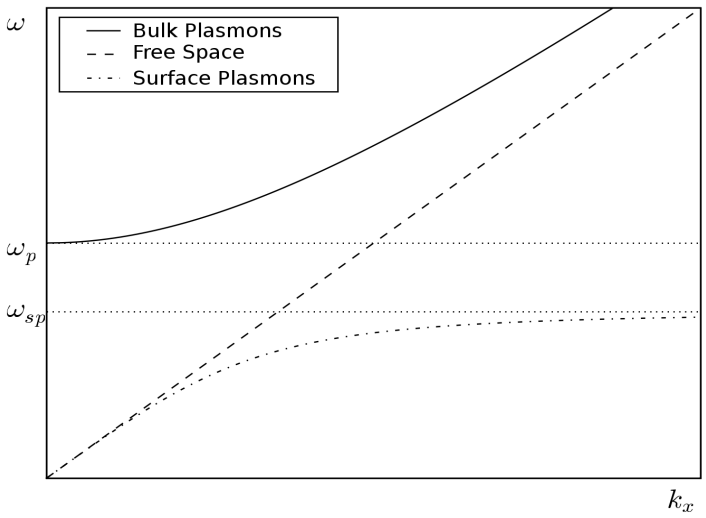

Fig. 5 Dispersion relations of light for bulk plasmons, free space and surface plasmons. ω is the frequency, k_x is the wavevector of the incident wave[44]

When reducing the size to nanoparticles, the situation is slightly different. Nanostructures, in fact, have a size that is generally smaller than the wavelength, such that the amplitude of the electrical field associated with the incident light can be considered constant (eq.3).

$$E = E_0 \frac{3\varepsilon_d}{\varepsilon + 2\varepsilon_d}$$

Eq. 3 Electrical field near a metallic particle. E_0 represents the incident electrical field

If the value ε of the dielectric constant of the metal can assume negative values, and this is possible being the particle metallic (for which the relationship between the dielectric constant and the frequency is known, and represented in eq.4), a condition of resonance may arise if the so called "Fröhlich condition" is verified (eq.5), namely when the particle is in a dielectric medium.

$$\varepsilon = 1 - \frac{\omega_p^2}{\omega^2}$$

Eq. 4 Drude model for the dielectric constant of a metal

$$\varepsilon = -2\varepsilon_d$$

Eq. 5 Fröhlich condition

As a consequence, the electrons of the nanoparticle oscillate collectively, creating an entity called "localized surface plasmon" or "polariton", at a typical frequency (eq.6).

$$\omega_{lsp} = \frac{\omega_p}{\sqrt{1+2\varepsilon_d}}$$

Eq. 6 Localized surface plasmon frequency

The electrical field around the particle is enhanced, being partially made up of the incident field, and partially due to the collective oscillation of electrons that create a charge delocalization (fig.6). This effect is of primary importance for the verification of the conditions to have the "metal enhancement of fluorescence effect" that will be described later on.

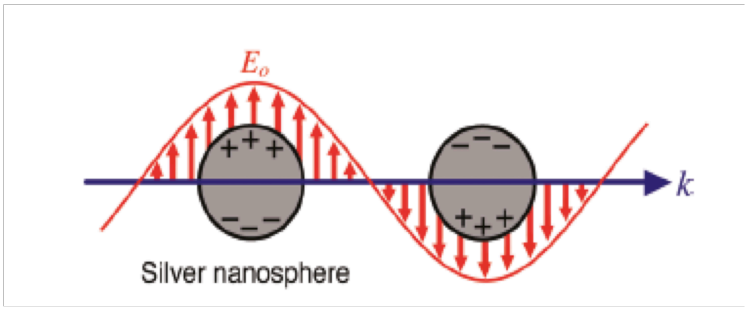

Fig. 6 Charge displacement and the oscillating field around silver nanoparticles, in resonance with the incident beam[45]

At the same time, the oscillating electrons induce a polarization in the opposite direction of the surrounding medium, which consequently reduces the restoring force, shifting the plasmon frequency to lower values. If the particle is small, only dipole-type oscillation arises, resulting in a single peak in the surface plasmon resonance spectrum; as the size increases, multiple oscillations may occur, resulting in several peaks. For small particles, electron confinement produces a variation in the mean free path of the electrons, namely the time between two scattering events. The mean free path is given by the product between the Fermi velocity and the inverse of the damping constant (eq.7 and eq.8): the reduction of the mean free path results in enhanced electron surface scattering, which accounts for the size-dependence of the surface plasmon absorption.

$$l = v_F \Gamma^{-1}$$

Eq. 7 Mean free path

$$\Gamma(r) = \Gamma_0 + \frac{A v_F}{r}$$

Eq. 8 Damping coefficient as a function of the radius of the particle. Γ_0 is the bulk damping value, A is a constant, v_F is the Fermi velocity

Plasmon absorption is the only damping effect in small particles, while both absorption and scattering are present in larger particles. Considering that the dielectric constant of a metal consists of a real ($\varepsilon_1(\omega)$) and an imaginary ($\varepsilon_2(\omega)$) part (fig.7), their relative values contribute to scattering and absorption, respectively.

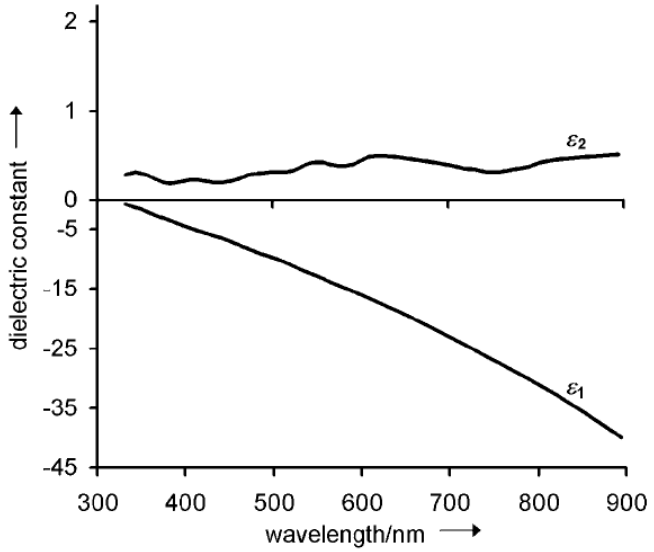

Fig. 7 Plot of the real (ε_1) and imaginary (ε_2) part of the dielectric constant of silver vs wavelength[46]

$|\varepsilon_1(\omega)|$ rapidly increases with the wavelength, hence scattering competes with absorption, becoming the dominant term over absorption, which does not increase as much. Being the value for the extinction cross-section (C_{ext}, which represents the amount of light extinguished by an object, eq.9) the summation of absorption (Cabs) and scattering (C_{sc}), from Mie's theory, extinction is hence mostly driven by scattering for large particles, since it is a faster phenomenon, which only involves electrons and not the interaction with lattice phonons (required for absorption). In the case of silver nanoparticles, the value of C_{ext} is larger than the geometric cross-section, which represents the physical region of space that is involved in collisional processes. This means that a silver nanoparticle interacts with both the amount of light (photons) colliding with the particle itself, but also with some photons passing in close proximity. This can be explained as follows[47]: when two particles, each having a geometrical cross-section, collide, the interaction is driven by the larger of the two objects. Photons have a geometrical cross-section that is much larger than particles, being related to their wavelength, providing the conditions for C_{ext} to be larger than the geometrical cross section of the particle. This also depends on the possibility that the particle has to dissipate energy from the field: for nanoparticles this is achieved by absorption and scattering via excitation of localized surface plasmons. Hence, C_{ext} for Ag nanoparticles will be

always smaller than the geometric cross-section of the photon. The value of C_{ext} for nanoparticles is provided in eq.9. As previously explained, though, the Fröhlich condition has to be satisfied in order to achieve the resonance condition.

$$C_{ext} = \frac{24\pi^2 r^3 \varepsilon_d^{3/2}}{\lambda}\left[\frac{\varepsilon_2}{\left(\varepsilon_1 + 2\varepsilon_d\right)^2 + \varepsilon_2^2}\right]$$

Eq. 9 Extinction cross section for nanoparticles.

The size-dependance of absorption and scattering from the particle size is different and it is shown in equation 10.

$$C_{abs} \propto r^3$$
$$C_{sc} \propto r^6$$

Eq. 10 Dependence of absorption and scattering cross sections on particle size

The scattering cross-section increases with the volume of the particle rather than its geometrical-cross section, which, again, accounts for the enhanced scattering from bigger particles. This is the reason why particles illuminated with a different light source exhibit a different coloration and, in turns, explains the principle of the Lycurgus cup. This model, as a first approximation, works well also for core-shell structures; a more complete theory, called "hybridization model" has been described by Prodan et al.[48]. In this model the arising plasmon comes from the interaction of a nanosphere and a nanocavity.

Finally, optical properties depend also on the shape of the nanostructure. Fig.8 shows the extinction, absorption and scattering spectra for silver nanostructures of different shapes, dispersed in water. For the spherical shape, a clear peak is visible at 410 nm, indicating the dipole resonance. At 370 nm, the shoulder for the quadrupole resonance (corresponding to two dipoles of opposite sign) is present. This latter is due to the non uniformity of the incident light across the sphere, as a result of energy losses.

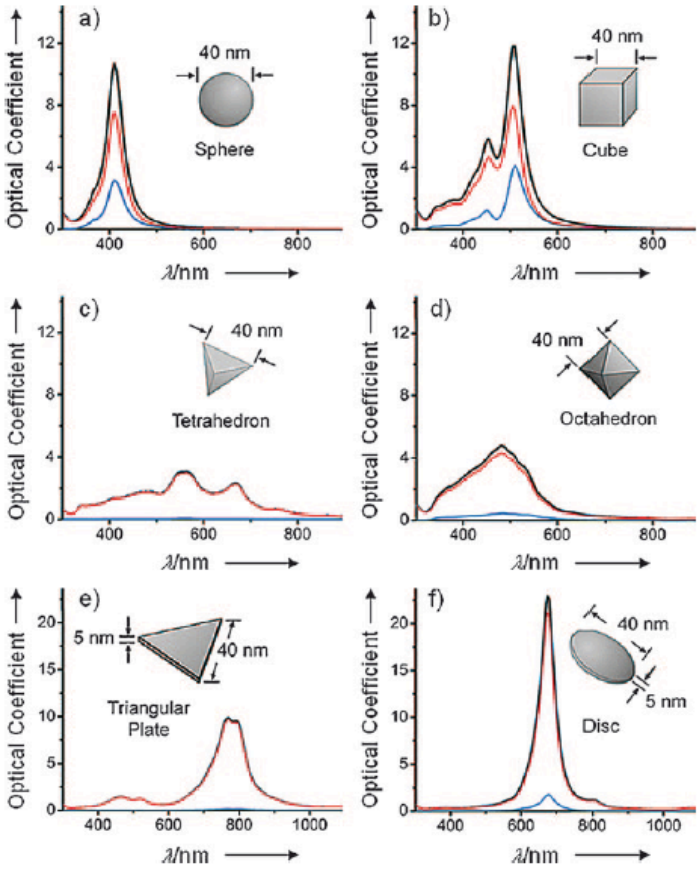

Fig. 8 Calculated UV-extinction (black), absorption (red) and scattering spectra (blue) for Ag nanostructures having different shape[49]

At this size, the resonance is mostly due to light absorption, which occurs in the range of wavelength corresponding to blue, giving the Ag nanoparticle solution a yellow color. The solutions of Ag nanoparticles that have been herein produced, as described in chapters 1.2 and 1.3, have these same characteristics. In principle, the charge separation that results from the polarization of electron density relative to the lattice of positive ions provides the main restoring force for electron oscillation and largely determines the frequency and intensity of the resonance peak for a given metal. Thus, variations in nanocrystal size, shape, and dielectric environment can affect the surface polarization and alter the spectral profile of the resonance. For simple geometrical shapes, both corner sharpness and shape symmetry can influence the surface polarization. In particular, sharpness affects the position of the peak and shape symmetry affects the spectra with the number of peaks being correlated to the number of modes in which the electron density can be polarized. Additionally, shape symmetry affects the intensity of the resonance peak. When the surface charges on a nanoparticle are separated by mirror symmetry (without the mirror plane bisecting through a vertex), the effective dipole moment will be very large and the greater the effective dipole moment the greater the intensity of the dipole resonance.

Table 2 features of metal nanoparticles; the main advantages of using silver over other metals for plasmonics applications is evident.

METAL	PLASMONIC ABILITY	CHEMICAL	NANOSTRUCTURE FORMATION	COST (PER OUNCE)
Aluminum (Al)	good in UV region	stable after surface passivation	very few nanostructures; used in lithographic patterning	$0.049
Copper (Cu)	Interband transitions below 600nm	Easy oxidation	Very few nanostructures	$14.8
Gold (Au)	Interband transitions below 500nm; high quality factor	Very stable; biocompatible	Many nanostructures	$950
Palladium (Pd)	Low quality factor;not suitable for plasmonics	Stable	Many nanostructures	$265
Platinum (Pt)	Low quality factor; not suitable for plasmonics	Stable	Many nanostructures	$1207
Silver (Ag)	Highest in quality factor	Oxidation; biocompatibility issues	Many nanostructures	$13.4

Table 2 Comparison among common metals (adapted)[50]

1.1.2.4 Other properties of metal nanoparticles

1.1.2.4.1 Catalytic activity

Noble metals have been extensively used to catalyse many chemical reactions. When produced as nanoparticles or nanocrystals, their high surface-to-volume ratio allows for minimizing the cost. In particular, the shape of the nanostructure is particularly important, since it affects both the reactivity and the selectivity of the catalyst. In the case of nanocrystals, the shape determines which facet of the crystal itself is at the surface, hence driving the reaction. Researches are focused on obtaining metal nanocrystals with high-index planes having many unsaturated atomic steps, edges and kinks, which act as more active sites for catalysis.

1.1.2.4.2 Electronic properties

With the continuous miniaturization of electronic devices, nanoparticles and nanocrystals with peculiar electronic properties may be promising materials to be incorporated as interconnecting or transport elements in integrated circuits. Silver, for example, has the highest electrical and thermal conductivity among all metals, and, in the form of nanowires or nanobeams, may be used as nanoscale conductor of heat and electrons. It was demonstrated[51] that for a nanobeam with diameter of 20 nm the resistivity is twice of bulk silver, and then decreasing with increasing diameter. This means that, despite at this small size, properties of bulk silver are maintained. Moreover, the maximum current that can be supported increases with increasing cross-section.

1.1.2.4.3 Magnetic properties

Having small size and, consequently, high surface-to-volume ratio, ferromagnetic metal nanoparticles (e.g., Co, Ni, Fe) have also attracted attention for their potential use as high-density storage media for magnetic memory devices. However, the "superparamagnetic limit", which consists of a coupling of the miniaturization of the particles with a reduction of the magnetic barrier for flipping spin orientation[52], has to be overcome. In superparamagnetic materials, the thermal energy (kT) is enough to switch the magnetic spin direction, thus reducing the magnetization to zero, with the temperature of transition from ferromagnetism to superparamagnetism (blocking temperature, T_b) depending on the size of the nanoparticle (eq. 11).

$$T_b = \frac{K_u V}{25k}$$

Eq. 11 Blocking temperature. K_u is the magnetic anisotropic constant, V is the volume of the nanoparticle

Magnetic coercitivity (H_c) also depends on the nanocrystal size (eq. 12), with direct proportionality; this trend is valid only up to a critical dimension, beyond which multiple magnetic domains form.

$$H_c = \frac{2K_u}{m_s\left[1-5\left(kT/K_u V\right)^{1/2}\right]}$$

Eq. 12 Magnetic coercitivity. m_s is the saturation magnetization value

The formation of multiple domains may be a limitation for the implementation of nanoparticles as magnetic storage media; however, it has been found that within a single domain both T_b and H_c are dependent on the shape of the nanoparticle, providing a potentially powerful way to tune the properties of the nanoparticle itself[53].

1.1.2.5 Core@shell particles: definition and synthesis

A particular type of zero-dimensional nanostructure is the core-shell particle, often indicated as "core@shell". It consists of a nanoparticle covered with a shell, of various thickness, that can be either of a similar material to the one of the particle, or a different one. In the first case, the shell can be epitaxially grown onto the particle, with the two materials having a similar crystalline structure. More interesting are core@shell structures in which the two materials differ in terms of composition, crystal structure and physical properties: for example, metal@oxides, metal@polymer or oxide@polymer. Depending on the specific materials involved, the fabrication methods may be different, like coating, self-assembling or PVD (physical vapour deposition). The properties of the core-shells change not only depending on the materials used, but also on the core-to-shell thickness ratio. The shell can modify the charge, the functionality and the reactivity of the core material, as well as its stability and ability to be dispersed in solvents. However, it is still quite challenging to obtain uniform and homogeneous shells.

Basically, three general methods are used to prepare core-shells assemblies[54]:

1. The first approach consists in the preparation of the core and the shell separately, and combine them via a *coupling agent*, that functionalizes the surface of the core and allows the linkage with the shell material. Some of the most used coupling agents are APS (3-aminopropyltriethoxysilane), APTMS (3-aminopropyltrimethoxysilane), PTMS (propyltrimethoxysilane) and PVP (polyvinylpirrolidone)[55]. Graf et al., for example, demonstrated a method to cover several colloidal particles with silica by using PVP[56]. The advantage of using PVP is that it affects the potential on the colloid surface and allows nanoparticles to be dispersed in a wide range of solvents.
2. The second approach is called "*controlled precipitation*" because the shell is directly formed in presence of the cores in the reactive mixture. The most important factors are the concentration of the species and the amount of cores in the mixture, which may determine the thickness of the forming shell[57].
3. The third approach is a "*layer-by-layer*" technique, in which alternating layers of opposite charge are synthesized onto a core material that will be dissolved to create hollow shells. Understanding the properties of the materials used is fundamental because core and shell must not interdiffuse, but, at the same time, be similar enough such that heterogeneous nucleation is favoured.

Depending on the materials, many different methods have been used which are extensively described in literature[58].

An example of core@shell structures is given by noble metal particles covered with a layer of silica, often with the aid of coupling agents. By varying the quantity of precursors and experimental conditions, the thickness of the silica shell can be conveniently tuned. Examples of these core@shell structures are shown in fig. 9a-b: the particles in the picture have been synthesized for the purposes of the present works and details of the preparation are given in the following sections.

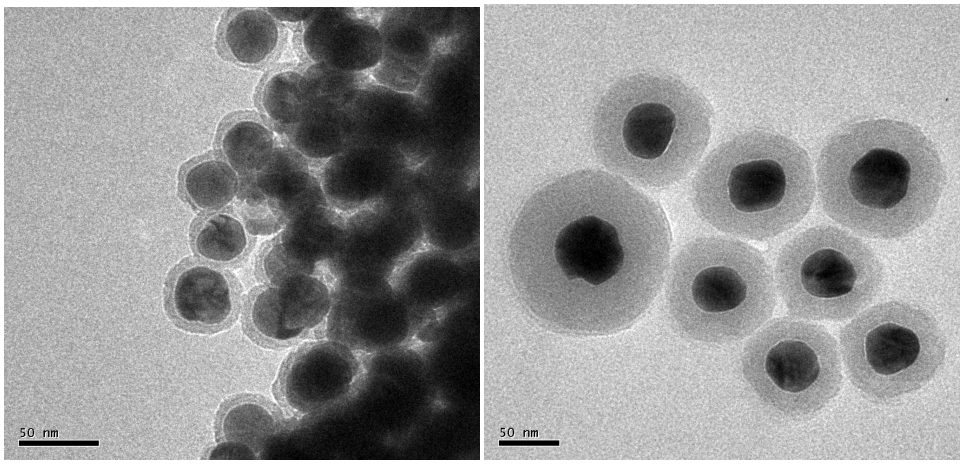

Fig. 9-a,b Silver@silica core-shell structures with different silica shell thickness prepared for the purposes of the present work: a)AS2; b)AS1

1.2 Synthesis and characterization of Ag@SiO_2: my work

1.2.1 Step I: Silver nanoparticles

The procedure for the production of silver nanoparticles with a diameter approximately of 50nm was derived from the work of Li et al.[59] (protocol #3). . This procedure consists of a conventional citrate-mediated reduction of silver nitrate in water, in presence of ascorbic acid, that makes the reduction of silver ions faster.

$$4Ag^{+} + C_6H_5O_7Na_3 + 2H_2O \rightarrow 4Ag^{0} + C_6H_5O_7H_3 + 3Na^{+} + H^{+} + O_2 \uparrow$$

The growth of uniform and quasi-spherical silver nanocrystals in water is difficult due to the secondary nucleation that occurs because the reduction *via* citrate is not fast enough. Furthermore, hydrolysis of Ag ions and oxidation and decomposition of newly formed Ag nanocrystals may occur. Ascorbic acid, being a strong reducing agent, leads to fast reduction of Ag^{+} ions to Ag^{0}. Hence, citrate plays to stabilize the newly formed particles, while ascorbic acid mainly drives the reduction. A sudden change of color of the solution, from colourless to clear yellow, is a first hint of the occurrence of the reaction (fig.10). A synthetic scheme of the procedure is provided in scheme 6. Briefly, a solution of ascorbic acid (SOLUTION ③ of the experimental section) is added to boiling milliQ water. After 4 min, an aqueous solution (SOLUTION ④) of $AgNO_3$ and sodium citrate is also added to the boiling water. The mixture is kept boiling for one hour and then cooled down to room temperature.

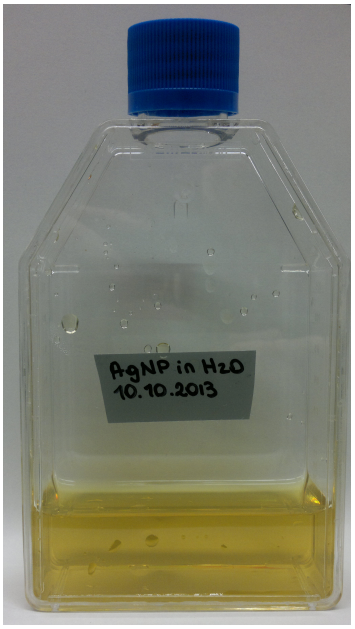

Fig. 10 Pictures of one of the prepared batch of silver nanoparticle, having a characteristic clear, yellow color.

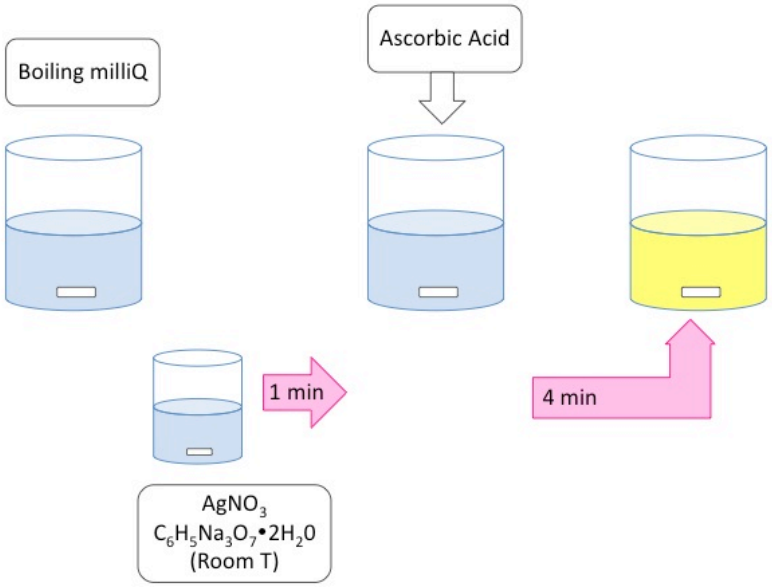

Scheme 6 route for silver nanoparticles synthesis

Furthermore, the absorption spectra of the as-prepared particle were recorded to verify that the absorption wavelength was in good agreement with theoretical values. The absorbance spectra have been collected using 0,2mL of Ag nanoparticle solution (the concentration of nanoparticles is 1% wt) and 1,8mL of milliQ water. Fig. 11 shows the absorbance spectra of one batch of particles, named AG1. The other batches, named AG2 to AG4, have been prepared with the same procedure; Table 3 summarizes the values of wavelength at the maximum. It is believed that the small differences in the wavelength positions of the peak are due to small differences in size and shape.

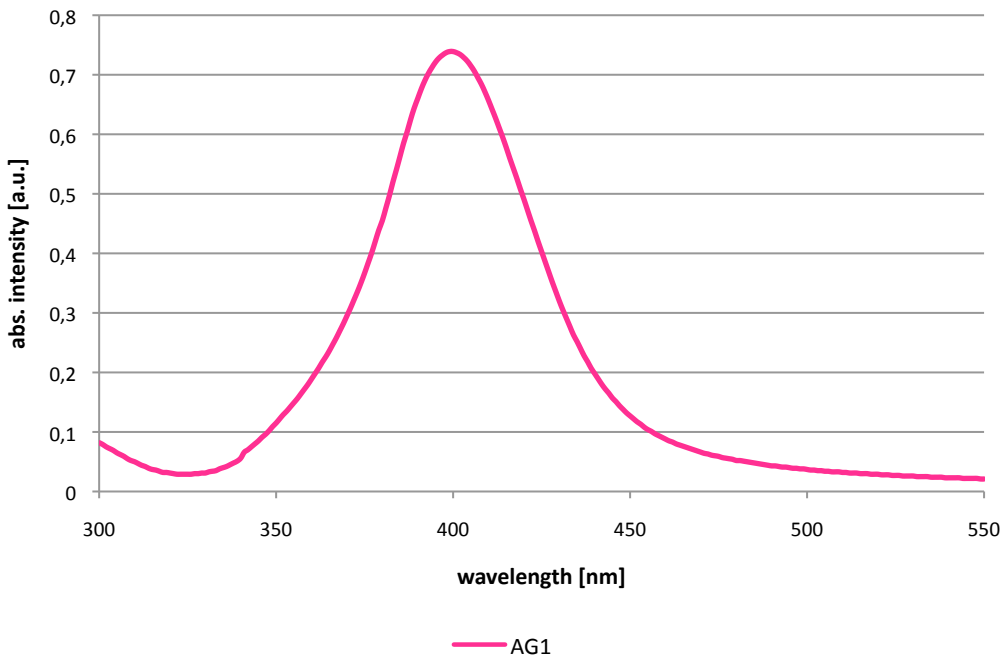

Fig. 11 Absorbance spectra of silver nanoparticles in H_2O

Sample	Max. λ [nm]
AG1	399.5
AG2	404
AG3	404
AG4	399

Table 3 Summary of silver nanoparticle runs and absorption peak position

TEM (Transmission Electron Microscope) was also used to determine shape and dimension of particles (fig.12a-d). TEM samples have been prepared depositing 5 µL of the solution to be analyzed onto standard copper grids, placed on a glass Petri dish as support. The Petri dish was then placed in a vacuum pump until complete drying of the solution (about 5 min).

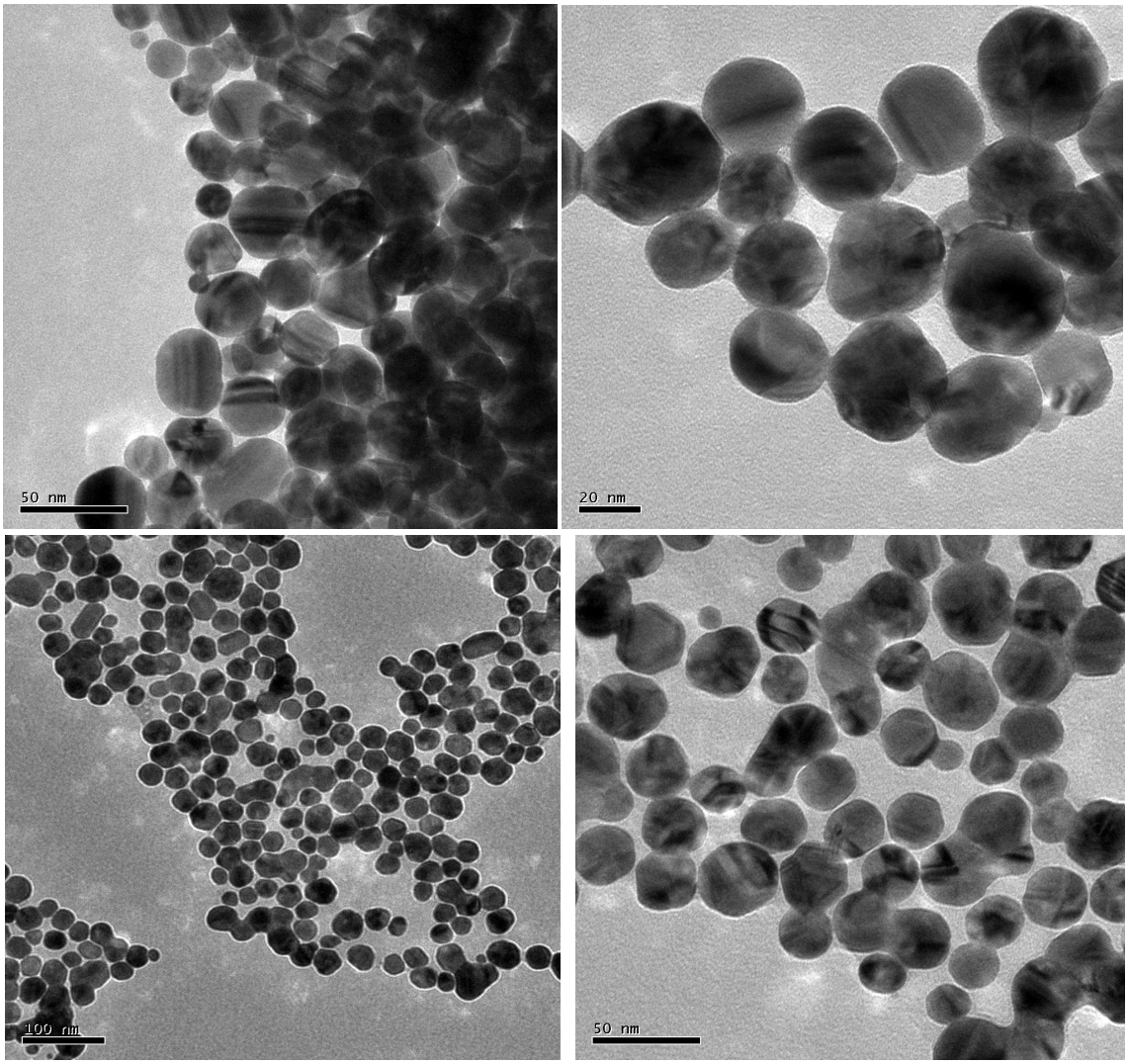

Fig. 12 a-d (from left to right and from top to bottom) TEM pictures of different batches of silver nanoparticles: a) and b) AG1; c) and d) AG4

Shape of the particle is mostly quasi-spherical, as it was expected by the production method adopted. Particle size looks also prevalently homogeneous; nevertheless, some aggregates were sometimes observed as well as rod-like structures (fig.13a-b).

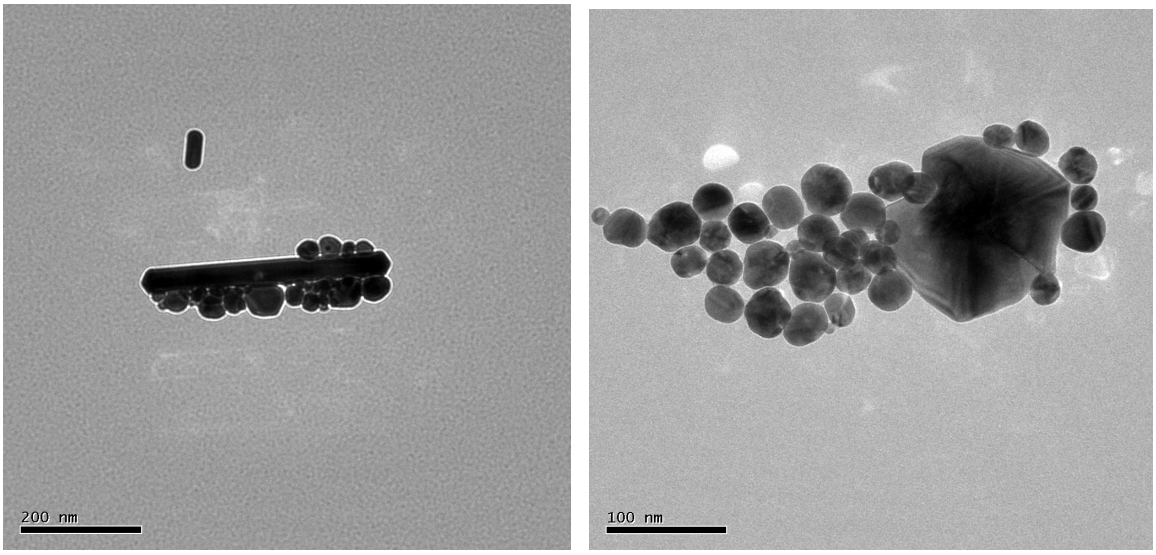

Fig. 13 a-b Examples of different structures present in the colloid: a)rod and b)aggregates

The occurrence of such structures may be related to a not efficient stirring, as well as an insufficient protection from the light. To confirm the size distribution of the silver particles, DLS (Dynamic Light Scattering) measurement have also been performed on the solution of fig. 12c-d, AG4. The measurement resulted in an average size of 43 nm. Measurements on sample AG1 resulted in particles mean size of 50 nm.

Stored in refrigerator at 5°C and protected from light, the as-prepared particles have a stability superior to two months, at least.

1.2.2 Step II: coating with silica shell

1.2.2.1 Silica shell formation

The procedure was derived from Baida et al.[60]. A few drops of dimethylamine (DMA) have been added to a solution of silver particles in ethanol: accordingly, pH values shift from approximately 5-6 to 8-9. 10 mL of a TEOS (tetraethoxysilane) solution (SOLUTION ⑤ of the experimental section), is added portionwise within 2,5 hours. TEOS is the conventional precursor for the formation of stable silica nuclei, as described the first time by Stöber and co-workers[61]. The "standard" method, derived from literature, makes use of a 10mM TEOS solution in ethanol. After the reaction is completed, the solution is washed three times with fresh ethanol, each washing step following a centrifugation to an easier separation of the solvent. A synthetic scheme of the process is provided below (scheme 7).

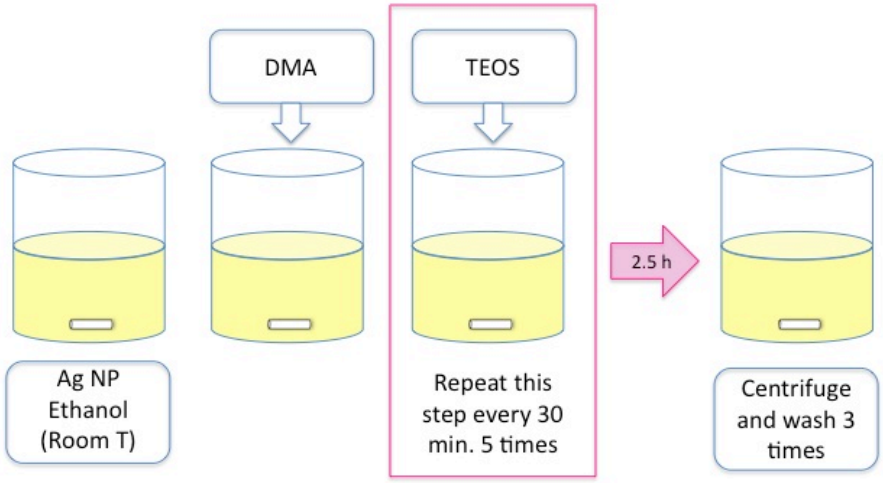

Scheme 7 Representation of the "standard" procedure, as derived from literature, to obtain the silica shell

At first glance, if the color of the solution does not change after the centrifugation step, the procedure can be considered successfully accomplished. A color change to red/brown may indicate aggregation of the particles, while a change to silver indicates the insufficient coating. Fig.14 provides examples of three different batches of particles, exhibiting a different coloration as a consequence of a different degree of coating.

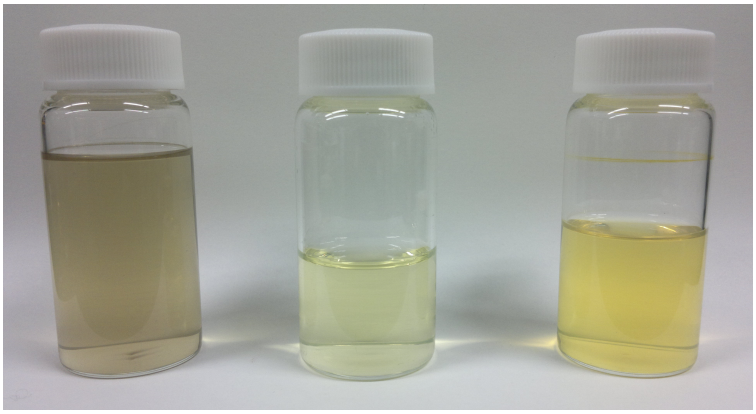

Fig. 14 Core@shell solutions exhibiting a different coloration. From left to right, aggregated silver particles (brown), uncoated particles (light yellow with silver shades) and successfully coated particles (yellow) are shown

The prepared core@shells have been characterized at first by UV-vis spectroscopy (Fig. 15), since a red-shift in the peak position, with respect to bare particles, indicates a change in the index of refraction of the nanostructures and hence a successful coverage.

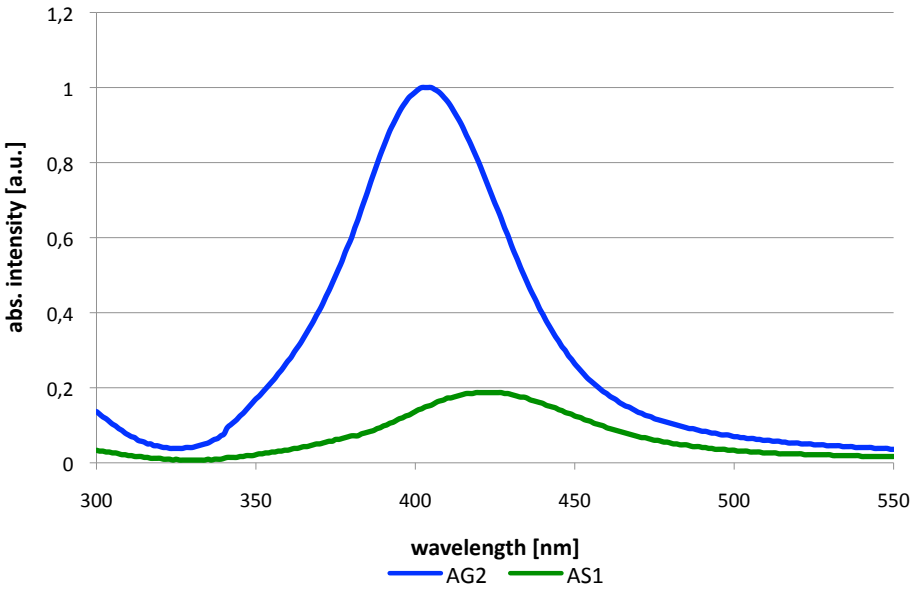

Fig. 15 UV-vis absorption spectra of silver nanoparticles (AG2) and core@shell particles (AS1)

As it can be seen from fig.15, the spectrum of AS1 (core@shell particles) is 16nm red-shifted (from 404 nm to 420 nm), thus indicating the formation of a silica shell. The decrease in absorbance is not meaningful, as core@shells have not the same concentrations, due to the preparation method, and diluted with respect to the original particles.

To assess the morphology and the thickness of the shell, TEM images have also been collected (fig.16a-b). The preparation of TEM samples is the same as previously described.

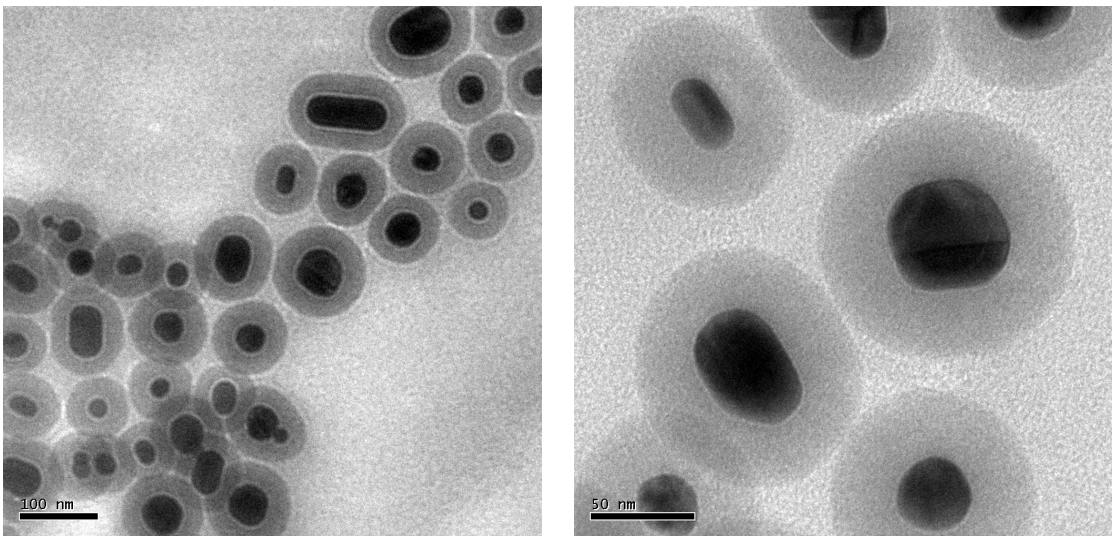

Fig. 16 a-b a) and b) Silica coated silver nanoparticles, AS1, obtained with the procedure described in the literature[62].

1.2.2.2 Optimization of silica shell thickness and homogeneity

A homogeneous silica shell is observed on all the particles (fig.16), even though a few double-core particles can also sometimes be found. No coreless particles, nor isolated silica aggregates are observed.

The silica shell has a double function: it protects the silver particles, preventing from aggregation, and allows achieving the correct spacing between the metal nanoparticles and the fluorophore that is a fundamental requirement to get a clear MEF signal. Apparently, MEF signal is maximum when the spacing is around 10nm[63], decreasing with the increase of the shell thickness.

Since the first run for the preparation of $Ag@SiO_2$ was successful and a homogeneous and stable shell was obtained, next experiments have been performed in order to optimize the thickness of the shell by working on the operational parameters. Changes involved:

- TEOS concentration
- TEOS total volume
- Number of TEOS addition or volume per addition
- Solvent or catalyst

Specifically, such modifications aimed at reducing the shell thickness, thus modifying the relative distance between the metal core and the fluorophore. A reduction of TEOS concentration was the most intuitive possible influencing parameter, but other ones have been also considered. In particular, 2-propanol was chosen because it has been reported[64,65] that it may avoid the formation of coreless particles, as it may happen in ethanol. As DMA is reported to promote the formation[66] of a thick silica shell, NH_3 was also tested to obtain a thinner dielecric layer. However, Ag may oxidize in presence of NH_3 and the formed $Ag(NH_3)_2^+$ dissolves in water and causes a damping of the surface plasmon band of silver with time as it does not absorbs in the visible. Table 4 summarizes the modifications taken into consideration, where the "O" symbol indicates a successful result, while"X" means not successful (a shell could not be observed).

TEOS CONC.	SOLVENT	CATALYST	N° ADDITIONS	VOLUME PER ADDITION [mL]	RESULT	RUN
10mM	ethanol	DMA	5	2	O	SOLUTION ⑤ AS1
8mM	ethanol	DMA	5	2	O	SOLUTION ⑥ AS2, AS3, AS4
5mM	ethanol	DMA	5	2	×	SOLUTION ⑦ AS7
1mM	ethanol	DMA	5	2	×	SOLUTION ⑧ AS8
10mM	ethanol	DMA	10	1	O	SOLUTION ⑤ AS5
10mM	ethanol	DMA	2	5	×	SOLUTION ⑤
8mM	2-propanol	DMA	5	2	O	AS6
8mM	ethanol	NH_3	5	2	×	AS9

Table 4 Summary of the modifications, with respect to the standard procedure (grey row), considered to tune the silica shell thickness

A homogeneous silica shell could be also be obtained by using 2-propanol instead of ethanol as solvent, but the thickness of the shell was higher, and some double-core particles could be observed (fig 17).

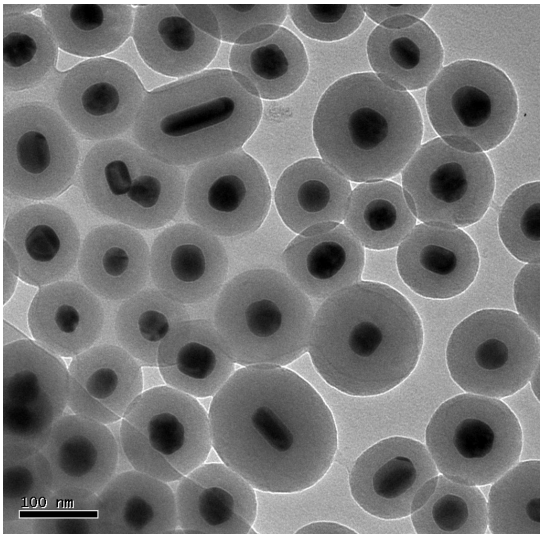

Fig. 17 Ag@SiO_2 in 2-propanol, AS6

On the contrary, changing the catalyst to NH_3 or decreasing the TEOS concentration was not effective, as can be seen in figures 18a-c.

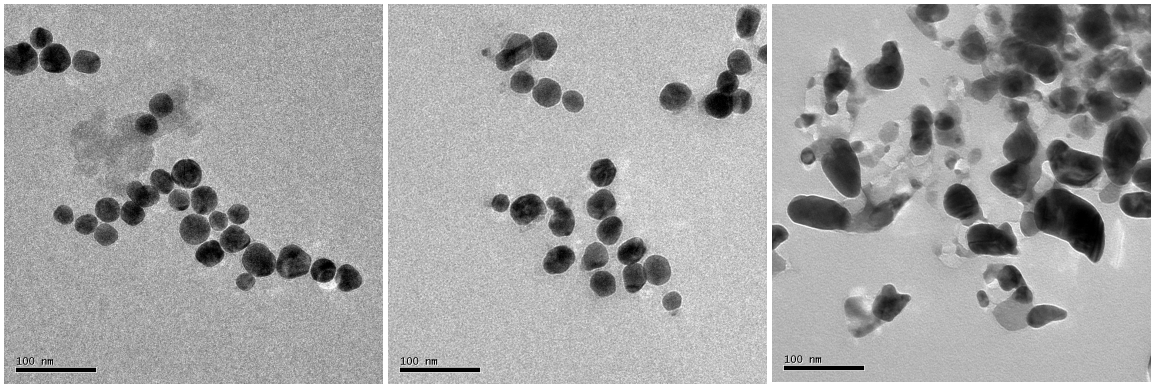

Fig. 18 a-c (from left to right) Uncoated silver particles obtained with a)1mmol TEOS, AS7; b)5mmol TEOS, AS8; c)NH_3 as catalyst, AS9

The particles have been characterized either via TEM and DLS to assess morphology and size. By decreasing the concentration of TEOS, the silica shell obtained is thinner: the lower limit of TEOS concentration is 8mM, below which the shell is not formed and many silica aggregates can be found. An important parameter is also the diameter of the silver nanoparticles, since it is easier to obtain a thinner shell if particles are bigger. Controlling the shell thickness is hence extremely easy. The following pictures (fig. 19a-e) show five different batches of particles, each with a different thickness of the silica shell.

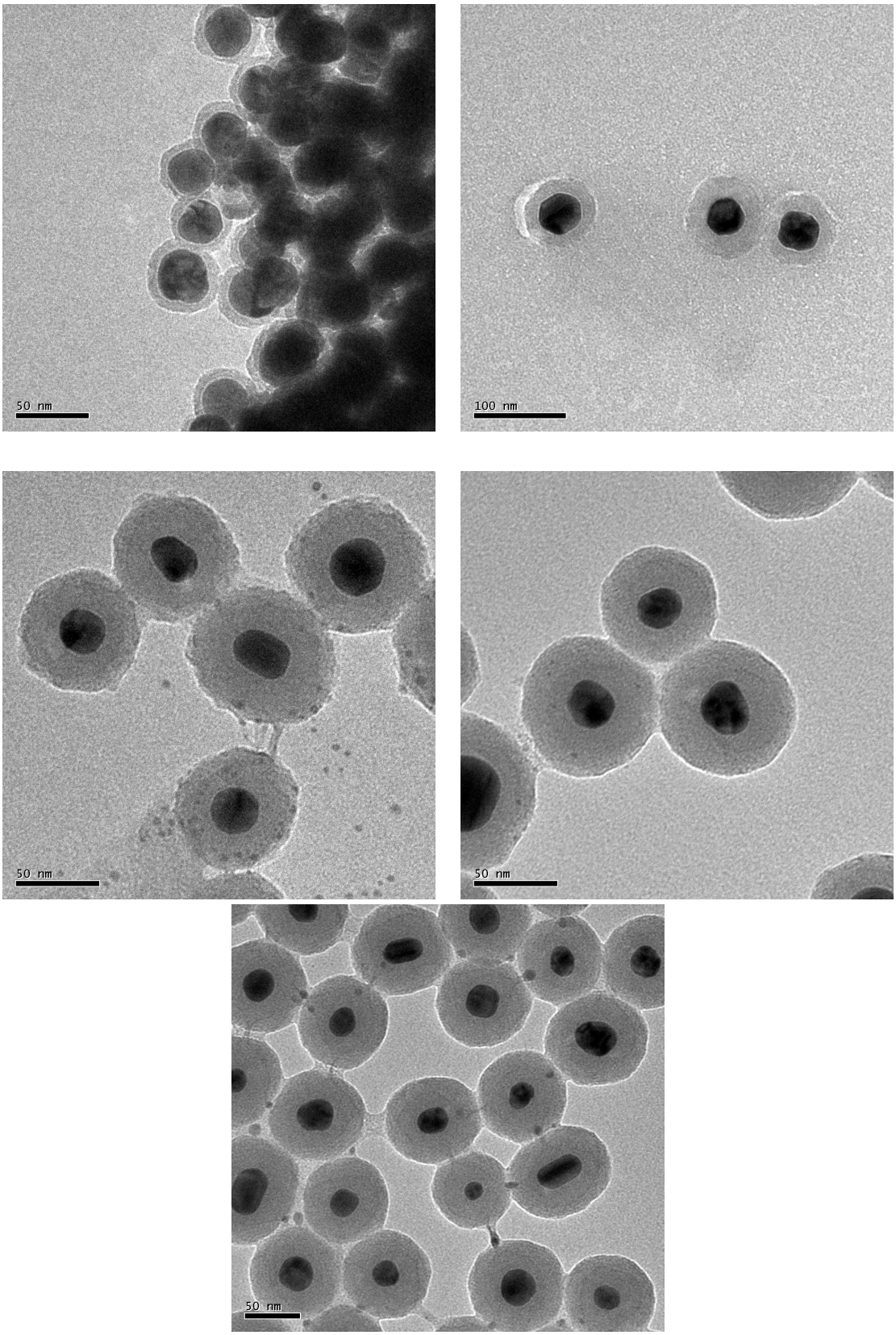

Fig. 19 a-e (from left to right and from top to bottom) TEM pictures of five different batches of Ag@SiO_2 particles. a) 8mM TEOS, AS2; b) 8mM TEOS ,AS3; c) 8mMTEOS, AS4; d) 10mM TEOS, AS1; e) 10mM TEOS x 10 times, AS5

Since the core@shells have been obtained with two different batches of silica nanoparticles and a direct comparison was not strictly possible, the core-to-shell ratio has been calculated. The

following table (table 5) summarizes the results of the DLS measurement and the calculated C/S ratio.

	d_{DLS} [nm]	C/S
A (AS2)	153	0,97
B (AS3)	159	0,91
C (AS4)	189	0,53
D (AS1)	147	0,83
E (AS5)	157	0,75

Table 5 Diameters (d_{DLS})and C/S of different batches of core@shells. A and B has been obtained from AgNP with a mean diameter of 50nm, while C, D and E with a mean diameter of 43nm

Stored in refrigerator at 5°C and protected from light, the shelf-life of the as-prepared core shells is over 6 months.

1.3 Experimental procedures

In this section, details of the experimental procedures will be provided. All experiments have been performed following the safety procedures, using gloves, mask, goggles and laboratory coat. If not specified, all chemicals have been used as received. To prevent contamination, all chemicals have been exposed to Ar gas after use, before sealing. All glassware was rinsed with milliQ water and acetone before use, otherwise differently specified. The water in all experiments was milliQ water (18,2 MΩ, Millipore). Acetone (99,5% min.) and ethanol (99,5% min.) were from Wako Pure Chemicals Ltd., Japan, for all experiments.

1.3.1 Synthesis of silver nanoparticles

As previously mentioned, the procedure to obtain silver nanoparticles is directly derived from the article by Li et al.[67]. Trisodium citrate dihydrate ($Na_3C_6H_5O_7 \bullet 2H_2O$), silver nitrate ($AgNO_3$ 99,8%) and ascorbic acid (AA 99,5%) were purchased from Wako Pure Chemicals Ltd., Japan.

10mL of aqueous solution of $AgNO_3$ (1 wt%) and 10mL of aqueous solution of sodium citrate (1 wt%) were prepared.
SOLUTION ①: 0,1g $AgNO_3$ in 10mL water. This solution is sensitive to light, so the screw vial in which it was contained was wrapped in an aluminum foil for all the experiment duration.
SOLUTION ②: 0,1g sodium citrate in 10mL water.
Also, 10mL of aqueous solution of AA was prepared. The concentration of AA in the total final solution (100mL) is 10mM.
SOLUTION ③: 0,176g AA in 10mL water.

95mL water were brought to boil in a triple-neck round flask, in a stirred oil bath. After water was boiling, SOLUTION ④ was prepared as follows: 2mL of SOL.② and 0,5mL of SOL.① were added subsequently to 2,5mL water under stirring at room temperature. After stirring SOL.④ for 4 minutes, 50µL of SOL.③ was added to the boiling water, followed by further one minute boiling before adding SOL.④. After this last addition, the boiling mixture suddenly changes colour from colourless to clear, transparent yellow. The reaction solution was further boiled for 1 h under stirring, the reaction system covered by aluminium foils to prevent light exposure. Finally, the reaction solution was cool down to room temperature before transferring it into a plastic bottle and stored in refrigerator.

1.3.2 Silica encapsulation

This procedure follows the indications found in the article by Baida et al.[68]. TEOS ($Si(OC_2H_5)_4$ tetraethoxysilane, 99,9%) was purchased by Alfa Aesar (Ward Hill, MA, USA). DMA (dimethylamine, ≈50%), ammonia (28%) and 2-propanol (99%) were purchased by Wako Pure Chemicals Ltd., Japan. This procedure leads to the production of total 60mL of $Ag@SiO_2$ solution.

Conventional protocol

20mL of a 10mM TEOS solution in ethanol was prepared.

SOLUTION ⑤: 44,8µL TEOS in 20mL ethanol. This solution is particularly sensitive to atmospheric conditions, so it has been treated with Ar gas anytime the screw vial containing it was opened.

10mL of Ag nanoparticle aqueous solution was added under stirring to 40mL ethanol. Subsequently, DMA was added dropwise to the solution until the pH reached a value between 8 and 9. Starting solution has a pH between 5 and 6: 6 drops of DMA (using a Pasteur pipette) are enough to promote the change. Then, 2mL of SOL. ⑤ was added every 30 min (5 additions in total). Particles were washed via centrifugation at 7000 rpm for 50 minutes and redispersed in ethanol (the washing step was repeated 3 times).

Modified protocols

Several alternative routes have been followed in order to optimize the thickness of the silica shell, changing the operational parameters one at a time to check their influence on the final result. The washing stage remained unchanged.

1. Reduction of TEOS concentration from 10mM to 8mM, 5mM and 1mM. Respectively:
   SOLUTION ⑥: 35,8µL TEOS in 20mL ethanol
   SOLUTION ⑦: 22,4µL TEOS in 20mL ethanol
   SOLUTION ⑧: 4,47µL TEOS in 20mL ethanol
   Each solution was used with the methodology of the "conventional protocol"

2. Reduction of total volume of TEOS added
   6mL of SOL.⑤ was added in 3 additions of 2mL each
   5mL of SOL.⑤ was added in 5 additions of 1mL each

3. Modifications of the number of additions, keeping the total amount of TEOS added constant and equal to 10mL
   10mL of SOL.⑤ was added in 2 additions of 5mL each
   10mL of SOL.⑤ was added in 10 additions of 1mL each

4. Modification of solvent or catalyst. In both cases, SOL.⑥ was used.
   Ethanol was changed to 2-propanol for the initial dissolution of silver nanoparticles
   DMA was changed to ammonia as pH modifying agent.

Bibliography

1. "*National Technology Initiative 2000 Leading to the Next Industrial Revolution", a report by the Interagency Working Group on Nanoscience, Engineering and Technology* (Washington DC: Committee on Technology, National Science and Technology Council), www.whitehouse.gov/documents
2. Milner, Robin, and Susan Stepney. "Nanotechnology: Computer science opportunities and challenges." *Submission by the UK Computing Research Committee to the Nanotechnology Working Group of the Royal Society and the Royal Academy of Engineering* (2003).
3. Roco, Mihail C. "Nanotechnology: convergence with modern biology and medicine." *Current Opinion in Biotechnology* 14.3 (2003): 337-346.
4. Naik, A. B., and N. B. Selukar. "Role of nanotechnology in medicine." *Everyman's Science* 44.3 (2009): 151-153.
5. Vo-Dinh, Tuan, ed. *Nanotechnology in biology and medicine: methods, devices, and applications*. CRC Press, 2007.
6. Aricò, Antonino Salvatore, et al. "Nanostructured materials for advanced energy conversion and storage devices." *Nature materials* 4.5 (2005): 366-377.
7. Pumera, Martin. "Electrochemistry of graphene: new horizons for sensing and energy storage." *The Chemical Record* 9.4 (2009): 211-223.
8. Moore, Gordon E. "Cramming more components onto integrated circuits." (1965).
9. Cao, Guozhong. *Nanostructures and nanomaterials*. Imperial college press, 2004
10. www.google.it; Last access 7.04.2014
11. Krätschmer, Wolfgang, et al. "C60: a new form of carbon." *Nature* 347.6291 (1990): 354-358.
12. Iijima, Sumio. "Helical microtubules of graphitic carbon." *Nature* 354.6348 (1991): 56-58.
13. Kresge, C. T., et al. "Ordered mesoporous molecular sieves synthesized by a liquid-crystal template mechanism." *Nature* 359.6397 (1992): 710-712.
14. Cfr. 10
15. Cfr.9
16. LaMer, Victor K., and Robert H. Dinegar. "Theory, production and mechanism of formation of monodispersed hydrosols." *Journal of the American Chemical Society* 72.11 (1950): 4847-4854.
17. Xia, Younan, et al. "Shape-Controlled Synthesis of Metal Nanocrystals: Simple Chemistry Meets Complex Physics?." *Angewandte Chemie International Edition* 48.1 (2009): 60-103.
18. Faraday, Michael. "The Bakerian lecture: experimental relations of gold (and other metals) to light." *Philosophical Transactions of the Royal Society of London* 147 (1857): 145-181.
19. Turkevich, John, Peter Cooper Stevenson, and James Hillier. "A study of the nucleation and growth processes in the synthesis of colloidal gold." *Discussions of the Faraday Society* 11 (1951): 55-75.
20. Cfr.9
21. Wiley, B., Sun, Y., Mayers, B. & Xia, Y. 2005, "Shape-Controlled Synthesis of Metal Nanostructures: The Case of Silver", *Chemistry-A European Journal,* vol. 11, no. 2, pp. 454-463
22. Reetz, Manfred T., and Wolfgang Helbig. "Size-selective synthesis of nanostructured transition metal clusters." *Journal of the American Chemical Society* 116.16 (1994): 7401-7402.
23. Hu, Bo, et al. "Microwave-assisted rapid facile "green" synthesis of uniform silver nanoparticles: self-assembly into multilayered films and their optical properties." *The Journal of Physical Chemistry C* 112.30 (2008): 11169-11174.
24. Komarneni, Sridhar, et al. "Microwave-polyol process for Pt and Ag nanoparticles." *Langmuir* 18.15 (2002): 5959-5962
25. Bahadur, Newaz Mohammed, et al. "Fast and facile synthesis of silica coated silver nanoparticles by microwave irradiation." *Journal of colloid and interface science* 355.2 (2011): 312-320
26. Amiens, Catherine, et al. "Selective synthesis, characterization, and spectroscopic studies on a novel class of reduced platinum and palladium particles stabilized by carbonyl and phosphine ligands." *Journal of the American Chemical Society* 115.24 (1993): 11638-11639.

27. Rodriguez, Ana, et al. "Synthesis and isolation of cuboctahedral and icosahedral platinum nanoparticles. ligand-dependent structures." *Chemistry of materials* 8.8 (1996): 1978-1986.
28. Verelst, Marc, et al. "Synthesis and characterization of CoO, Co3O4, and mixed Co/CoO nanoparticules." *Chemistry of materials* 11.10 (1999): 2702-2708.
29. cfr. 17
30. Tausch-Treml, R., A. Henglein, and J. Lilie. "Reactivity of silver atoms in aqueous solution II. A pulse radiolysis study." *Berichte der Bunsengesellschaft für physikalische Chemie* 82.12 (1978): 1335-1343.
31. Michaelis, Matthias, and Arnim Henglein. "Reduction of palladium (II) in aqueous solution: stabilization and reactions of an intermediate cluster and palladium colloid formation." *The Journal of Physical Chemistry* 96.11 (1992): 4719-4724.
32. Mandler, Daniel, and Itamar Willner. "Photohydrogenation of acetylenes in water-oil two-phase systems: application of novel metal colloids and mechanistic aspects of the process." *Journal of Physical Chemistry* 91.13 (1987): 3600-3605.
33. Cfr.9
34. Cfr.19
35. Bönnemann, H. & Richards, R.M. 2001, "Nanoscopic Metal Particles− Synthetic Methods and Potential Applications", *European Journal of Inorganic Chemistry,* vol. 2001, no. 10, pp. 2455-2480.
36. Sarathy, K. Vijaya, et al. "Superlattices of metal and metal-semiconductor quantum dots obtained by layer-by-layer deposition of nanoparticle arrays." *The Journal of Physical Chemistry B* 103.3 (1999): 399-401.
37. Rao, CN Ramachandra, et al. "Metal nanoparticles and their assemblies." *Chemical Society Reviews* 29.1 (2000): 27-35.
38. Bönnemann, H. & Richards, R.M. 2001, "Nanoscopic Metal Particles− Synthetic Methods and Potential Applications", *European Journal of Inorganic Chemistry,* vol. 2001, no. 10, pp. 2455-2480.
39. Cfr.16
40. Mie, Gustav. "Beiträge zur Optik trüber Medien, speziell kolloidaler Metallösungen." *Annalen der physik* 330.3 (1908): 377-445
41. Betschon, Felix, and Markus Halter. "Method for producing an electro-optical printed circuit board with optical waveguide structures." U.S. Patent No. 8,383,327. 26 Feb. 2013.
42. Thylen, Lars H., Alexandre M. Bratkovski, and Petter Holmstrom. "NANOPARTICLE WAVEGUIDE APPARATUS, SYSTEM AND METHOD." U.S. Patent No. 20,130,215,495. 22 Aug. 2013.
43. Cheng, T., C. Rangan, and J. E. Sipe. "Metallic nanoparticles on waveguide structures: effects on waveguide mode properties and the promise of sensing applications." *JOSA B* 30.3 (2013): 743-765.
44. Del Zoppo, Mirella. Lecture of the course "*Nanophotonics*", A.Y. 2012/2013, Politecnico di Milano
45. Ghosh Chaudhuri, Rajib, and Santanu Paria. "Core/shell nanoparticles: classes, properties, synthesis mechanisms, characterization, and applications." *Chemical reviews* 112.4 (2011): 2373-2433.
46. Evanoff, David D., and George Chumanov. "Synthesis and optical properties of silver nanoparticles and arrays." *ChemPhysChem* 6.7 (2005): 1221-1231.
47. Cfr.45
48. Prodan, E., et al. "A hybridization model for the plasmon response of complex nanostructures." *Science* 302.5644 (2003): 419-422.
49. Cfr. 17
50. Cfr. 46
51. Wiley, Benjamin J., et al. "Synthesis and electrical characterization of silver nanobeams." *Nano letters* 6.10 (2006): 2273-2278.
52. Weller, Dieter, and Andreas Moser. "Thermal effect limits in ultrahigh-density magnetic recording." *Magnetics, IEEE Transactions on* 35.6 (1999): 4423-4439
53. Jiles, David C. *Introduction to magnetism and magnetic materials*. CRC Press, 1998.
54. Kalele, S., Gosavi, S., Urban, J. & Kulkarni, S. 2006, "Nanoshell particles: synthesis, properties and applications", *Current science,* vol. 91, no. 8, pp. 1038-1052

55. Chou, Kan-Sen, and Chen-Chih Chen. "Fabrication and characterization of silver core and porous silica shell nanocomposite particles." *Microporous and mesoporous materials* 98.1 (2007): 208-213.
56. Graf, C., Vossen, D.L., Imhof, A. & van Blaaderen, A. 2003, "A general method to coat colloidal particles with silica", *Langmuir,* vol. 19, no. 17, pp. 6693-6700.
57. Baida, H., Billaud, P., Marhaba, S., Christofilos, D., Cottancin, E., Crut, A., Lermé, J., Maioli, P., Pellarin, M. & Broyer, M. 2009, "Quantitative determination of the size dependence of surface plasmon resonance damping in single Ag@ SiO2 nanoparticles", *Nano letters,* vol. 9, no. 10, pp. 3463-3469
58. Caruso, F. 2001, "Nanoengineering of particle surfaces", *Advanced Materials,* vol. 13, no. 1, pp. 11-22
59. Li, H., Xia, H., Wang, D. & Tao, X. 2013, "Simple Synthesis of Monodisperse, Quasi-Spherical, Citrate-Stabilized Silver Nanocrystals in Water", *Langmuir*
60. Cfr. 57
61. Stöber, W., Fink, A. & Bohn, E. 1968, "Controlled growth of monodisperse silica spheres in the micron size range", *Journal of colloid and interface science,* vol. 26, no. 1, pp. 62-69
62. Cfr.57
63. Dragan, A. I., and C. D. Geddes. "Excitation volumetric effects (EVE) in metal-enhanced fluorescence." *Physical Chemistry Chemical Physics* 13.9 (2011): 3831-3838.
64. Hardikar, Vishwas V., and Egon Matijević. "Coating of nanosize silver particles with silica." *Journal of colloid and interface science* 221.1 (2000): 133-136.
65. Niitsoo, Olivia, and Alexander Couzis. "Facile synthesis of silver core–silica shell composite nanoparticles." *Journal of colloid and interface science* 354.2 (2011): 887-890.
66. Kobayashi, Yoshio, et al. "Silica coating of silver nanoparticles using a modified Stöber method." *Journal of colloid and interface science* 283.2 (2005): 392-396.
67. Cfr. 59
68. Cfr.57

2. PLAMSON-ASSISTED FLUORESCENCE ENHANCEMENT FROM PAPER SUBSTRATES

2.1 Principles of Fluorescence

Luminescence is the emission of light from electronically excited species and, depending on the excited state, it can be distinguished into fluorescence and phosphorescence. Fluorescence occurs as decay from the first singlet excited state to the ground state of the molecule. In excited singlet states, the electron in the excited orbital is paired with another one in the ground state, having opposite spin. The fluorescent decay is, hence, spin-allowed and occurs rapidly (typically 10^8 s^{-1}), so that a typical lifetime for the excited state is about 10 ns[1]. Typically, fluorescent molecules contains aromatic groups, with quinine being one of the most encountered in daily life (it is present also in tonic water!), observed for the first time in 1845 by Sir John Fredrich William Herschel[2]; some are represented in fig.20.

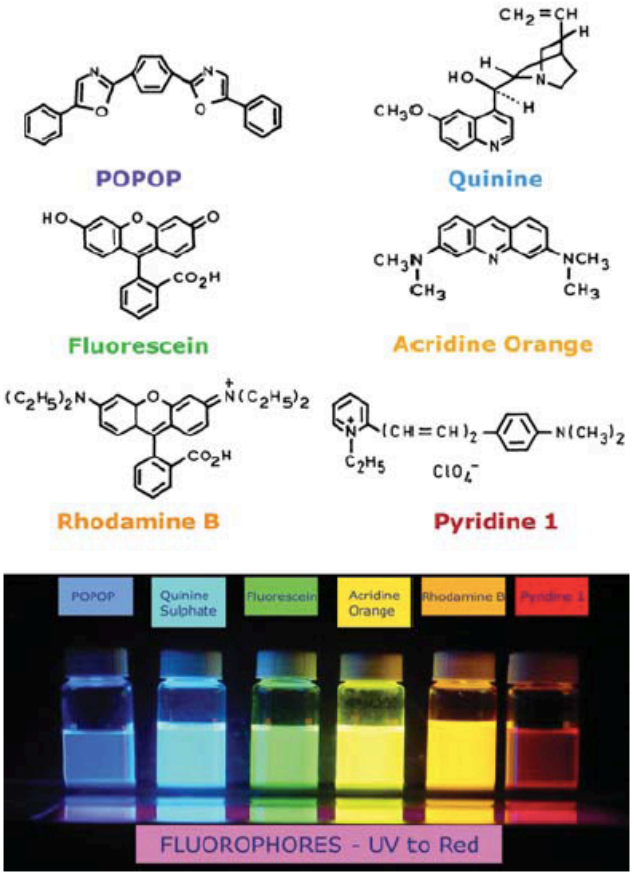

Fig. 20 Chemical structures of some common fluorescent dyes and their emission colour upon irradiation[3]

2.1.1 Jablonski diagram

The de-activating processes occurring after light absorption are described by the Jablonski diagram, which is represented in fig.21 in the complete form. S_0, S_1 and S_2 are the ground and two excited states for the singlet, respectively, while T_1 is a triplet excited state and vibrational states (indicated by the numbers 0, 1 and 2) are associated to each of these electronic levels. Due to light absorption, $h\nu_A$, electrons are promoted form the ground to the excited states. According to the Franck-Condon principle, nuclei displacement is neglected. Subsequent decay processes may occur: Internal Conversion is a rapid process that brings electrons from higher excited states to lower vibrational states, until reaching S_1, from which two competitive effects may occur. Additionally, vibrational relaxation can occur within the S_1 state. Luminescence by fluorescence occurs through a radiative $S_{1,0} \rightarrow S_{0,n}$ transition the emission of a photon with typical frequency, $h\nu_F$. Spin conversion to the state T_1 can also occur via intersystem crossing, from which another luminescent decay process may happen, namely phosphorescence, with emission of photons $h\nu_P$. Phosphorescence typically becomes a relevant deactivating process when molecules contain heavy atoms.

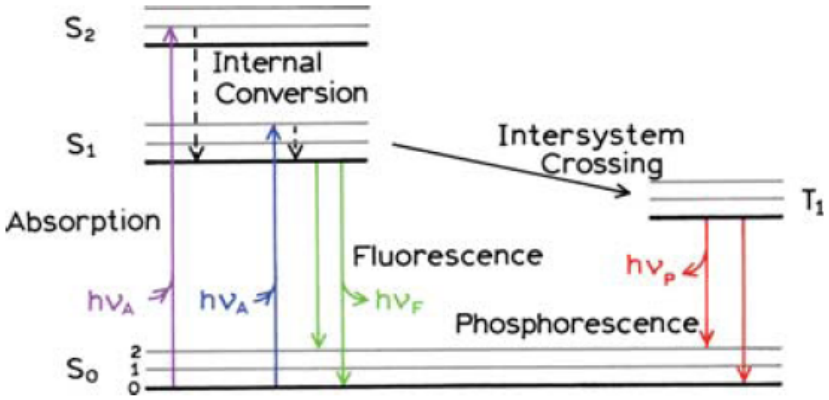

Fig. 21 Complete Jablonski diagram, representing all possible radiative and non-radiative processes[4]

Fluorescence implies that photons at a longer wavelength than that of absorption are emitted: this phenomenon was first observed by Sir G.G. Stokes in 1852 at Cambridge[5], and it is named "Stokes shift". Energy losses between excitation and emission are observed universally for fluorescent molecules in solution. One common cause of the Stokes shift is the rapid decay to the lowest vibrational level of S_1. Furthermore, fluorophores generally decay to higher vibrational levels of S_0, resulting in further loss of excitation energy by thermalization of the excess vibrational energy. In addition to these mechanisms, fluorophores can display further Stokes shifts due to solvent effects, excited-state reactions, complex formation, and/or energy transfer. Another important feature is that fluorescence, does not generally depend on the excitation wavelength (Kasha-Vavilov rule)[6]. Few exceptions refer to molecules having two ionization states, or molecules emitting from S_2. Moreover, many dyes follow the mirror-image rule, having mirrored absorption and emission spectra for the inverse transition (fig.22).

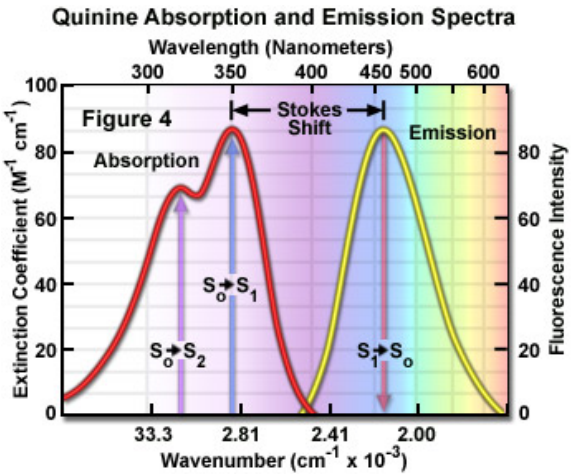

Fig. 22 Absorption and emission spectra of quinine[7]

Probably, the most important characteristics of fluorophores are the quantum yield and the lifetime. Quantum yield is the number of emitted photons, with respect to the number of absorbed photons. The higher the quantum yield, the brighter the dye. Lifetime is a measure of the time experienced by the electron in the excited state, and it is important for the interaction of the fluorophore with the environment. If it is too high, the fluorophore may interact with the environment, such that deactivation processes, other that fluorescent emission, may occur. To explain in detail these two concepts, it is easier to consider a simplified version of the Jablonski diagram (scheme 8).

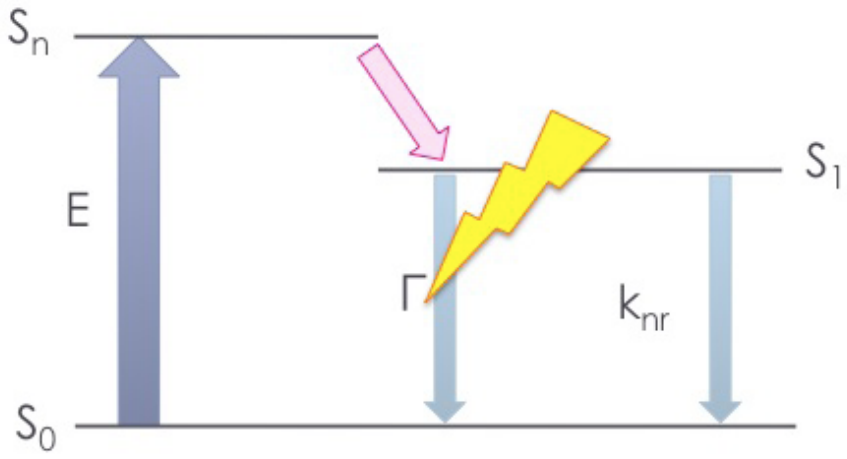

Scheme 8 Classical Perrin-Jablonski diagram of a fluorophore

When a stimulus is applied, like a striking electromagnetic wave, represented by *E*, electrons may be excited from the ground state to a generic excited state of higher energy, S_n. This process, absorption, is very fast, requiring about 10^{-15} s. Subsequently, fast decay to S_1 state occurs *via* internal conversion or vibrational relaxation (pink arrow). Once the electrons are found in the S_1 state, they may decay, both radiatively or non-radiatively. Non-radiative processes are indicated by the rate k_{nr}, while *Γ* represents the number of electrons decaying radiatively that is, in turn, the number of emitted photons. Other de-activation processes may actually occur with a rate k_q (not shown). These processes are named generally “quenching processes”, and include a variety of

mechanism; one of the most relevant is collisional quenching, that occurs when the excited state fluorophore is deactivated upon contact with some other molecule in solution, called quencher. The quantum yield of a fluorophore, Q_o (eq.13), is calculated as the rate between the number of electrons radiatively decaying, versus the total number of electrons that decay (or absorbed photons). Clearly, the higher Γ, the higher the quantum yield. Similarly, the excited lifetime, τ_0 (eq.14), is defined as the inverse of the total number of electrons decaying

$$Q_0 = \frac{\Gamma}{\Gamma + k_{nr} + k_q}$$

Eq. 13 Quantum yield

$$\tau_0 = \frac{Q_0}{\Gamma} = \frac{1}{\Gamma + k_{nr} + k_q}$$

Eq. 14 Lifetime of a fluorescent molecule

Most changes in quantum yield depend on the surrounding environment, and act by modifying the value of k_{nr} or k_q.

Solvent polarity is one of the most influencing factors. Typically, the fluorophore has a larger dipole moment in the excited state (μ_E) than in the ground state (μ_G). Following excitation the solvent dipoles can reorient or relax around μ_E, which lowers the energy of the excited state. As the solvent polarity is increased, this effect becomes larger, resulting in emission at lower energies (or longer wavelengths). In general, only fluorophores that are polar display a large sensitivity to solvent polarity. Nonpolar molecules, such as unsubstituted aromatic hydrocarbons, are much less sensitive to solvent polarity. Fluorescence lifetimes (1–10 ns) are usually much longer than the time required for solvent relaxation. For fluid solvents at room temperature, solvent relaxation occurs in 10–100 ps. For this reason, the emission spectra of fluorophores are representative of the solvent relaxed state. Fig.23 evidences why absorption spectra are less sensitive to solvent polarity than emission spectra.

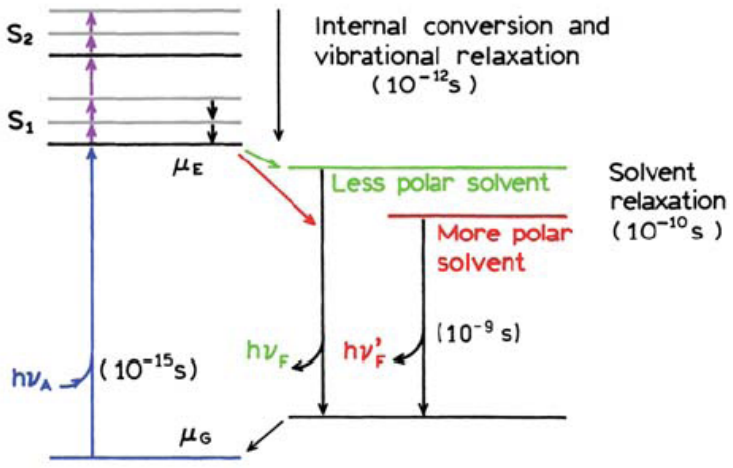

Fig. 23 Jablonski diagram for fluorescence with solvent relaxation[8]

Absorption of light occurs in about 10^{-15}s, a time too short for motion of the fluorophore or solvent. Accordingly, absorption spectra are less sensitive to solvent polarity because the molecule is exposed to the same local environment in the ground and excited states. In contrast, the emitting fluorophore is exposed to the relaxed environment, which contains solvent molecules oriented around the dipole moment of the excited state. The effect of solvent polarity may be dramatic, as depicted in fig.24.

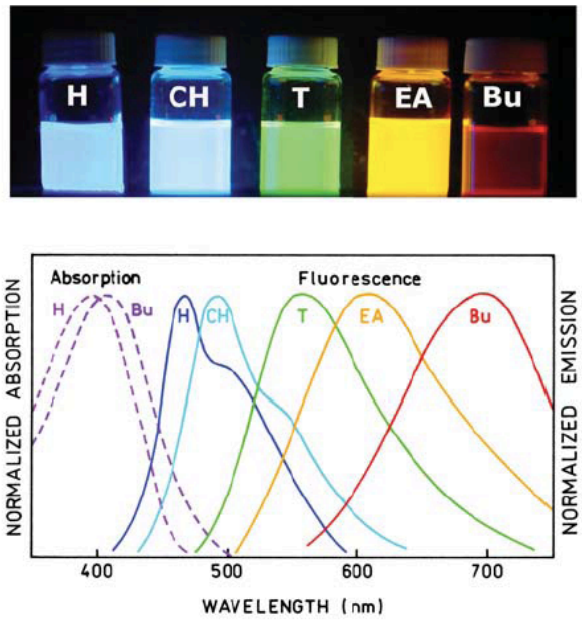

Fig. 24 Photograph and emission spectra of DNS (4-dimethylamino-4'-nitrostilbene) in solvents with increasing polarity: H, hexane; CH, cyclohexane; T, toluene; EA, ethylacetate; Bu, n-butanol[9]

Other factors include:

- Solvent viscosity
- Rate of solvent relaxation
- Probe conformational changes
- Rigidity of the local environment
- Internal change transfer
- Proton transfer and excited state reactions
- Probe-probe interactions
- Changes in radiative and non-radiative decay rate

2.1.2 Fluorescence as detection technique in life sciences: from conventional techniques towards Metal-Enhanced Fluorescence

A variety of chemical and biological analyses are based on fluorescence signals for reporting specific molecular events, detection of chemical or biological analytes/species, or for the understanding of microenvironments (viscosity, polarity and voltage measurements). The major issues to have a significant quality of such measurements are the fluorophore brightness (quantum yield) and photostability, which represents also the main limitation factors. The need

for bright and stable probes has constantly increased in life sciences and, also, the request for easy-to-use assays.

In almost all applications of fluorescence, the chromophore is excited and then emits into a homogeneous environments, and little consideration is given to the surrounding environment, neglecting the complex relations that arise in the near-field, namely, when a dipole is located less than one wavelength of light away from a substrate. The term "Metal-Enhanced Fluorescence (MEF)" was first introduced by Geddes in 2002[10], but the same effect is also known as Surface Enhanced Fluorescence (SEF), Plasmon-Enhanced fluorescence and Metal-Induced Fluorescent Enhancement (MIFE). MEF is a physical effect that occurs when fluorophores are placed in the near-field (i.e. at nanometric distances) from a metal. MEF is characterized both by an increased fluorescence intensity and a decreased fluorescence lifetime, where the decreased lifetime is associated to an increased photostability, as the fluorophore lies for a shorter time in the excited state prior to return to the ground state[11]. The use of metallic surfaces or structures supporting surface plasmons to increase both the brightness and photostability of fluorophores, has gained increasing attention in recent years, offering some opportunities to increase the potential of conventional fluorescence-based techniques. In the present work, silica-coated silver nanoparticles have been used as MEF substrate to increase the luminescent output of Rose Bengal (fig.25), a low quantum yield dye widely applied in bio-systems and medicine. Its sodium salt is commonly used in eye drops to stain damaged conjunctiva and cornea cells and thereby identify damage to the human eye.

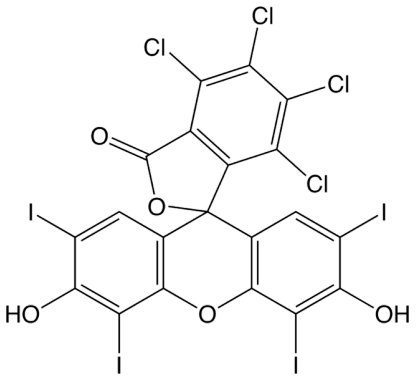

Fig. 25 Chemical structure of Rose Bengal (4,5,6,7-tetrachloro-2',4',5',7'-tetraiodofluorescein)

Although applications of MEF have been recently proposed in the literature, the main novelty of this thesis work is the application of metal@silica nanoparticles on paper, as potential tool to expand the capability of μPADs (microfluidic paper-based analytical devices). Microfluidic technology is discussed in chapter 3.

2.2 MEF – Metal Enhancement of Fluorescence

MEF investigation started in the 1960s, when Drexhage observed that a fluorescent molecule, close to a metal film, exhibited modified decay times and angular distribution of fluorescence[12-13]. Specifically, it was demonstrated that a fluorophore placed near a thick silver film resulted in the oscillations of the emissive lifetime with the distance from the metal surface. This could be explained by the back-reflected far-field radiation from the fluorophore, which depends on the distance from the metal surface. When the reflected field amplitude at the fluorophore was increased the lifetime decreased, and viceversa. When the distance was less than 20 nm, the lifetime dropped and fluorescence was quenched. This pioneering work opened up to a number of experimental studies[14-19]. The interest in MEF has intensified over the last decade, and several interpretations of the mechanisms involved have been proposed and continuously implemented, to get a clear view of such phenomenon. Nevertheless, MEF is still not fully understood yet; in particular, debate is still going on, regarding the most influential parameters on the enhancement. Several critical reviews and articles have been published, aimed at describing and explaining the mechanism of MEF[20-27]. In chapter 1, some concepts are introduced, that are now used to describe the theory MEF is based on.

2.2.1 Theory and models of MEF

2.2.1.1 Metal-fluorophore interaction

Understanding MEF means understanding the interactions between fluorophores and metals. When discussing such interactions, a preliminary clarification is required: *far-field* indicates a wave propagating in the space away from the source, while *near-field* is the field around an oscillating dipole at distances closer than the wavelength. It is assumed that the *near-field* exists for excited fluorophores, while the *far-field* is created after the molecule releases a photon and turns back to the ground state. The interaction of fluorophores with metals can be modelled as the interaction of an oscillating dipole with a conducting metal surface, and can be described using classical electrodynamics[28-29].

Consider an oscillating dipole above a metallic surface (fig.26). This dipole (μ) can be described by

$$\mu = \mu_0 \exp\left[-i\left(\omega + \Delta\omega\right)t\right]\exp\left[-bt/2\right]$$

Eq. 15

where $b=1/\tau$ is the inverse lifetime and $\Delta\omega$ is the frequency shift caused by the metal. The reflected field (by the metallic surface) is given by

$$E_R = E_0 \exp\left[-i\left(\omega + \Delta\omega\right)t\right]\exp\left[-bt/2\right]$$

Eq. 16

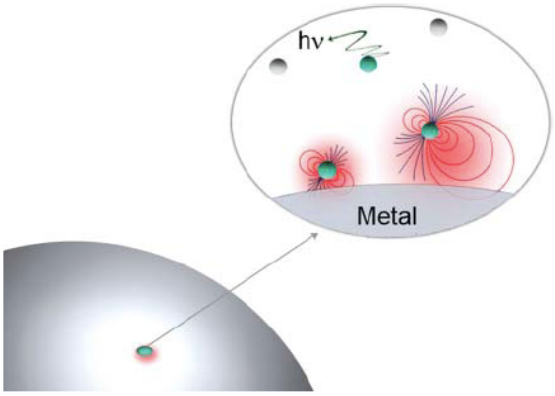

Fig. 26 Fluorophore near a metal surface[30]

The decay rate of the reflected field is the same as the decay time for the fluorophore. The frequency shift $\Delta\omega$ is small and can be neglected. Calculation of the effect of the metal on the fluorophore requires calculation only of the reflected field. The decay ratio in the absence ($b_0=1/\tau_o$) or presence ($b=1/\tau$) of metal is given by

$$\frac{b}{b_0}=\frac{\tau_0}{\tau}=1+\frac{3qn_1^2}{2\mu_0 k_1^3}\mathrm{Im}\left(E_R\right)$$

Eq. 17

where q is the quantum yield, n_1 is the refractive index of the medium surrounding the dipole, k_1 is the wavevector for a frequency ω in the same medium, and $\mathrm{Im}(E_R)$ is the reflective field at the dipole. This equation can be used to calculate the radiative decay rate for dipoles parallel (II) or perpendicular (⊥) to the metal surface.

$$\frac{b_{II}}{b_0}=1+\frac{3}{4}q\,\mathrm{Im}\int_0^\infty\left[\left(1-\mu^2\right)R^{II}+R^{\perp}\right]\exp\left[-2l_1k_1d\right]\frac{\mu}{l_1}d\mu$$

$$\frac{b_{\perp}}{b_0}=1+\frac{3}{2}q\,\mathrm{Im}\int_0^\infty R^{II}\exp\left[-2l_1k_1d\right]\frac{\mu^3}{l_1}d\mu$$

Eq. 18 Radiative decay rates for dipoles that are parallel (TOP) or perpendicular (BOTTOM) to the metallic surface

with the reflection coefficients given by

$$R^{II}=\frac{\varepsilon_1 l_2-\varepsilon_2 l_1}{\varepsilon_1 l_2+\varepsilon_2 l_1}$$

Eq. 19

$$R^{\perp}=\frac{l_1-l_2}{l_1+l_2}$$

Eq. 20

and

$$l_1=-1(1-\mu^2)^{1/2}$$

Eq. 21

$$I_2 = -i\left(\frac{\varepsilon_2}{\varepsilon_1} - \mu^2\right)^{1/2}$$

Eq. 22

For this system, in which a fluorophore is in front of the metal, the total decay rate corresponds to

$$b = b_{\perp} + 2b_{//}$$

Eq. 23 Fluorophore total decay rate in proximity of a metal

From the analysis of the previous equations, it is rather unclear which are the most influential parameters. To have more insights, it is convenient to consider the far-field approximation, where the variable μ is simply described by

$$\mu_{FF} = \frac{k_x}{k_1} = \sin\theta$$

Eq. 24 Dipole moment under *far-field* approximation

being θ the angle from the normal axis. In this case, equations 9 and 10 can be more easily understood. In the *far-field*, when sinθ < 1, the integral is real and describes energy radiating away from the interface. If sinθ > 1, the integral is imaginary and describes the decay of the evanescent field. Plasmons create an evanescent field in the medium surrounding the fluorophore (just as totally internally reflective beam creates an evanescent field in the distal medium). Another interpretation, leading to the same results, states that the integral between 0 and 1 is real and results in *far-field* radiation, while the integral from 1 to infinity is imaginary and represents non-radiative fields. When μ=1, the field created by the dipole is in resonance with surface plasmons. This explains why induced electron oscillation becomes non radiative when the fluorophore is close to the surface.

2.2.1.2. Underpinning mechanisms of MEF

Metal colloids can interact strongly with the incident light, because they have large optical cross-sections (eq. 9, in chapter 1), much larger than those of fluorophores, making metal colloids valuable probes for imaging and sensing. However, the scattered light from a metallic particle has the same wavelength of the incident light. Hence, the advantage of high optical cross sections for metallic colloids is partially reduced by the absence of a wavelength shift (Stokes shift), as it occurs with fluorescence. Wavelength shift is a property widely used for sensing, imaging and bioimaging. Using fluorophores and metal particles in proximity, allows for taking the advantages of both the large extinction coefficients and the Stokes shift. Furthermore, some peculiar effects arise. Metal-fluorophore interaction occurs via three mechanisms:

1. Energy transfer from the fluorophore to the metal, with a d^3 dependence. The proximity of a metal surface can dampen the oscillating dipole, causing quenching of the fluorescence.

This is a non-radiative effect dominating at small distances, due to the coupling between the fluorophore and the plasmon polariton at the surface of the metal. Nevertheless, an important observation is that, while there is quenching at short distances from a planar surfaces, there is, on the contrary, enhancement near metallic particles or thin metal films[31]. An interpretation might be that metallic surfaces do not necessarily quench fluorescence, except when there is some underlying absorption not due to electron motions (interband absorption). Oscillations created in the metal at short distance with the fluorophore cannot radiate because of constraints at the metal-sample interface: plasmons can be trapped because of peculiar optical properties, and decade as heat. So, plasmons will radiate whenever allowed by optical conditions. For continuous surfaces, the plasmons will radiate if there is wavevector matching at the metal-dielectric interface. In colloids, the induced plasmons will radiate if the scattering cross section of the colloid dominates on the absorption cross section[32]. Plasmons are induced in the metal as a consequence of the charge distribution induced by excited fluorophores in proximity. If the plasmon can radiate, then the fluorophore emission is observed as plasmon-coupled emission; if the plasmon cannot radiate, then the fluorophore appears to be quenched. These fundamental observations will be clarified later on, when discussing the modified Perrin-Jablonski diagram for fluorophores-metal interaction.

2. Concentration of the electromagnetic field, with the metal structure acting as an antenna concentrating the field where the fluorophore is located, thus enhancing the fluorescence.

This effect can be explained by solving the Maxwell's equations around the metallic structure. In specific frequency ranges, resonance can occur in the metallic structures themselves (visible-near IR for metal nanoparticles). These electromagnetic properties of metallic nanopaticles (Drude's model) have already been discussed in chapter 1.

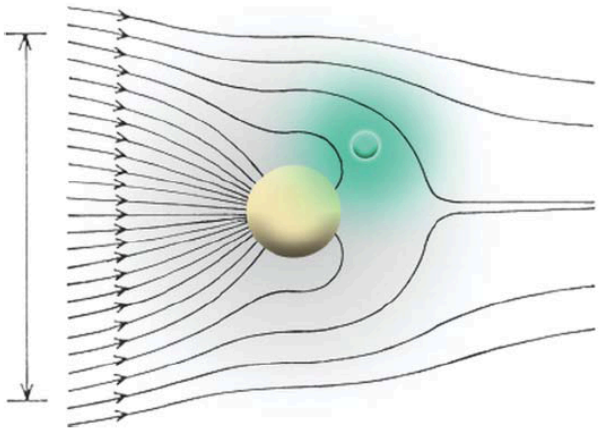

Fig. 27 Interaction of a metal colloid (yellow) with incident light; the lines show the direction of light propagation. As a result of the large extinction cross-section, the lines concentrate around the particle. A fluorophore (green) is also shown in the near field[33]

3. Modification of the radiative decay rate of the fluorophore, by modifying the photon density of states

Usually, there is no control over the radiative decay rate. Consequently this metal-mediated effect is peculiar and particularly important to achieve high fluorescent outputs. For a better explanation, it is useful to consider a modified Jablonski diagram, represented in scheme 9.

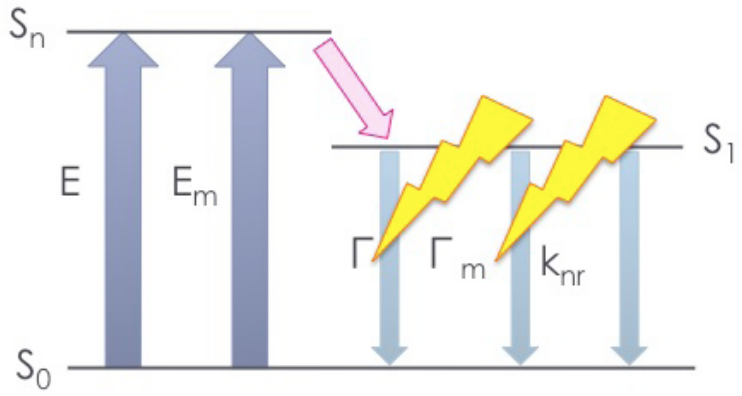

Scheme 9 Modified Jablonski diagram, representing the interaction between a fluorophore and a metal particle

In the scheme, an additional electric field, E_m is represented: this term is the field increased by the oscillation of surface plasmons in the metal, which provides additional energy to excite electrons of the ground state of the fluorophore. If more electrons are excited, then more electrons can decay radiatively, Γ_m, resulting in an enhanced fluorescent output. Accordingly, the values of the quantum yield and the excited lifetime also change (eq.25 and eq.26), in opposite direction, Φ_m increasing and τ_m decreasing.

$$Q_m = \frac{\Gamma + \Gamma_m}{\Gamma + \Gamma_m + k_{nr} + k_q}$$

Eq. 25 Modified quantum yield

$$\tau_m = \frac{1}{\Gamma + \Gamma_m + k_{nr} + k_q}$$

Eq. 26 Lifetime after coupling with plasmons of the metallic particles

2.2.1.3 Parameters affecting fluorescence enhancement

2.2.1.3.1 Effect of quenchers

When there is no metal surface in close proximity to a fluorophore, environment strongly affects its lifetime and intensity, but does not, directly, affect the decay rate Γ, and quantum yield is modified by variation of k_{nr} or k_q. Generally, polar fluorophores in polar fluids have large Stoke's shifts due to the interaction of the excited state dipole moment of the fluorophore with the surrounding polar solvent molecules. On the contrary, in presence of metal surfaces, fluorophores can undergo modification of decay rates, increased by a term Γ_m. Additionally, it is less likely that

in presence of metal particles the collisional quenching decay rate ($k_q[Q]$) undergoes modifications. The Stern-Volmer equation (eq.27) describes the fluorescence intensities in presence (I) or absence (I_0) of a quencher, being k_q the bimolecolar quenching constant and τ_0 the unquenched lifetime

$$\frac{I_0}{I} = 1 + k_q \tau_0 [Q]$$

Eq. 27 Stern-Volmer equation

This equation represents the concept that fluorophores with longer lifetimes are quenched more than those with shorter lifetimes. For a low quantum yield dye, in presence of quenchers and a metallic surface, the intensity is expected to increase closer to the surface because of an increase in the radiative rate, which competes more effective than quenching. Emission from quenched fluorophores can still be observed near metal particles.

2.2.1.3.2 Quantum yield

This observation points out another important property concerning MEF, namely the quantum yield. As a consequence of the increased radiative decay rate, quantum yield also increases. It has been observed that the largest enhancement in quantum yield is gained for the weakest fluorophores, as shown in fig.28. At sufficient high values of Γ_m/Γ, the quantum yield of the fluorophore approaches unity. Fig.28 shows the effect of an increased radiative decay on both quantum yield (Q_m) and lifetime τ_m., considering three dyes with different values of Q_0.

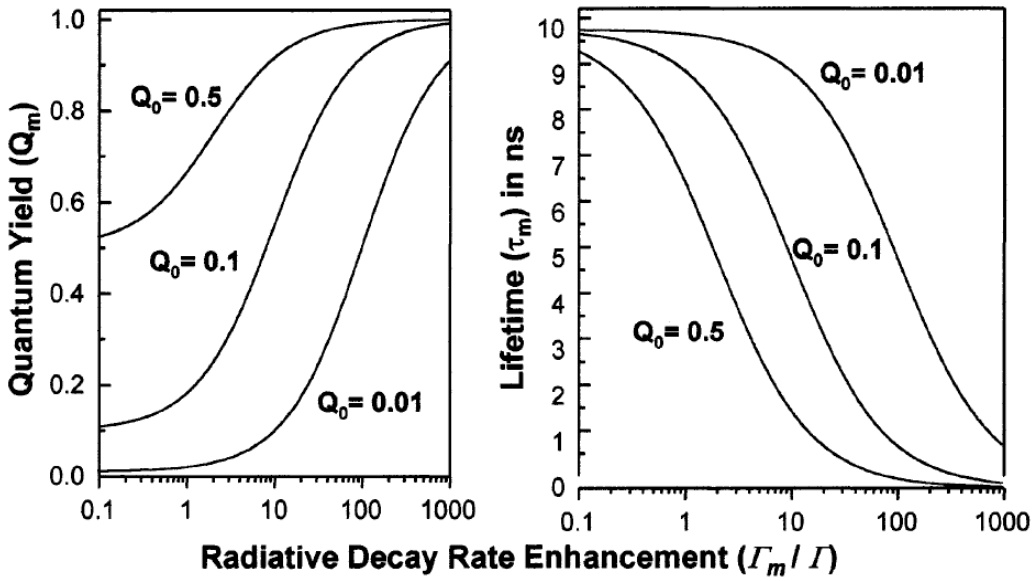

Fig. 28 a-b: Modifications of a)enhanced quantum yield (Q_m) and b)lifetime (τ_m) for three dyes with quantum yield Q_0 varying from 0,5 to 0,01. It is assumed that τ_0= 10 ns[34].

It is clear that increasing Γ_m has a weaker effect for Q_0= 0,5 and a stronger effect for Q_0=0,01 on the final value of quantum yield. This effect is quite intuitive: for a dye having low quantum yield, hence normally weakly fluorescent, the effect of MEF is to excite more electrons than usual, which would then decay radiatively, generating fluorescence. If a dye is strongly fluorescent, only

a limited portion of electrons is available for excitation via MEF, and the relative enhancing effect is reduced. The lifetime decreases rapidly in all three cases, resulting in a higher photostability. In fact, spending longer time in an excited state could lead to a lower probability that the electron decay with processes other than radiative (non fluorescent). Additionally, the fluorophore less likely undergoes saturation, emitting more photons per second than an equivalent fluorophore with a longer lifetime.

2.2.1.3.3 Volumetric effect and role of the surrounding electrical field

From these previous observations, it can be stated that MEF≈ $1/Q_0$. Despite some experimental data, shown in fig.28, Geddes and Dragan proposed that there is not direct correlation between quantum yield (Q_0) and enhancement in the *near-field*[35]. According to their publication, the two basic mechanisms of MEF (enhanced absorption and enhanced emission) cannot explain by themselves why MEF≈ $1/Q_0$. In a previous work, they suggested that *far-field* excitation intensity changes the near-field volume of enhancement[36]. It follows that *far-field* excitation irradiance needs to be considered when considering fluorophores of different quantum yield close to metals, as the natural tendency to shine more light on weakly fluorescent species accounts for the experimentally observed MEF≈ $1/Q_0$. Studying different dyes with different values of Q_0 in carefully controlled conditions, the authors showed that the enhancement can be modulated by changing the surface properties of metallic nanoparticles, which are able to alter the surface electric field distribution, as mentioned before. In their opinion, there is no *direct evidence* of such inverse proportionality, and previous observation by other researchers can be explained by changes in the *near-field* excitation volume and the need to shine more light on weakly fluorescent dyes. Considering metal nanoparticles, Geddes and Dragan showed that the magnitude of MEF enhancement correlates with the intensity of the *near-field* generated around a nanoparticle in response to incident light irradiance[37]. Both the irradiance and the MEF intensity decay exponentially with the distance of the fluorophore from the nanoparticle. The *near-field* around the nanoparticle has a specific volume, or spatial distribution of high-frequency energy, interacting with the oscillating dipole system of the chromophore. This interaction has an important role in enhancing the fluorescence of the dye. The effects of both size and density of silver nanoparticles on MEF and the intensity of the incident light were investigated by using silver nanoparticles, grew on glass slides, forming silver island films (SiFs) with deposition time, and fluorescein as dye (fig.29b).

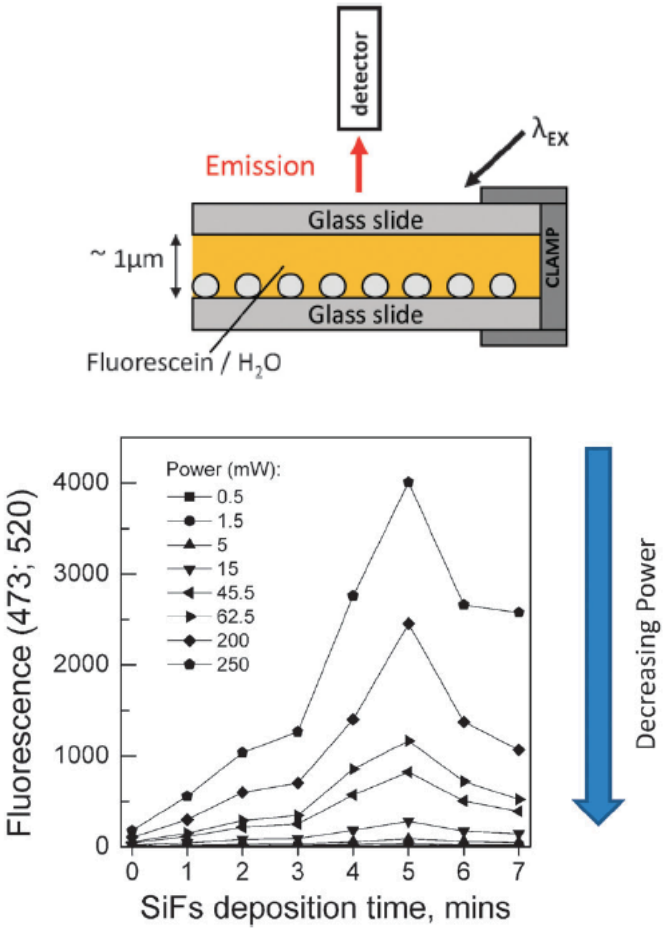

Fig. 29 a-b: a)Experimental set-up and b)fluorescence intensity of fluoresceine as a function of SiFs deposition time. λ_{exc}= 473 nm; λ_{em}= 520 nm[38]

Figure 29b shows the fluorescence intensity of fluorescein vs. deposition time of SiFs, collected with different source powers. The fluorescence intensity follows the time of deposition of SiFs, in particular:

1. Larger particle more effectively enhance fluorescence
2. When the density of SiFs is high, the mean distance between nanoparticles is short, electrical conductivity increases and there is a upper limit in MEF
3. At the point in which particles condense in a continuous film, MEF drops

The function in fig.29b has a maximum, which does not correlate with the morphology of SIFs (there is no such sharp modification in the morphology of the film, rather than a gradual change): the authors hypothesised that such maximum is caused by the specific change in power volume of the *near-field* generated around silver particles, by the *far-field* incident light. Such sudden increase may be due to plasmon resonance interparticle interaction that occurs at a certain short distance between silver islands. This also accounts for the sharp drop, when the film becomes continuous. More interesting, MEF depends on the intensity of the incident light (fig.30).

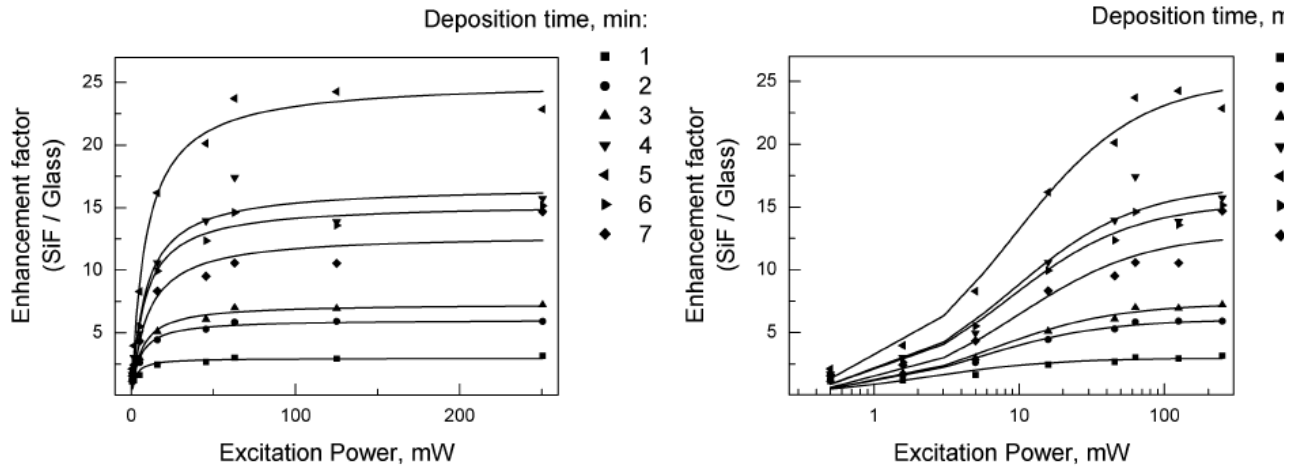

Fig. 30 a-b: a)Dependence of enhancement factor upon laser excitation power, for different deposition times. b)On the right, the same plot with a $\log_{10}$ power axis[39]

The maximum enhancement factor, ≈25, was observed with a deposition time of 5 minutes, not linearly increasing with the excitation power, until saturation. The asymptotic value is determined by deposition time (fig.30a), while the character of the relationship between enhancement and excitation power (fig.30b) depends on more complex photophysical processes. MEF interaction is the consequence of the coupling of a chromophore with the *near-field*, generated around the nanoparticle by incident light. By FDTD (finite-difference time-domain) simulations, it has been demonstrated that an increase in *far-field* intensity ($|E(\lambda_{exc})|^2$) expands the electric field around the nanoparticle (fig.31) and that the maximum intensity of the far-field linearly depends on the intensity of excitation light (fig.32):

$$\left|E(\lambda_{exc})_{\max}\right|^2 = \beta \times I_{exc}$$

Eq. 28 Maximum intensity of the electrical *far-field*

β being the slope of the function that does not depend on I_{exc}, rather on the size and density of SiFs, and the properties of the surrounding medium (as shown in fig.32).

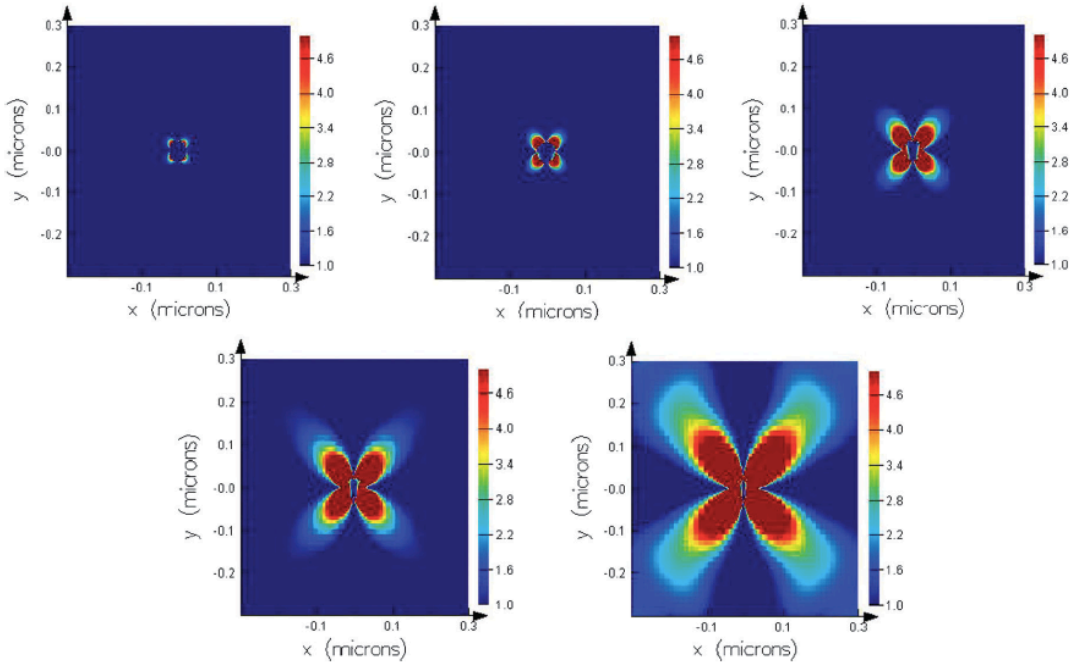

Fig. 31 Distribution of near-field intensity around a 50 nm Ag NP upon intensity of incident light that is, from left to right and from top to bottom: I_{exc}=1, 16, 36, 64, 100 a.u.[40].

Additionally, the exponential character of the electrical field intensity changes upon the distance from the NP, and it is the same for Ag and Au NPs, reflecting the general validity of such mechanism (fig.33).

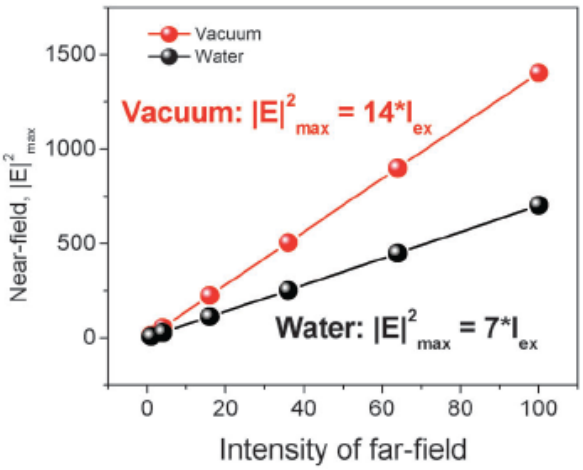

Fig. 32 Intensity of the *near-field*, linearly depending on far-field excitation intensity[41]

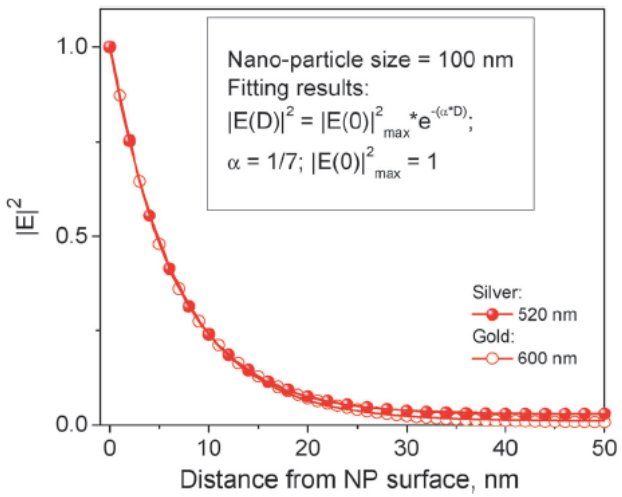

Fig. 33 Normalized intensity of the near-field as function of the distance from the nanoparticle, for different metals[42]

The electrical field decay function can be written as a function of distance (*d*) as:

$$\left|E(d)\right|^2 = \left|E_0\right|^2_{\max} \cdot e^{-7d} = 7 \times I_{exc} \cdot e^{-7d}$$

Eq. 29

The volume of the electrical field was calculated as the volume of a sphere minus the volume of the NP (with radius *r*)

$$V = \frac{4}{3}\pi\left[\left(d+r\right)^3 - r^3\right]$$

Eq. 30

being *d* the distance of the *near-field* from the nanoparticle

$$d = \frac{\ln\left[7 \times \frac{I_{exc}}{\left(\left|E\right|^2\right)}\right]}{1/7}$$

Eq. 31

Considering the interpretation given by this model, it was possible to explain the strong enhancement at about 10 nm from the particle surface. The distance dependence of MEF was studied also by Dragan and co-workers, by using fluorescent-labeled DNA scaffolds of different length, that the enhancement followed quite closely the theoretical decay of the *near-field* of the nanoparticles[43].

2.2.1.3.4 Effect of incident wavelength

Another influencing parameter is the wavelength of the excitation light beam. Zhang et al[44]. used 6-propionyl-2-dimethylaminonaphthalene (Prodan), a dye that has high sensitivity to solvent polarity, namely whose emission wavelength shifts as polarity changes (fig.34). Accordingly, MEF wavelength dependence was investigated by simply changing the solvent, using SiFs. As Prodan does not exhibit significant modifications of quantum yield or lifetime, a simple comparison of the

spectra can be performed, and. an increase of enhancing factor upon a shift in wavelength was demonstrated (fig.35). A similar study was carried out by Caires and co-workers with tryptophan, leading to analogous results[45].

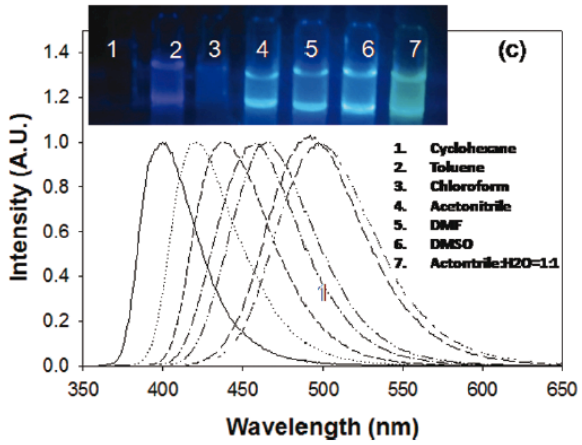

Fig. 34 Emission spectra of Prodan in different solvents: Cyclohexane (1); Toluene (2); Chloroform (3); Acetonitrile (4); DMF (5); DMSO (6) and Acetonitrile:H_2O=1:1 (7)[46]

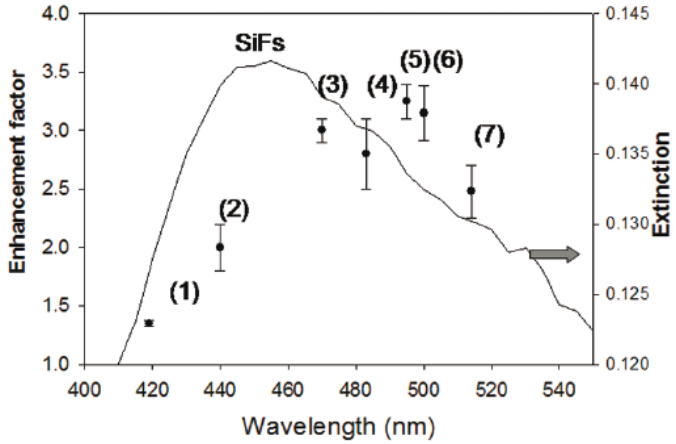

Fig. 35 Enhancement factor of Prodan near SiFs for different excitation wavelengths, number refers to the solvents in fig. 15[47]

2.2.1.3.5 Metal-fluorophore spectral overlap

Finally, the spectral overlap between the dye and LSPR (localized surface plasmon resonance) modes of nanoparticles has to be taken into account. A difficulty in rationalising this effect is due to the broadening of spectra in case of not homogeneously size-distributed colloidal systems. Ginger et al.[48] studied such effect, using fluorophores placed at a fixed distance from silver nanoprisms thanks to using DNA biological linkers.

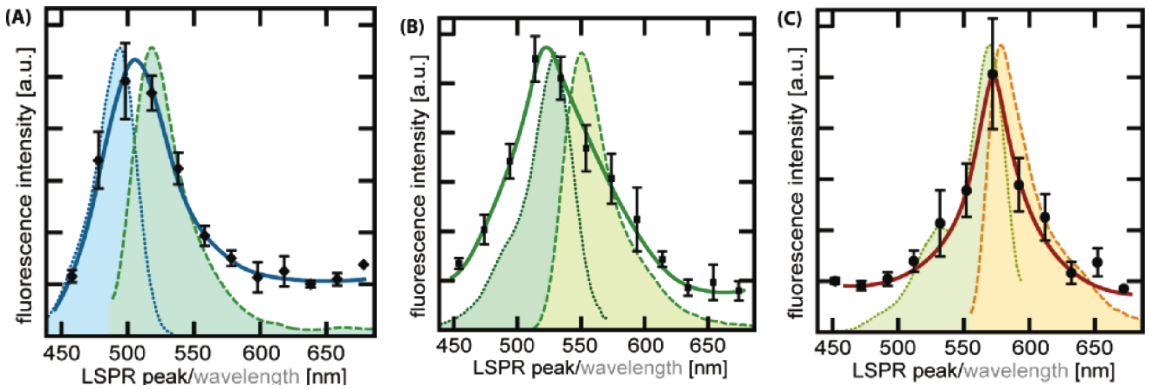

Fig. 36 a-c: Fluorescence intensity from: A) Alexa Fluor 488; B) Alexa Fluor 532; C) Rhodamine Red. For each dye, the excitation spectra (dotted line) and emission spectra (dashed line) are given; the solid line is a guide for easier detection of the fluorescence intensity, as a function of the LSPR peak[49]

Analysing fig.36, the maximum fluorescence intensity is obtained at a value of wavelength close to the maxima in absorbance and emission of the dye (this is understood comparing the wavelenght of both dashed and dotted peak). This means that there is a good spectral overlap between dye and LSPR of nanoparticles. This strong spectral correlation is explained, as follows.. The apparent brightness of a fluorophore-functionalized metal nanoparticle is

$$Y_{APP} = \gamma_{exc}(\omega_{exc})Q_{em}(\omega_{em})\eta_{coll}(\omega_{em})\sigma$$

Eq. 32

Where $\gamma_{exc}(\omega_{exc})$ is the *near-field* excitation rate of the fluorophores at the excitation frequency ω_{exc}, $Q_{em}(\omega_{em})$ is the quantum yield for a *far-field* emission at the same frequency, $\eta_{coll}(\omega_{em})$ is the collection efficiency of the *far-field* light in the experimental geometry, accounting for any modification of the free-space spatial emission profile and the fixed angular acceptance of the detector. Finally, σ is a normalization factor, accounting for attachment density and the total area excited. σ and η_{coll} are usually neglected, as they are often of secondary importance. The *near-field* excitation rate, as already pointed out, will depend on the absorption coefficient of the dye and the local (enhanced) field intensity. The enhancement is frequency (or wavelength) dependent, so that the highest excitation rate should occur for dyes adsorbed on nanoparticles with a LSPR peak that directly overlaps the maximum in the absorption spectra of the dye.

2.2.2 MEF from silver particles and core@shell particles

Gold is widely applied as a fluorescent quencher, but it is an attractive MEF substrate due to its chemical stability and well-developed and facile surface chemistry; there are several works that make use of gold with different morphologies for fluorescence enhancement[50-53] and MEF from gold particles has been observed for long wavelength fluorophores[54]. Aluminum is also thought to be a quencher, but there are few reports on this effect[55]; Ray and co-workers demonstrated the possibility to use aluminum also as enhancer[56]. Despite few articles, the metal that exhibits the biggest potential as enhancer is silver. The imaginary component of the dielectric function of silver determines its big absorption cross section, thus making silver a favourable material. Gaponenko and co-workers were able to develop a mathematical model that describes plasmonic

enhancement near silver nanoparticles of different sizes[57], showing how the enhancement depends on size itself. Results are given in fig. 37-38 and prove that the ideal size of silver nanoparticles to have the strongest enhancement is 50 nm. Indeed, although fig. 38a seems to indicate that the highest value of enhancement occurs with bigger particles, this is true only for the long-wave portion of excitation wavelength with respect to the intrinsic plasmon resonance (350 nm). An increase in size, as shown in fig.38b, not only simply rises *F*, but also shifts the whole spectrum to red. This because the scattering component of the extinction spectrum becomes dominant, when particle size is not negligible with respect to the excitation wavelength.

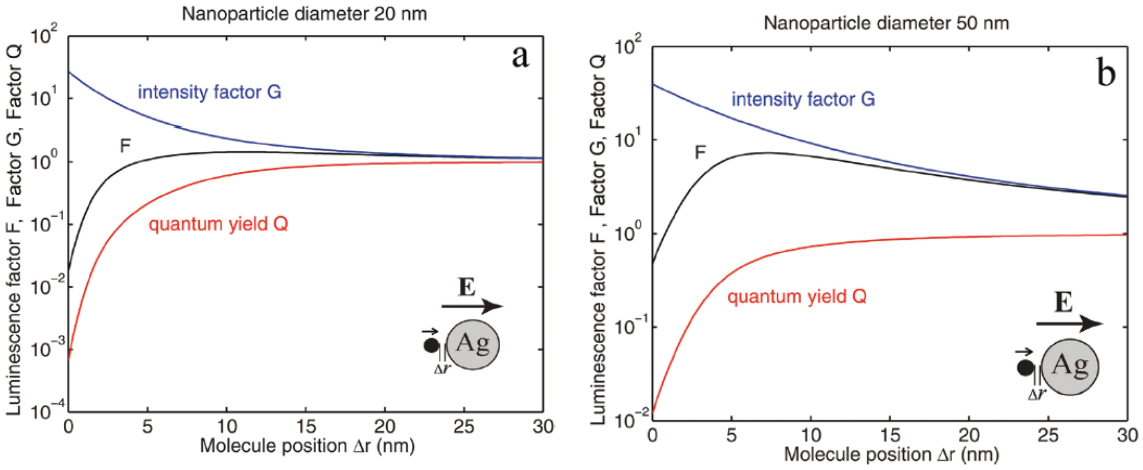

Fig. 37 a-b: Dependence of total luminescence intensity factor (F), quantum yield (Q) and incident intensity modification factor (G) on the fluorophore-metal distance, for two silver nanoparticles of different dimension[58]. For bigger nanoparticles, the factor F is higher and peak occurs at longer distance

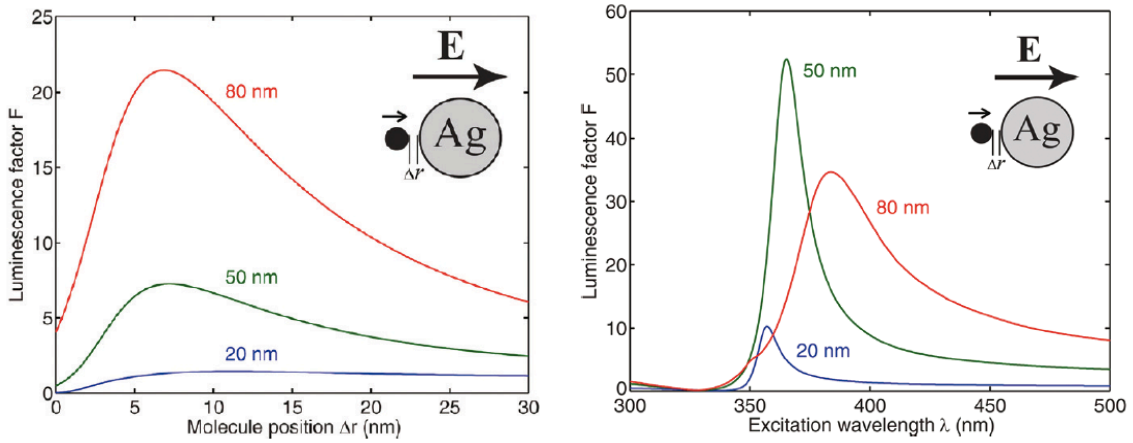

Fig. 38 a-b: a)Dependency of factor F on fluorophore-metal distance; b)dependency of the same factor on excitation wavelength, for different nanoparticle size[59]

MEF has various potential applications[60-61]. One of the most important is in protein imaging, for example, by using immunoassays[62]. Immunoassay is based on highly specific antibody-antigen recognition. The antibody is usually immobilized on a substrate, for example a glass slide or, in most novel assays, on paper; subsequently, the fluorescent labeled antigen and labeled proteins are added and left for incubation. The fluorophore lights up as a consequence of the specific antigen-antibody binding interaction, *via* resonance energy transfer. Metal nanoparticle

functionalized substrates provide an easy tool for fluorescent enhancement, by exploiting MEF. Since MEF provides the opportunity to enhance the intensity upon a binding interaction ideally for almost any fluorophore, a strategy could be to couple such binding reaction close to a metal particle. Ultra-bright probes could be obtained by means of metal-fluorophores complexes in which the metal particle increases the brightness of the bound fluorophore. In principle, this can be achieved by trapping the fluorophores in metal shells or by coating metal particles with fluorophores. Core-shell structures, presented in chapter 1, fulfil all these requirements, combining different functionalities in a single hybrid nanostructure. The applicability of core@shell particles for MEF has been investigated only in recent times, but enhancement from silver particles in which the fluorophore was bound by a surface coating of silica has been already reported[63-67]. Biological applications, for example, would profit from this approach since particle-based biosensing and bioimaging require that metal nanostructures are monodisperse, bright, photostable and easily functionalizable to couple with biomolecules.

So far, there is only one publication reporting MEF with silver colloid (though not silica coated) from paper substrate[68]; MEF from plastic substrate with a similar assay has been also demonstrated[69-70].

2.3 MEF from paper substrates: my work

2.3.1 Overview on experimental procedures

The procedure for the investigation of MEF from paper substrate (see Scheme 10) was derived from the only article published about[71]. Actually, the experimental procedure was only therein roughly described, and no data, except the concentration of the fluorescent dye used, was provided. Hence, several different experimental conditions have been tested, in order to assess the best conditions to achieve the enhancement phenomena.

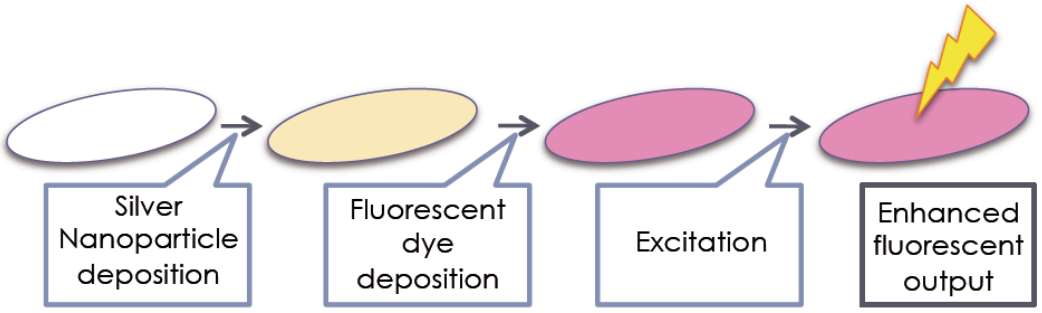

Scheme 10 Four sequential steps for paper functionalization and fluorescence detection

Circles of approximately 2,5 cm of diameter were cut out from filter paper disks #5C by Advantec ("Quantitative" Advantec filter paper), used as received. To avoid contamination of the filter paper, new gloves have been used anytime a new filter paper disk was handled, and scissors and tweezers were disinfected with ethanol. All circles have homogenous dimensions. The circles were then deposited in disposable Petri dish for the functionalization step.

The functionalization of the filter paper disk was performed by two different methods:

1. pipetting Ag or Ag@SiO_2 colloidal dispersions
2. dipping the paper disk into the solution

Concentration of the silver nanoparticle solutions has been varied to determine its influence on the fluorescent output.

CONCENTRATION OF PARTICLE SOLUTION
10x diluited
5x diluited
As prepared
5x concentrated
10x concentrated

Table 6 Summary of different concentrations of AgNP solution used

Once the paper was dried the fluorescent dye has been deposited. Also in this case, different quantities of dye have been tested, as well as several common dyes.

- Rose Bengal (Wako Chemicals, Japan)
- Rhodamine B (Kanto Chemicals, Japan)
- Fluorescein (Wako Chemicals, Japan)
- Coumarin 343 (Sigma-Aldrich®)
- Calcein (Dojindo)
- Acridine Orange (Sigma-Aldrich®)

Such dyes have been chosen considering the following criteria:

- ✓ Spectral overlap between emission of dye and absorption of particles
- ✓ Relatively low quantum yield
- ✓ Availability and low cost

Rose Bengal was tested only with the concentration value given in the reference paper[72], while for the others dyes variation of concentration has been considered in order to make the enhancement more significant. In paragraph 2.3.2.2.4, results for the already optimized conditions are provided. However, the majority of the experiments in this thesis work has been performed with Rose Bengal, which has turned out to be the only system clearly providing enhancement.

After drying, the paper samples were placed in HORIBA FluoroLog® spectrofluorimeter and the emission spectra were recorded. Excitation wavelength was chosen according to the absorption spectrum of each dye. Each sample,was tested four times in four different spots for a statistical analysis: the final emission data resulted the average of the collected spectra. As long as it was possible, samples were prepared in the afternoon, left drying overnight (in case of naturally dried samples) and measured on the day after. The Petri dishes used to contain the samples were always kept wrapped in an aluminium foil to prevent light exposure, since silver nanoparticles are light sensitive and prolonged exposure could also leads to photobleaching of the dye.

Furthermore, different substrates have been considered. According to the indications given by the manufacturer, filter paper types differ in surface roughness, porosity and particle retaining ability.

- Filter paper #1
- Filter paper #3
- Filter paper #4
- Filter paper #5

From Whatman

- Filter paper #4A
- Filter paper #5B
- Filter paper #5C
- Filter paper #6

From Advantec

- Copy paper
- OHP sheets
- PVDF

2.3.2 MEF investigation from paper substrates

2.3.2.1 Experimental observation of MEF

The first experiment was performed following the prescription of a previous report[73], even though the only indication concerned the concentration of the Rose Bengal. Circles were cut from Advantec filter paper #5C, using the bottom of a screw vial as a model (diameter ≈2,5 cm, fig. 39).

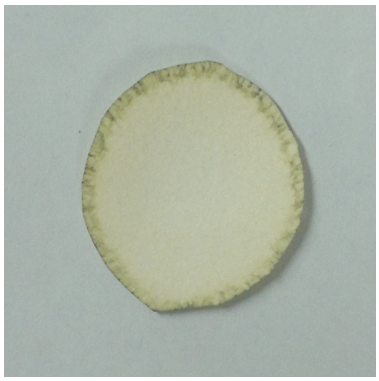

Fig. 39 Photograph of a paper sample functionalized with silver nanoparticles and naturally dried

Onto each sample, 0,5 mL of the Ag nanoparticles aqueous solution (1%wt) have been pipetted. Three different drying methods were adopted:

1. Drying in a vacuum pump (≈10min)
2. Drying in stove at 37°C
3. Naturally drying in environmental conditions, but protecting the containers from light by means of aluminum foils (overnight)

Once the paper was dry, 100 µL of a 10^{-4} M solution of Rose Bengal in ethanol was also pipetted onto the paper samples, and again drying was performed with the three different methods. Control samples have been prepared by pipetting only 100 µL of Rose Bengal on filter paper. The pictures (fig. 40-42) show the result of the fluorescent emission measurement (λ_{exc}= 532nm).

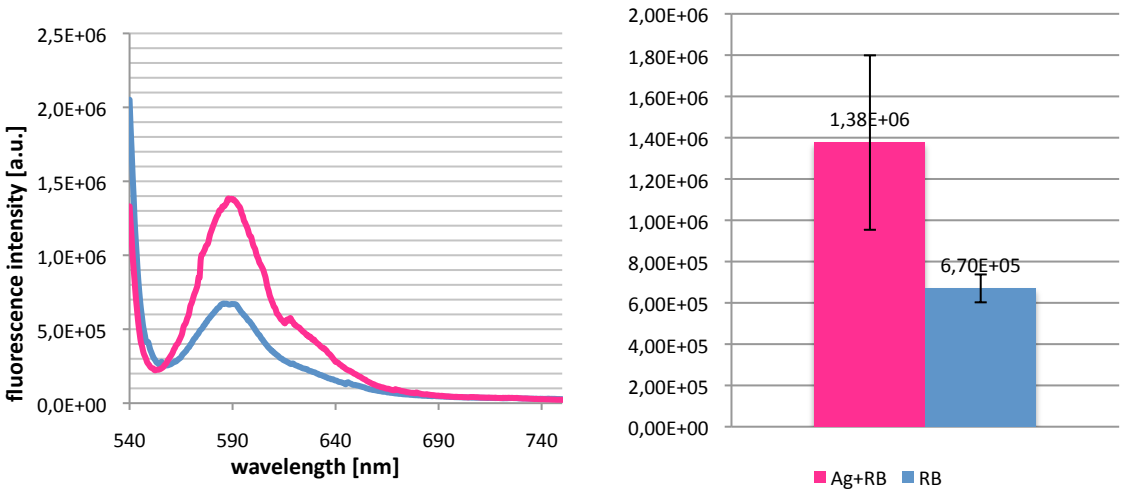

Fig. 40 Fluorescence intensity of vacuum dried paper samples and detail of the peak values and error bars

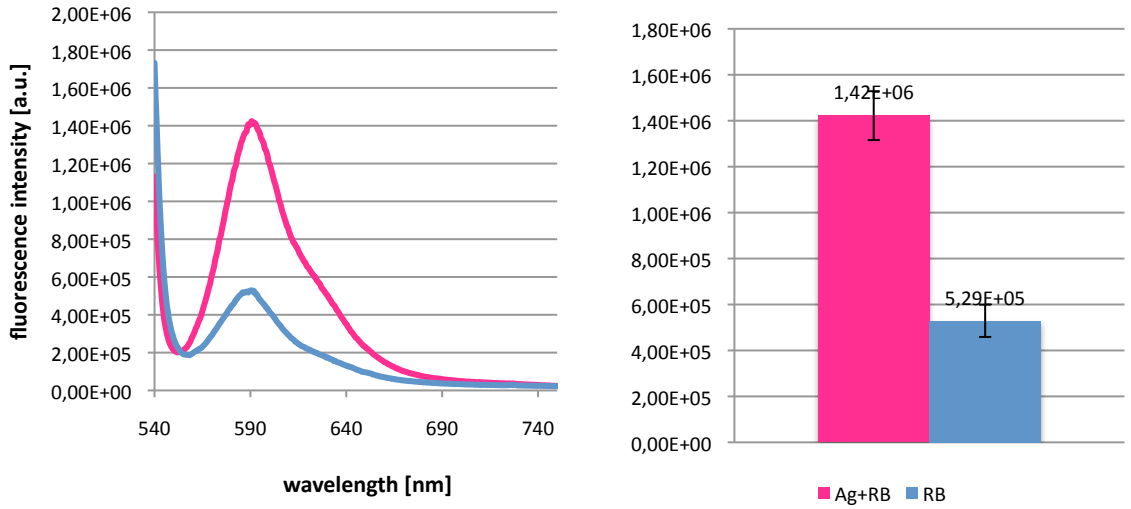

Fig. 41 Fluorescence intensity of oven dried paper samples and detail of the peak values and error bars

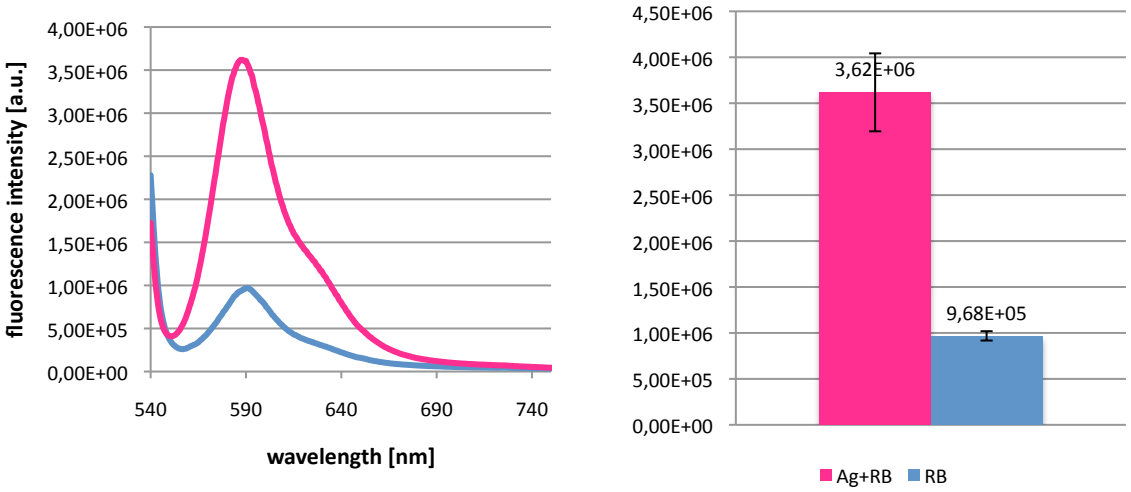

Fig. 42 Fluorescence intensity of naturally dried paper samples and detail of the peak values and error bars

According to the three plots, drying in vacuum exhibits the worst results, both in terms of enhancement (2,1-fold, compared to Rose Bengal only) and of reliability of the data, being the error bar quite large. Drying in oven provides a reliable result, with a better enhancement (2,7-fold), but the best results can be achieved by naturally drying the sample: in this last condition, the enhancement with bare silver nanoparticles is 3,7-fold. It can be hence stated that naturally drying the samples is the most effective drying strategy, which is also particularly easy to perform and inexpensive. On the other hand, it requires longer time, and it may suffer from environmental conditions (as an increase in humidity which is a typical situation occurring in the summer in Japan).

As a following step, some experimental conditions were changed in order to establish which other parameters are most relevant to achieve a bigger enhancement. In particular, the concentration of particles, the volume of particles solution deposited, the concentration of the Rose Bengal, the deposition method, as well as different types of filter paper have been considered.

2.3.2.2 MEF conditions optimization

2.3.2.2.1 Particle concentration

With respect to the original silver particle concentration (1%wt), fluorescence enhancement tests have been performed with solutions that were 10 times or 5 times more concentrated, and 10 times or 5 times more diluted.

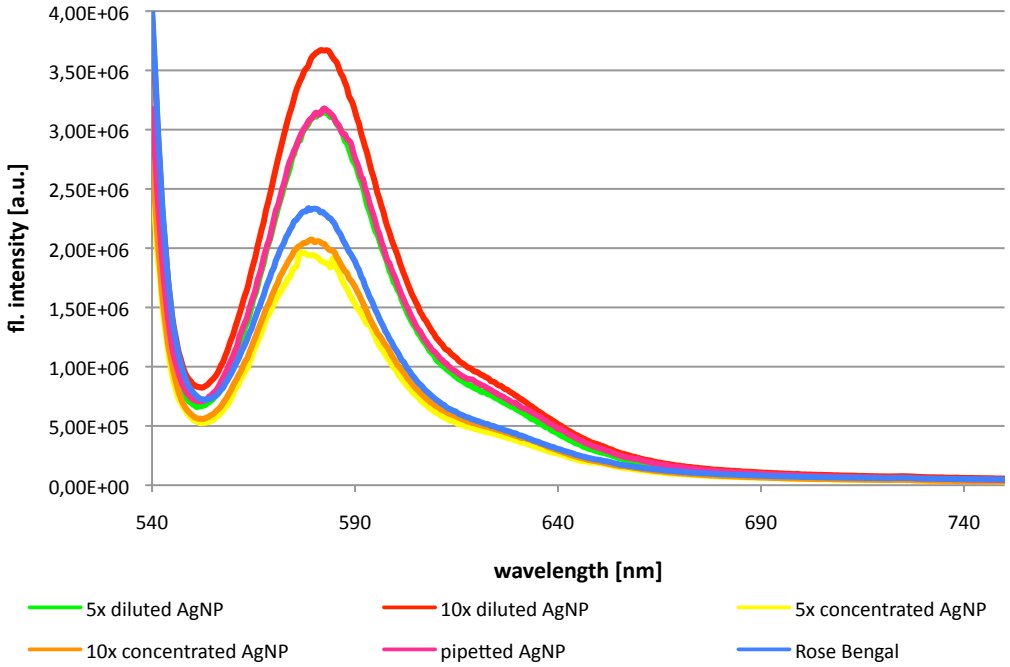

Fig. 43 Fluorescence spectra from Ag NP solutions having different Ag NP concentration, compared to Rose Bengal

Concentrating the particles is not an effective strategy, and both samples are even slightly less fluorescent than Rose Bengal only. This can be ascribed to a quenching effect due to the close space between the particles. On the contrary, dilution is favourable: diluting the particles 5 times leads to the same result as non-diluted particles (1.35-fold enhancement, with respect to the fluorescence value of Rose Bengal only), while 10 times diluted particles leads to a higher enhancement (1.6-fold). In figure 44 the data of fluorescence enhancement are summarized.

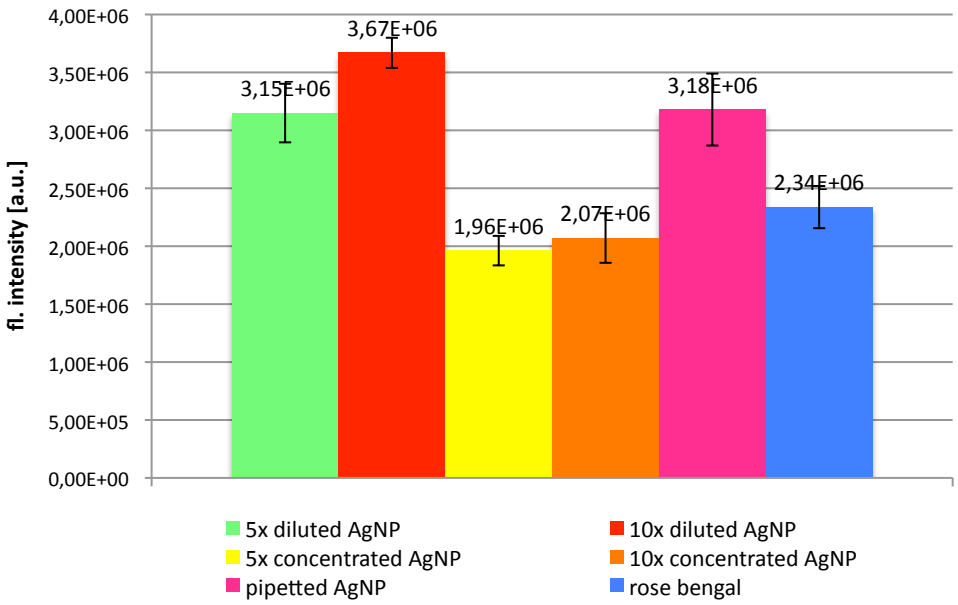

Fig. 44 Comparison of fluorescence intensities at maximum value from Ag NP solutions having different Ag NP concentration. Error bar is also reported

2.3.2.2.2 Deposition method

Despite pipetting is the method that resembles most the ink-jet printing, a comparison between functionalization via pipetting and dipping has also been performed. Paper samples have been dipped in the AgNP solution, having 1%wt AgNP concentration, for 60 s.

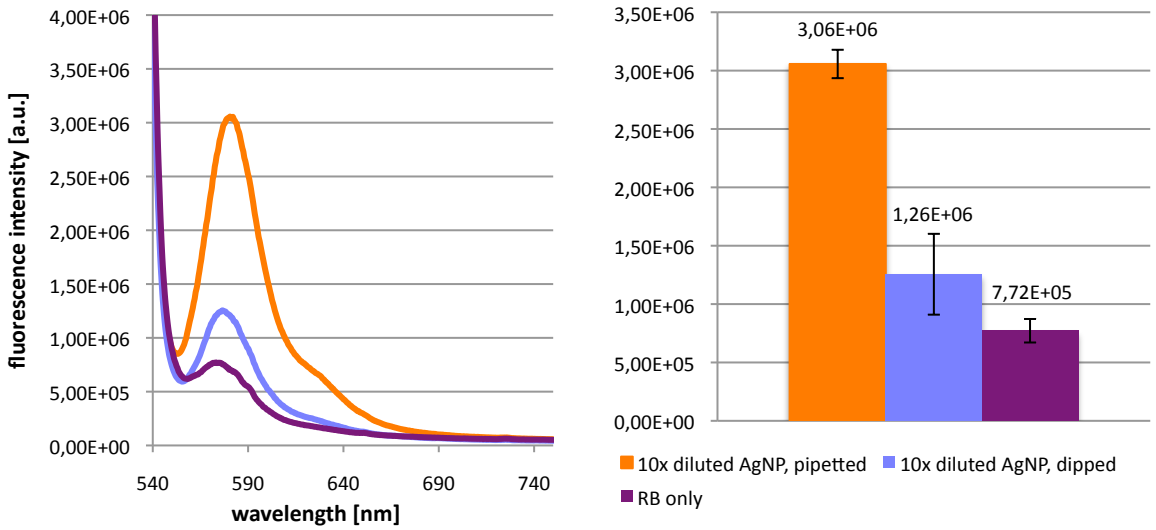

Fig. 45 Fluorescence intensities from samples onto which Ag NP were pipetted, or dipped into Ag NP solution. Detail of fluorescence intensity at the peak and error bars are provided

The enhancement factor for the pipetted sample is 4-fold with respect to dye only, while in the case of the dipped sample it is 1,6-fold. In addition, as can be seen from the larger error bar associated with the dipped sample, this method gives less reliable results.

SEM (Scanning electron microscope) images of paper samples functionalized by pipetting 0,5 mL of a core@shell aqueous solution has been taken to prove the effective deposition and retaining of such structures in the cellulose fibers. A solution of core@shell with average diameter of 189 nm was chosen, as large nanoparticles give the investigation easier. Figure 46 show the effective retaining of the particles in the paper fibers.

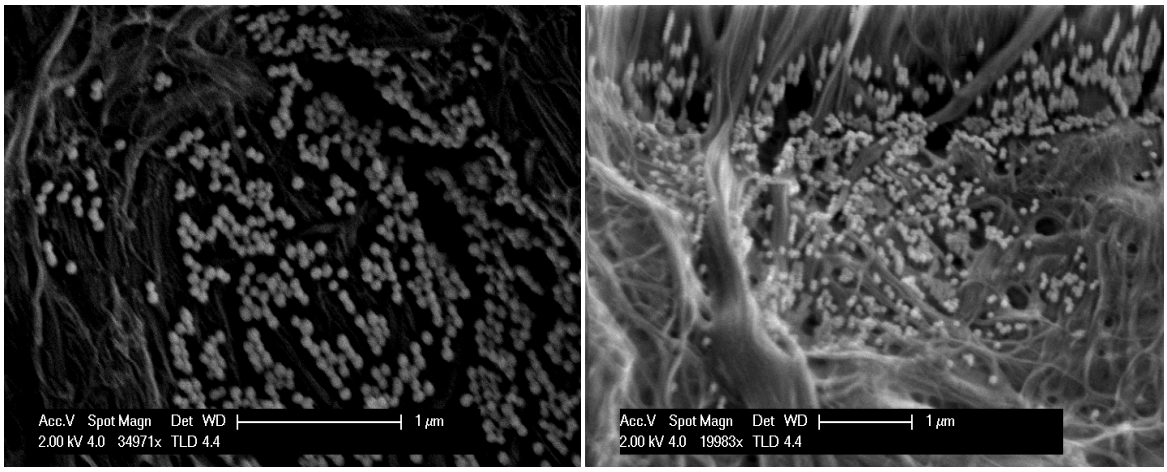

Fig. 46 a-b: SEM pictures at a)≈35000x and b)≈20000x of core@shell particles on filter paper

2.3.2.2.3 Filter paper type and other substrates

Advantec "quantitative" filter paper #5C was chosen at first as a substrate due to its fine structure, able to retain precipitates smaller than 5 µm in diameter, without being too expensive. In order to determine if the type of substrate affects the overall behaviour, several other types of filter paper have been tested, together with substrates other than paper. Filter papers differ for a series of parameters (particle retention, weight, thickness, ash percentage and residuals quantity, flow time, wet strength), and, also, some may be treated chemically (like Advantec #4A, that is washed in nitric acid), influencing their fields of application, as well as cost. Regarding Whatman filter paper types, type #1 is the lightest (88 g/m^2) and thinnests (180 µm), while type #3 is the heaviest (187 g/m^2) and thickest (390 µm). The main difference is in particle retention ability, that is 11 µm for #1, 6 µm for #3, 20-25µm for #4 and 2.5µm for #5. Also adavntec filter paper types differ for thickness, being type #5C the thickest and heaviest(220 µm, 118 g/m^2) and #4A the lightest and thinnest (120 µm, 96 g/m^2). Filter paper types are, obvioulsy, all hydrophillic, in contrast to copy paper which is strongly hydrophobic. Copy paper weighted 80 g/m^2. Transparent, hydrophobic OHP (Overhead Projector) sheets made of polypropylene, having a thickness of 0,1 mm were also used. Finally, the last type of substrate was PVDF (Polyvinyledene Fluoride) membrane purchased by Millipore, having a pore size of 0.22 µm. This last material is hydrophobic.

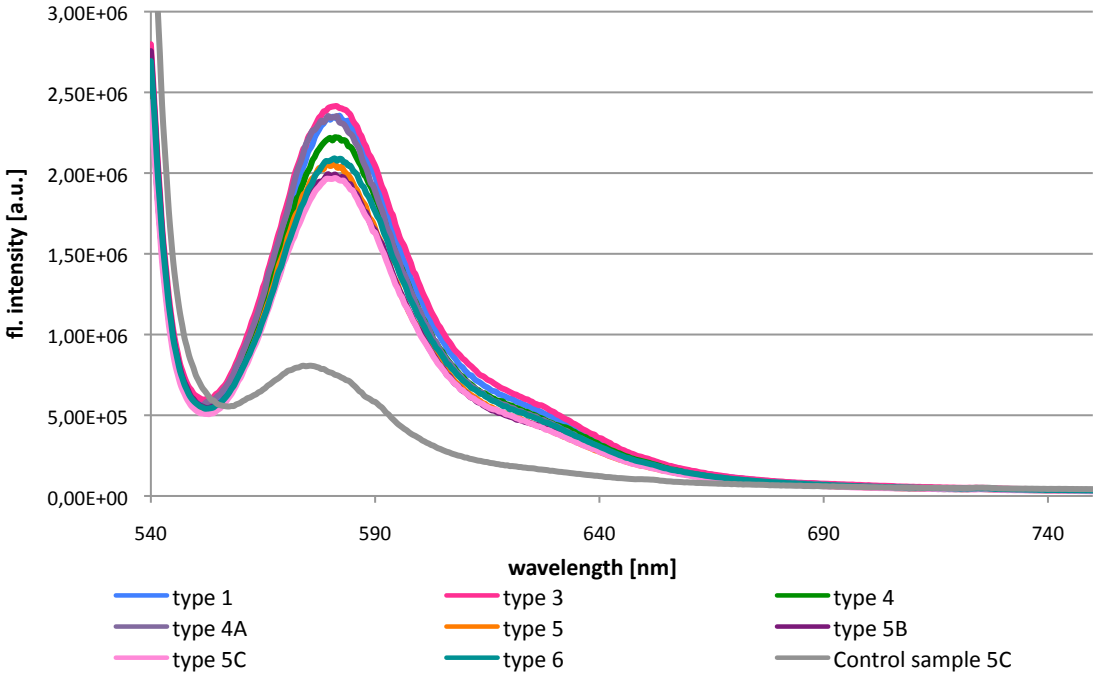

Fig. 47 Fluorescence intensities from AgNP deposited onto different types of filter paper samples

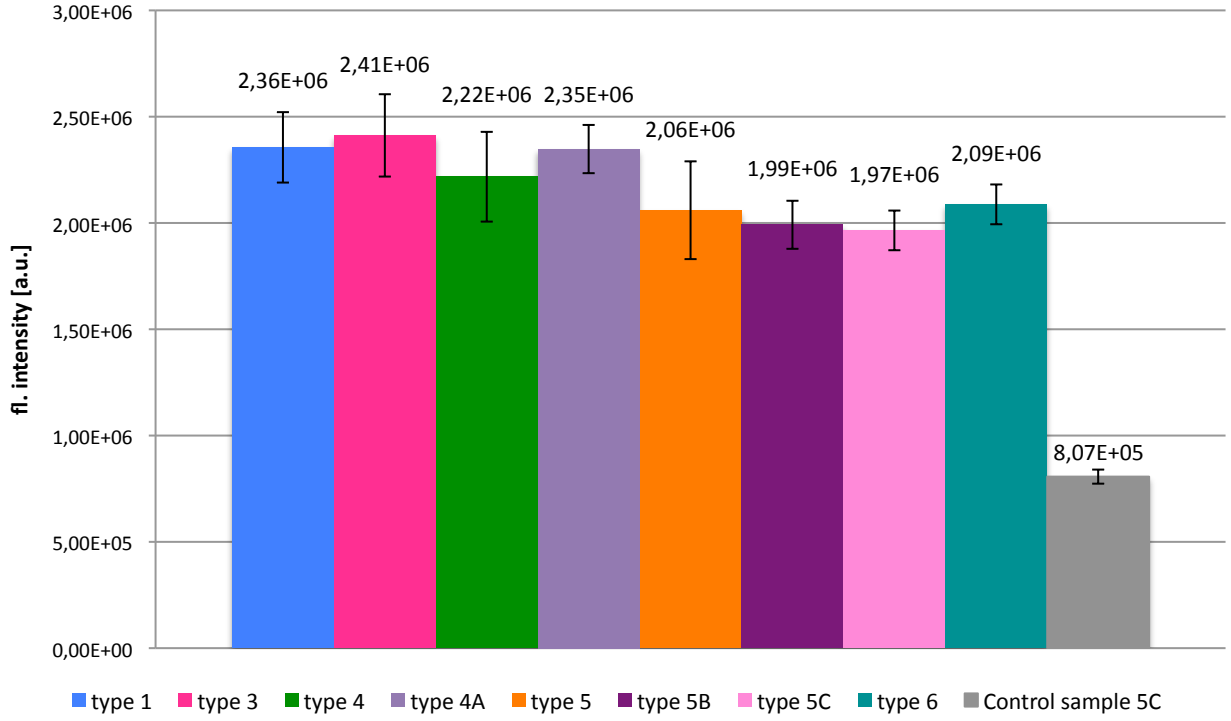

Fig. 48 Fluorescence intensity at the peak from AgNP onto different filter paper types samples

Comparing the results, it is possible to see small differences in enhancement values, from 3-fold of Whatman filter paper #3 to 2.5-fold of Advantec filter paper #5C. Moreover, the shape of the spectra is the same for all types, and the peak value is centred at the same wavelength (581 nm),

showing no substantial effect of the filter paper type on the NP plasmon. Since the filter paper type does not significantly affect the degree of enhancement, Advantec #5C filter paper has been kept for all the other experiments which have been carried out later on, since its low cost is particularly desirable for the fabrication of µPADs..

Filter paper is a porous and hydrophillic substrate. To investigate the role of these characteristic on fluorescence enhancement and, also, to consider the feasibility of µPADs on different substrates, experiments on copy paper, OHP (Overhead Projector) sheets and PVDF (Polyvinylidene Fluoride) have been performed. PVDF samples, provided by Millipore, are circles of 5 mm diamter: the quantities of silver nanoparticles solution and Rose Bengal have been adjusted to 50 µL and 5 µL, respectively, in order to retain the 10:1 ratio.

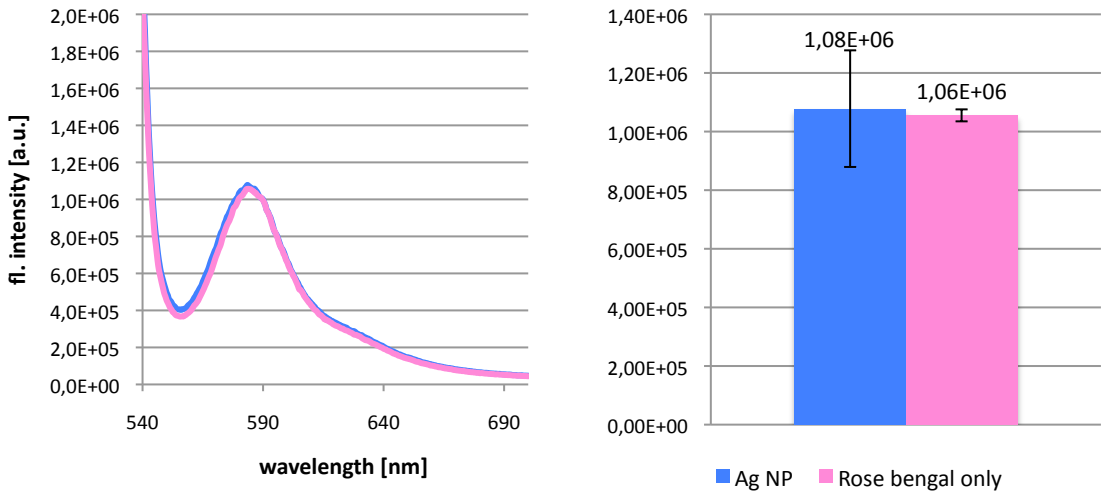

Fig. 49 Fluorescence intensity from AgNP deposited onto common copy paper and detail of peak value and error bar

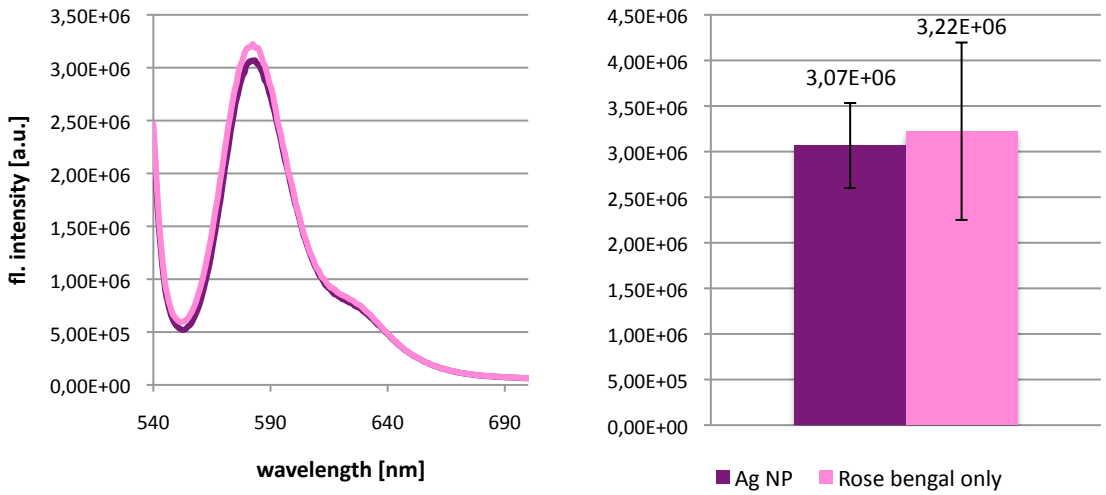

Fig. 50 Fluorescence intensity from AgNP deposited onto OHP sheet and detail of peak value and error bar

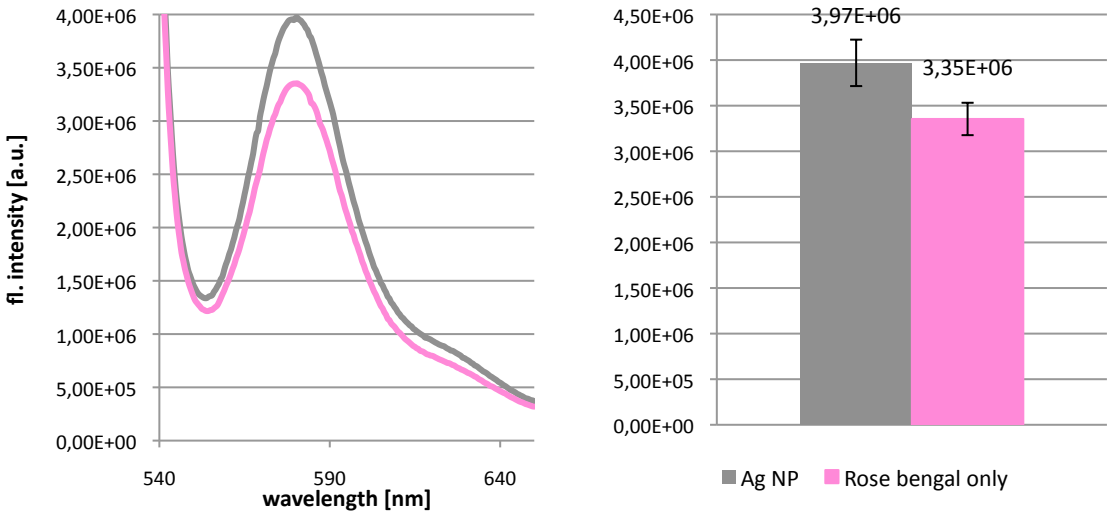

Fig. 51 Fluorescence intensity from AgNP deposited onto PVDF samples and detail of peak value and error bar

Analyzing the fluorescence spectra, OHP sheets lead to a reduction in the fluorescence with respect to Rose Bengal only, while both copy paper and PVDF samples give negligible enhancement. It follows that filter paper (or,likely an analogous hydrophilic substrate) is the only one suitable for the feasibility of ink-jet printing. To use hydrophobic substrates modification of the substrate and/or a different patterning technique are suggested.

2.3.2.2.4 Other dyes

Rose Bengal has been chosen as ideal dye to detect MEF, because of its very low quantum yield (11%),. Calcein (0,0006 g/10 mL milliQ), Fluorescein (0,003 g/10 mL EtOH) and Acridine orange (0,0003 g/10 mL EtOH) have been used at the same concentration of Rose Bengal (10^{-4} M). Coumarin 343 and Rhodamine B solutions in EtOH have been prepared in the same 10^{-4} M concentration (respectively, 0,0003 g and 0,00048 g) and then diluted 10 times. The following table provides the values of quantum yield for these dyes, as can be found in literature.

Dye	*Quantum yield [%]*
Calcein	38%
Fluorescein	79%
Coumarin 343	63%
Acridine Orange	20%
Rhodamine B	49%

Table 7 Summary of utilized dyes and their quantum yield [%]

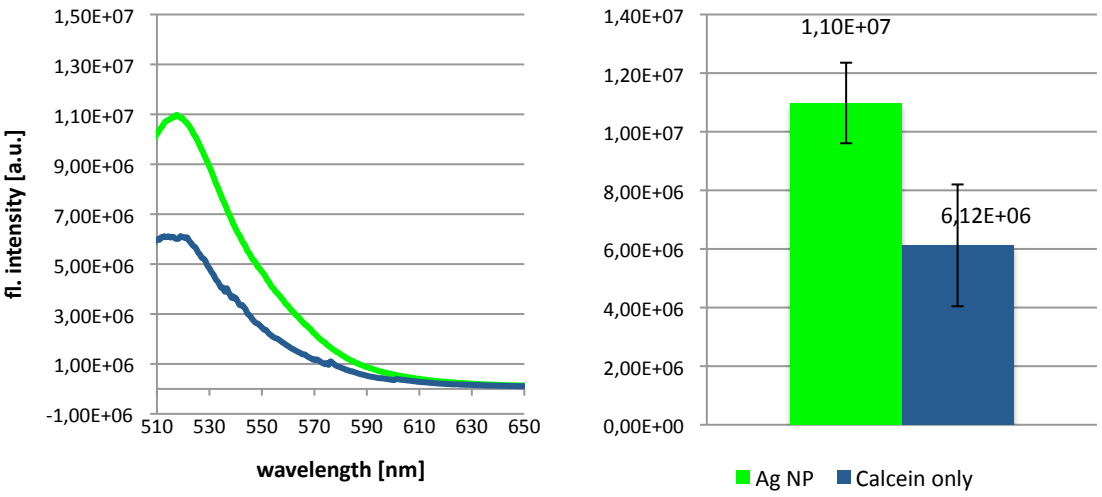

Fig. 52 Fluorescence intensity from AgNP and Calcein and detail of peak value and error bar

With calcein, a 1.8-fold enhancement has been measured, whereas fluorescein exhibited peculiar results. Indeed, fluorescence measurement in solution exhibited a 1.7-fold enhancement, when using Ag NP, and a 2.8-fold enhancement when using core@shell particles. Despite these good results, enhancement was not detected from paper measurements.

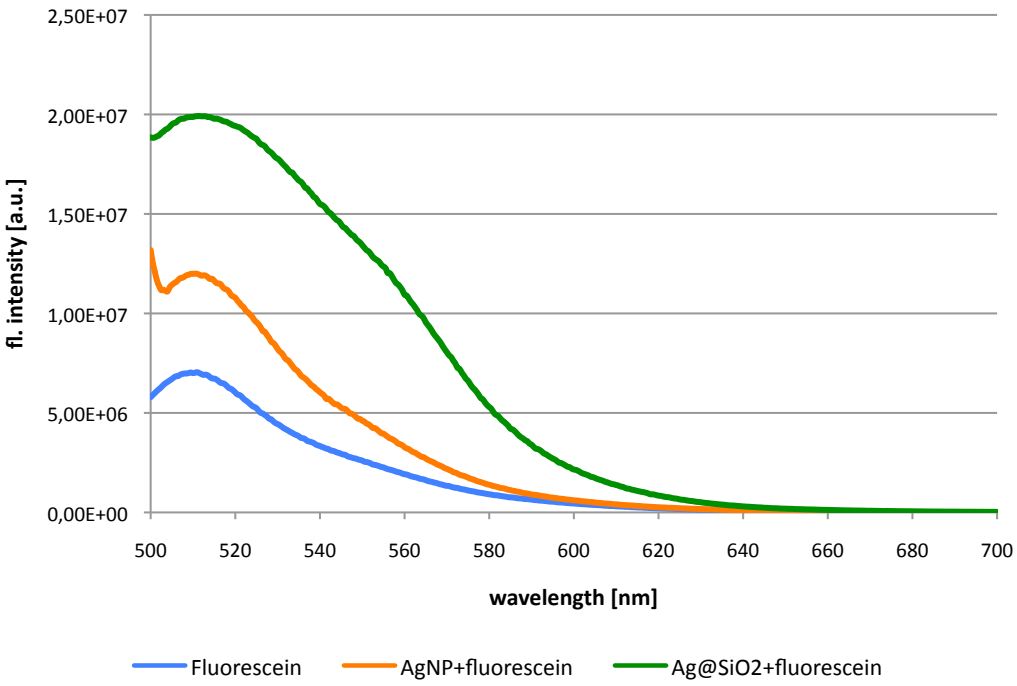

Fig. 53 Fluorescence intensity from Fluorescein in solution, from AgNP and core@shells

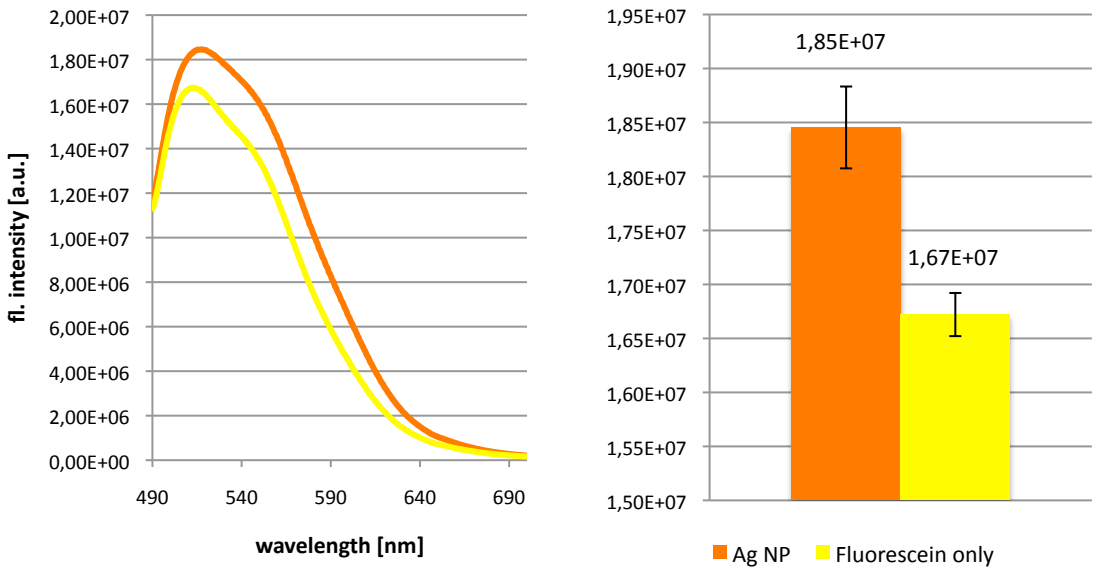

Fig. 54 Fluorescence intensity from AgNP and Fluorescein and detail of peak value and error bar

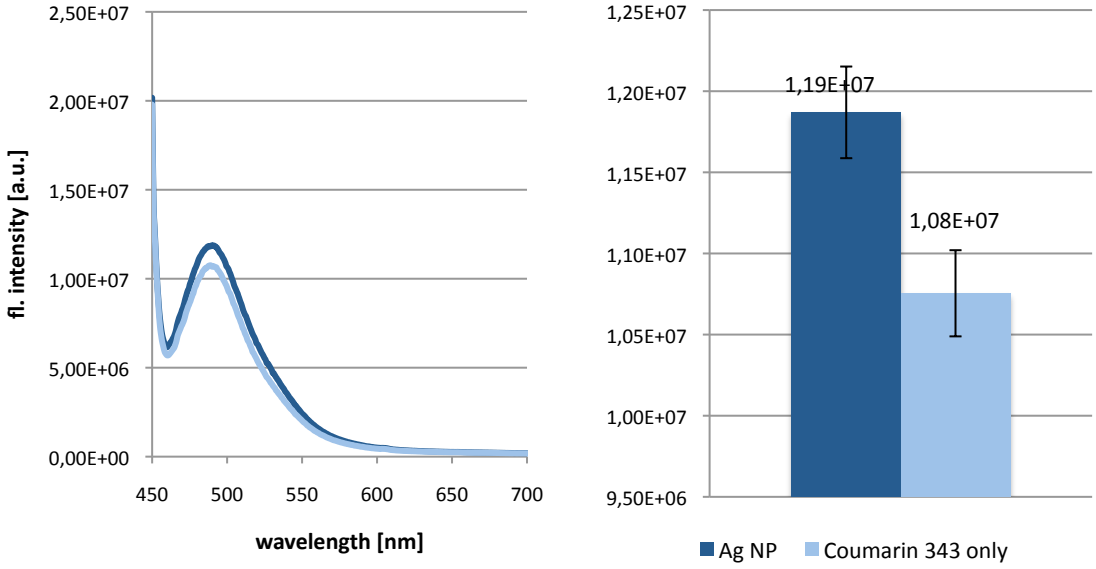

Fig. 55 Fluorescence intensity from AgNP and Coumarin 343 and detail of peak value and error bar

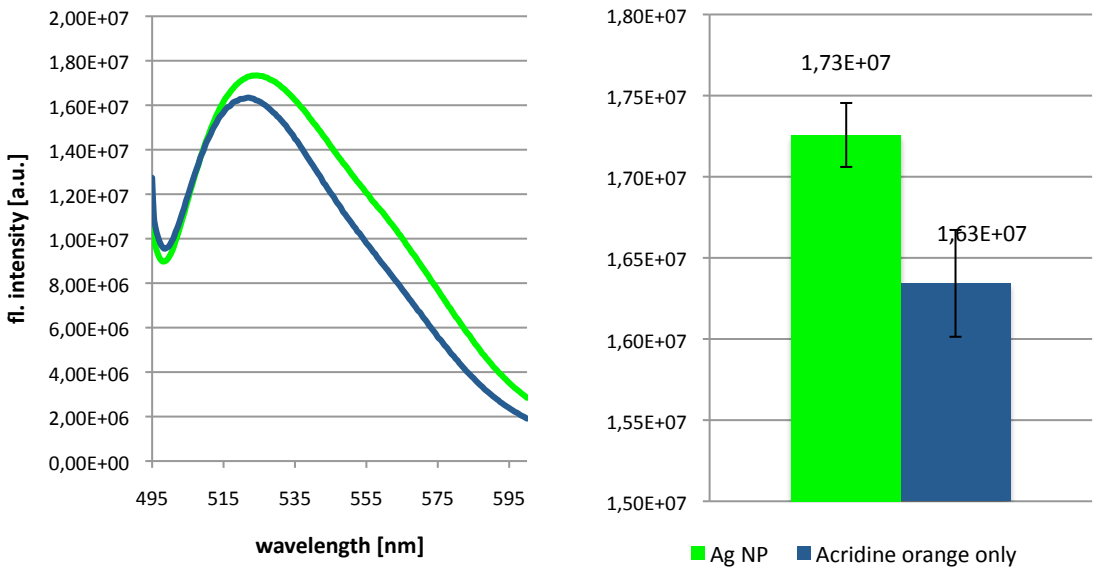

Fig. 56 Fluorescence intensity from AgNP and Acridine Orange and detail of peak value and error bar

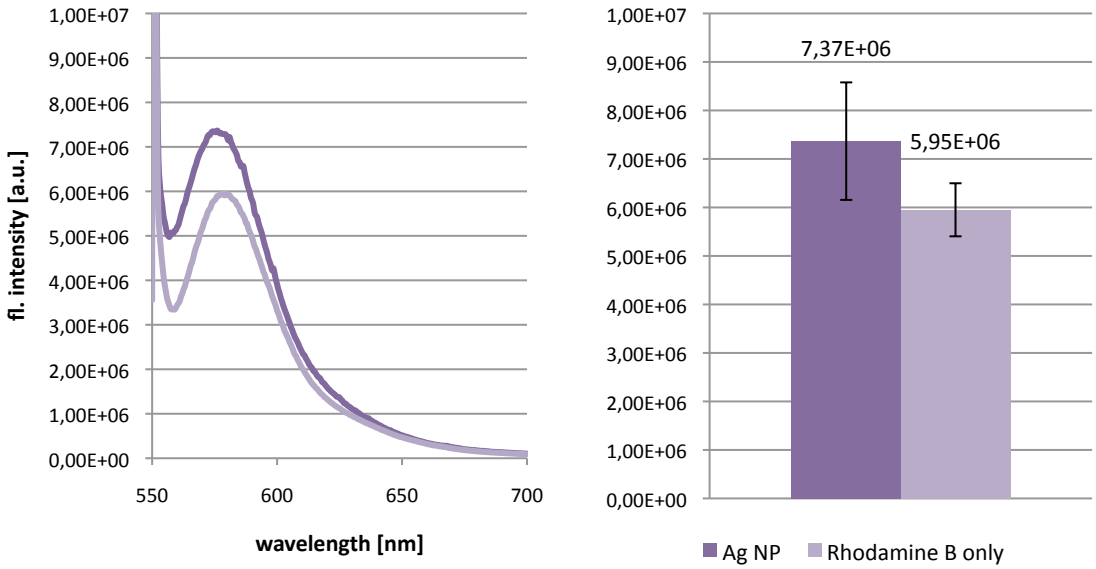

Fig. 57 Fluorescence intensity from AgNP and Rhodamine B and detail of peak value and error bar

Coumarin 343 has been used 10 times diluted respect to the original concentration and with a total volume of 20 µL. Unfortunately, no enhancement has not been obtained. A very little, practically negligible enhancement could be observed from Acridine orange which, given the low quantum yield, could have been a promising dye. Finally, a 1.3-fold enhancement could be observed when using a 10 times diluted solution of Rhodamine B. A possible explanation of the different behaviour of the various dyes is relative to their chemical structure (see the appendix): it

seems that protic lateral groups favour the enhancement, while non-polar groups, as in the case of Coumarin 343 and Acridine Orange, hinder the enhancement.

2.3.2.3 Enhancement from core@shell

The optimized conditions were then tested by using core@shell structures. Theoretically, the optimized distance between silver nanoparticles should be around 10 nm, to get the highest enhancement. The plots show that the enhancement factor is 4,36-fold by using core@shell with the thinnest silica shell (fig.58).

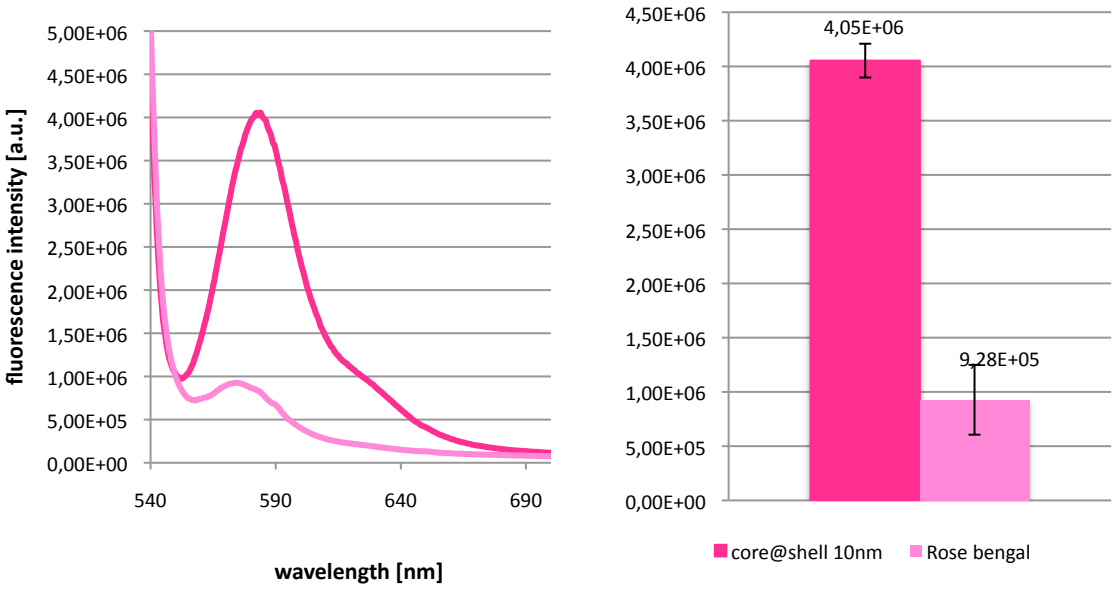

Fig. 58 Fluorescence intensity from $Ag@SiO_2$ on filter paper compared to Rose Bengal only

As a further confirmation that the enhancement effect derives from an interaction between the particles and the fluorophore, fluorescence intensity has been measured from samples having a different shell thickness. The five different batches of core@shell particles are those presented in chapter 1 (fig.19a-e), and data are collected in the table below.

	d_{DLS} [nm]	C/S
A	153	0,97
B	159	0,91
C	189	0,53
D	147	0,83
E	157	0,75

Table 8 Diameters (d_{DLS})and C/S of different batches of core@shells. A and B has been obtained from AgNP with a mean diameter of 50nm, while C, D and E with a mean diameter of 43nm (Cfr. Table 5 in chapter 1)

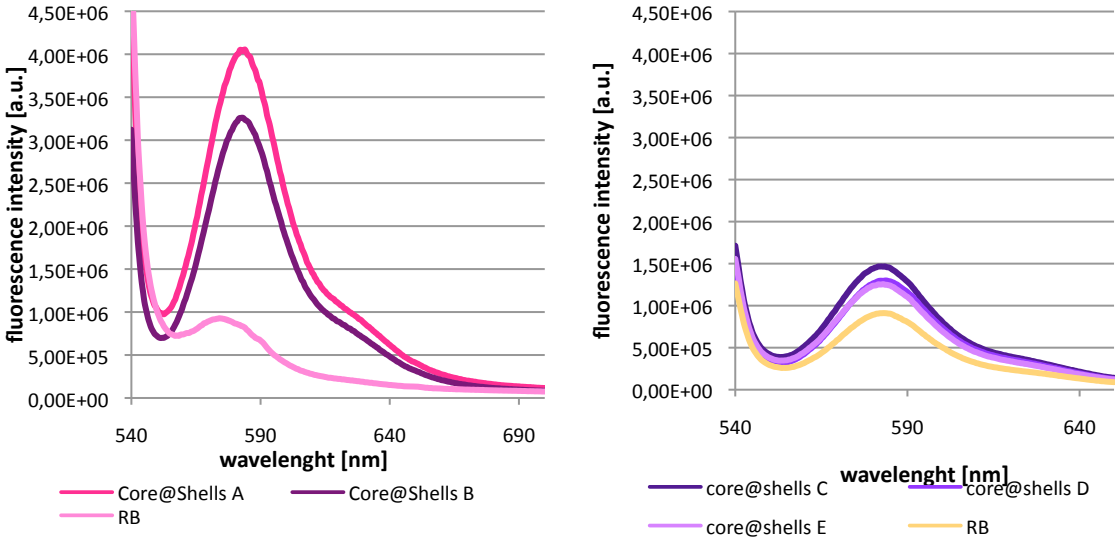

Fig. 59 Fluorescence intensities from Ag@SiO_2 particles having different shell thickness, compared to Rose Bengal only

These pictures show a different extent of enhancement depending on the shell thickness: thinner shell gives the higher enhancement, which is in good agreement with theoretical models. The shell does not "mask" the plasmonic effect of the encapsulated metallic particles, but provides effective protection from external conditions and a substrate for surface functionalization.

2.3.2.4 Comparison with different particles

To further confirm that the observed enhancement is due to MEF, that is related to the presence of a metal structures, the experiment has been performed using core@shells, an aqueous solution of ≈300 nm SiO_2 particles and an aqueous solution of ≈200 nm cationic particles. Result is provided below. Core@shell particles provide a 5-fold enhancement, with respect of the 2,6-fold of polymeric particles and 1,6-fold of silica particles.

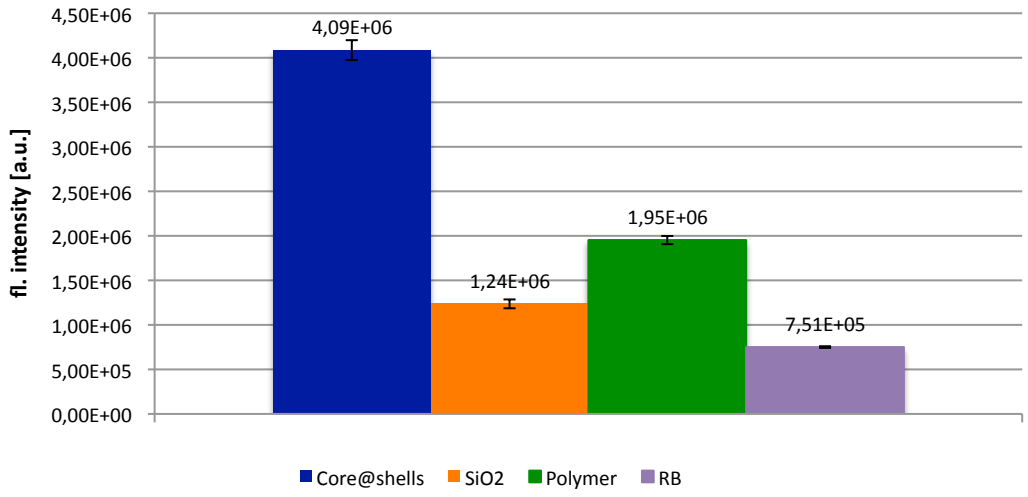

Fig. 60 Comparison of fluorescence intensities from different particles with respect to Rose Bengal only

2.3.2.5 The problem of water

A peculiar result has been obtained from paper samples that has been wetted with milliQ water, and then onto which Rose Bengal was deposited, as depicted in the following plot.

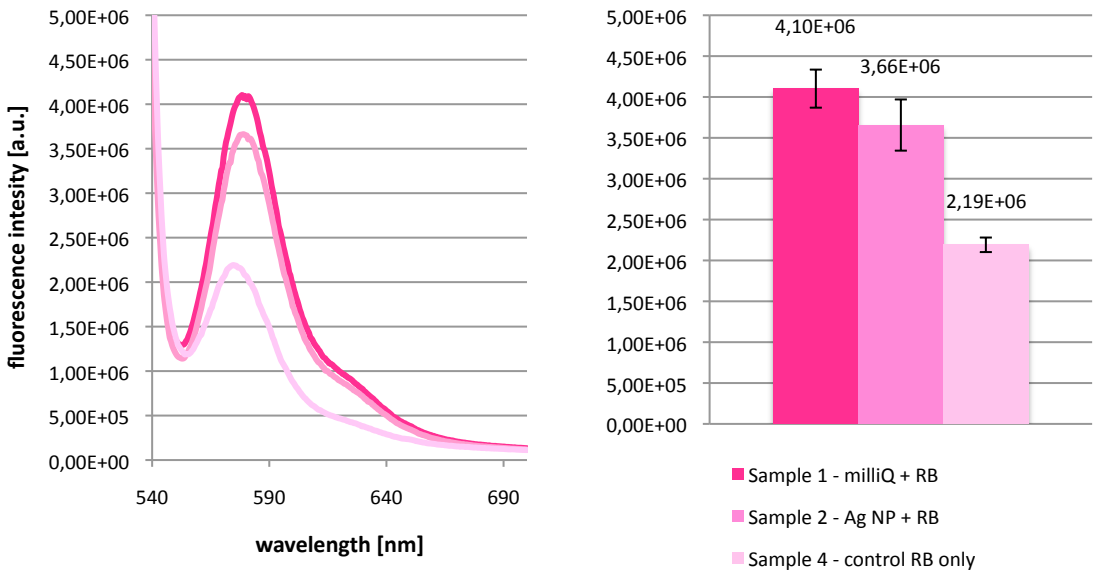

Fig. 61 Fluorescence intensities from paper samples onto which AgNP or milliQ water was deposited, together with Rose Bengal. Detail of peak value and error bar is provided

In this case, the enhancement from the sample in which particles were not present was even slightly higher than that one with silver nanoparticles, questioning if the enhancement recorded up to now was meaningful to be considered deriving from MEF.

2.3.2.5.1 Analysis of the paper structure

A possible explanation of the above reported results could be related to the wetting of the paper: an aqueous solution may modify the paper structure, for example by increasing the dimensions of the cellulose fibers. Accordingly, a reduction of pores size leads to retention of dye in the superficial layers. Since the fluorescence emission is recorded from the surface of the paper, this would imply a higher fluorescence just due to the spatial location of the dye. To confirm this hypothesis SEM (Scanning Electron Microscope) pictures of the surface of filter paper have been collected (10kV, 1000x magnification, fig 62-63).

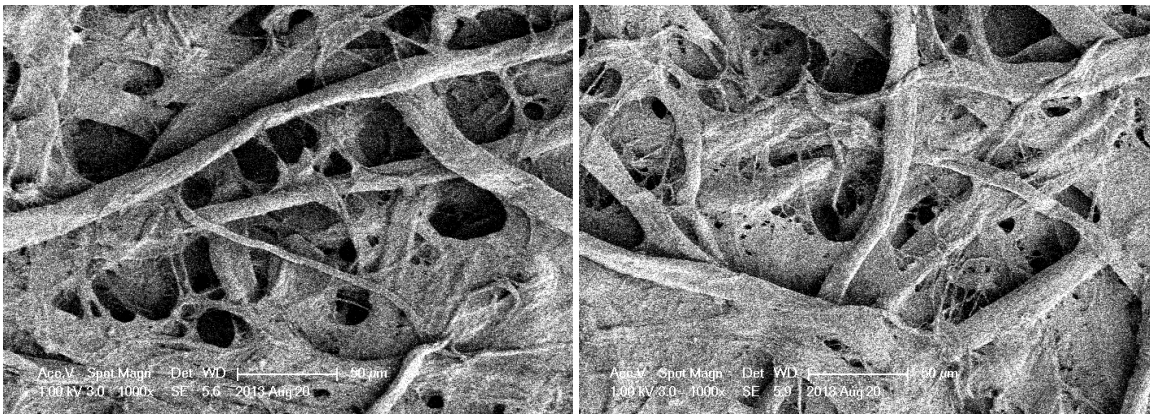

Fig. 62 a-b: SEM pictures of a)dry filter paper and b)milliQ wetted filter paper

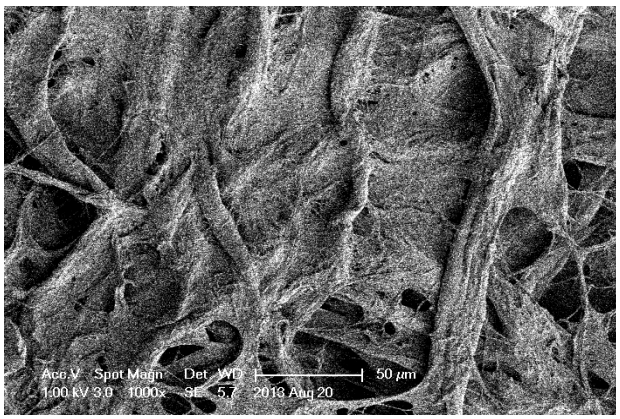

Fig. 63 SEM picture of silver nanoparticle functionalized filter paper

Even though the dry sample looks less dense, no remarkable differences can be observed from the other two samples, namely the wetted paper and the NP-functionalized paper, thus indicating that wetting does not provide the correct explanation of the overall phenomenon.

2.3.2.5.2 Modification of experimental procedures

Three different types of experimental procedures have been considered and performed using either silver nanoparticles or milliQ. Specifically, the first type of experiment was called “forward”, and consisted in the deposition of 0,5 mL of an aqueous solution of silver nanoparticles (1% wt) or milliQ water onto the paper samples, let dry naturally and then deposit the dye (50 µL of a 10^{-4}M solution of Rose Bengal, otherwise differently specified). The second type of experiment, as in scheme 11, has been called “mixing”, and consisted in the deposition onto the filter paper samples of a mixture of particles (or water) and dye. Finally, the third type of procedure, “backward”, consisted in the deposition of the dye on paper and, once dried, in that of particles (or, again, just water). The idea was to observe if there was any significant modification of the spectra, depending on the procedure adopted.

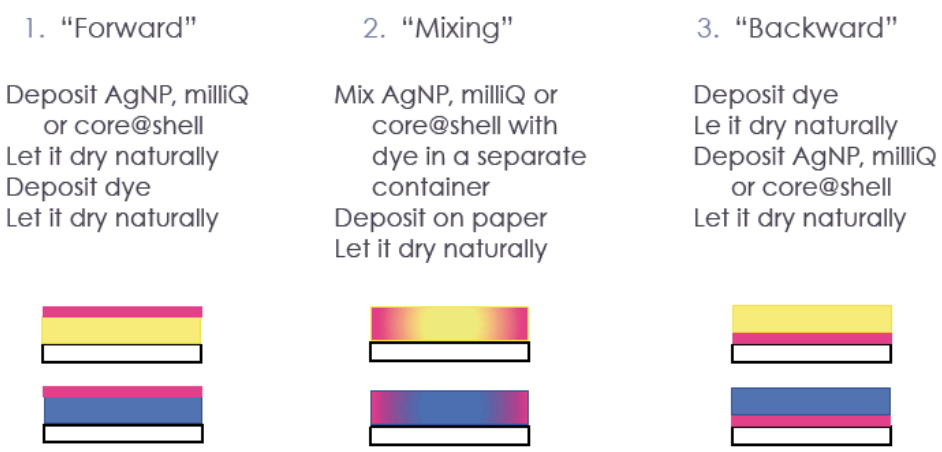

Scheme 11 Representation and description of the three different experimental procedures

Fluorescence emission values have been recordered, as usual. The following scheme (scheme 12) depicts the result of the fluorescence measurement depending on the specific procedure adopted: 6 samples (2 forward, 2 mixing and 2 backward) have been compared to a paper samples onto which only Rose Bengal was deposited.

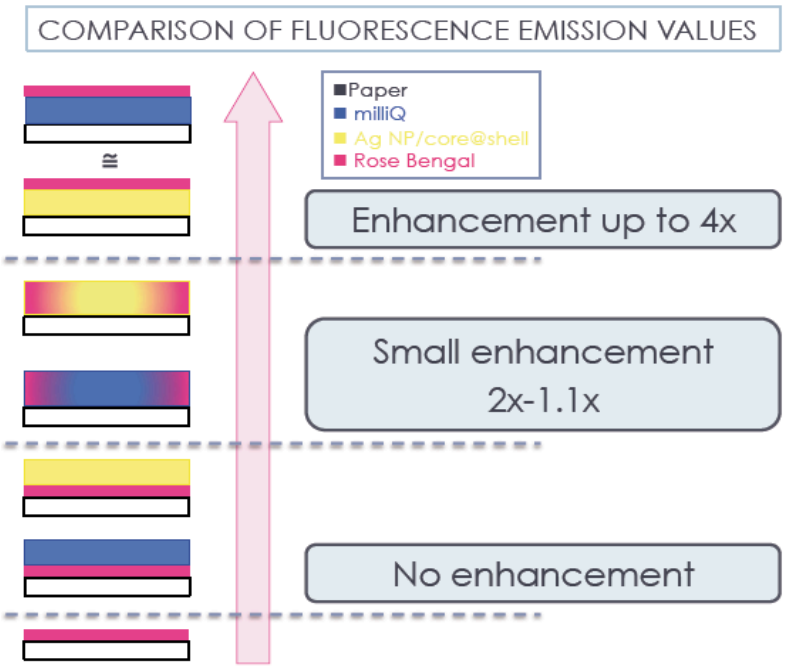

Scheme 12 Summary of enhancement values obtained with the different experimental procedures

Briefly, confronting the samples functionalized with particles (or water) and dye, with respecting to dye only, no enhancement was recorded from the samples prepared with the "backward" procedure. Small values of enhancements have been recorded from samples prepared with the "mixing" procedure. In particular, the samples with nanoparticles provided higher values of fluorescence, if compared to those without particles (2-fold enhancement *vs.* 1.1-fold). Finally, the highest enhancement values were observed for paper samples prepared *via* the "forward" method, both (the one with particles and the one with only water) having enhancement factors

around 4. Clearly, there is a correlation between the enhancement factors and the methodology, specifically, the order in which particles/water and dye are deposited. This suggested that a different dye penetration may vary accordingly.

2.3.2.5.3 Analysis of paper cross section

Aimed at correlating the emission values of fluorescence for the three deposition methods the cross section images of paper samples that give enhancement have been taken at 200x magnification. The results are shown in the figures 64-65.

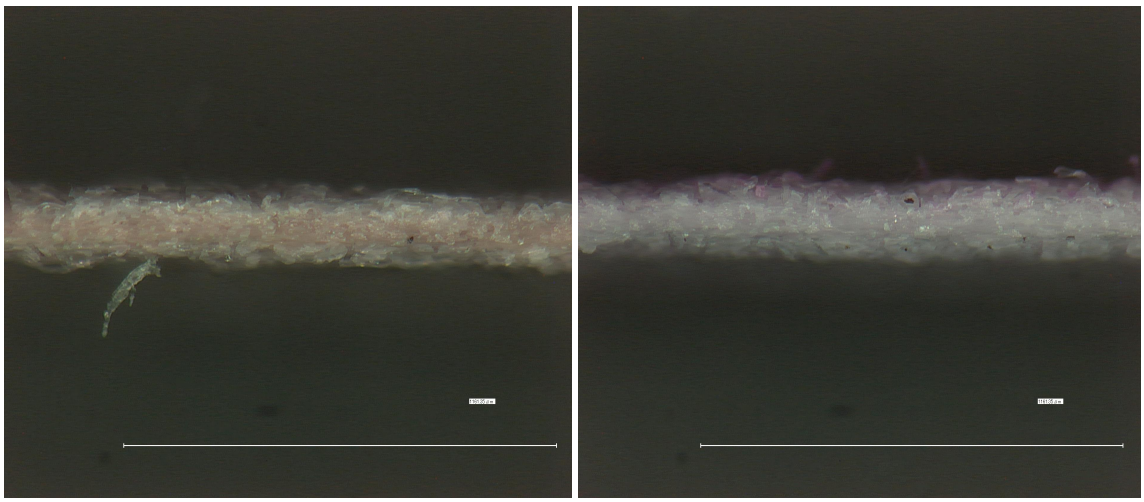

Fig. 64 a-b: Cross section of paper samples ("forward" method) functionalized with a)silver nanoparticles and Rose Bengal and b)milliQ water and Rose Bengal

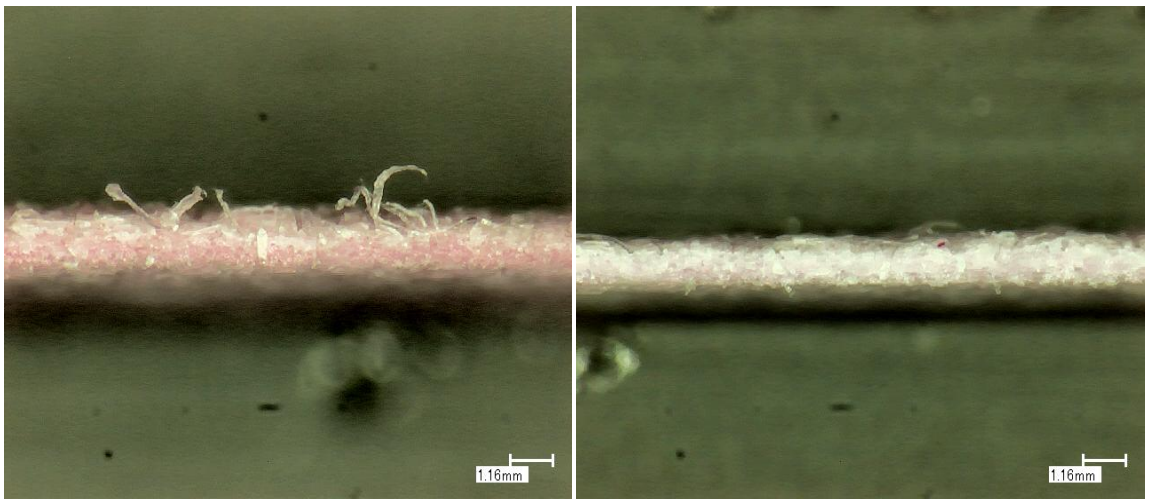

Fig. 65 a-b: Cross section of paper samples ("mixing" method) functionalized with a)silver nanoparticles and Rose Bengal and b)milliQ and Rose Bengal

Despite their similar fluorescence (about 4-fold the fluorescence with respect to the Rose Bengal only), samples of fig.64a and fig.64b show distribution of the dye remarkably different. When silver nanoparticles are present (figure 64a), the dye penetrates through the sample and distributes homogeneously. On the other hand, where only milliQ was present, the dye concentrates and distribute only in a thin layer at the paper surface (figure 64b). This last finding

confirms that the wetting shrinks the inter-fibers pores of the filter paper, thus preventing penetration of the dye. Moreover, the resulting fluorescence enhancement can be likely explained by the high concentration of the dye close to the paper surface. On the other hand, the same degree of enhancement is recorded from the sample of figure 30 where the dye is more distributed across the paper, which cannot be supported by the previous explanation. It leads to the hypothesis that the plasmonic interaction between silver nanoparticles and the Rose Bengal, which generates MEF, makes up for the lack in fluorescence due to the penetration of the dye. A similar situation occurs in the case of the "mixing" method,, as shown in fig.65, with a concentration of the dye, though deeper than in the "forward method". Moreover, where milliQ and rose bengal have been mixed together before applying on paper, it is quite difficult to even see the presence of rose bengal, that looks extremely diluted. Fluorescence from such sample is basically the same as paper with rose bengal only (1.1-fold enhancement).

The reason why sample in fig.65a, which looks similar to fig.64a from the point of view of the dye distribution in the cross section, has a different extent of fluorescence, is probably due to the reduction in fluorescence that is recorded from Rose Bengal when it is diluted in water rather than in ethanol. Investigations on this point have been made, and they are explained in section 2.3.3. Additionally, it may be that fig.65a is only one of the main spots that could be photographed of the sample cross section, and some differences and inhomogeneities could be observed by moving to different spots, while this was not the case for sample in fig.64a.

The same experiment has also been performed using the paper samples functionalized with the SiO_2 particles and the polymeric particles, to account for the recorded enhancement, even if relatively small, as shown in paragraph 2.3.2.4. Theoretically, there should be no enhancement where there is no metal structure, but the increase in fluorescence can be explained again by analysing the paper cross section.

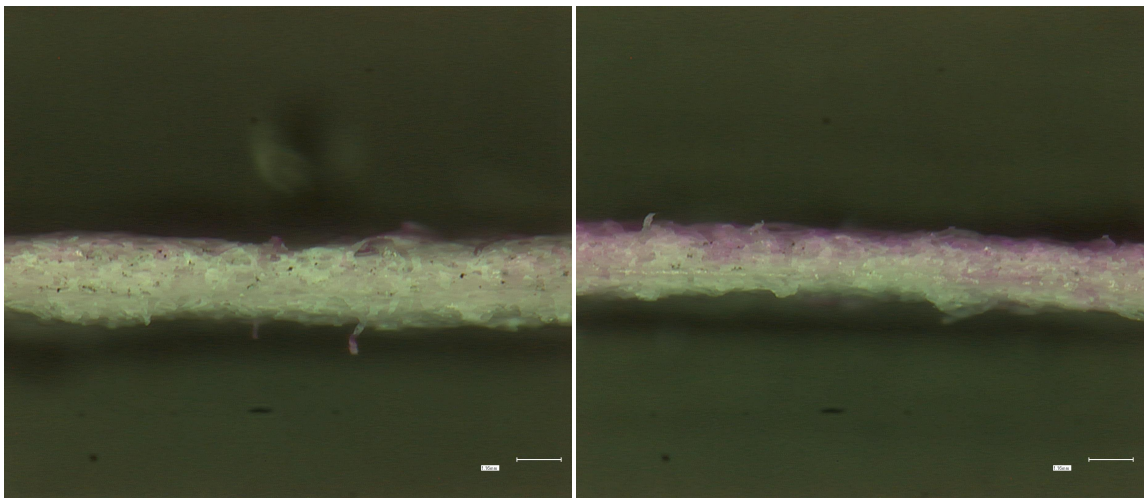

Fig. 66 a-b: Cross section of paper samples functionalized a)with SiO_2 particles and b)polymeric particles

Fig. 66a represents the distribution in the cross section of the silica particles, fig. 66b that of the polymeric particles. The distribution, especially in the case of polymeric particles, is clearly limited

to the surface of the paper sample: the fluorescence values, shown in fig. 60 are probably due to this close proximity with the surface, in a similar way to what happens to samples having only water and dye (fig. 64b). Additionally, fluorescence values are much lower than that of silver particles (fig. 60), which encourages the fact that fluorescence from metal particles-functionalized samples can be due to MEF.

2.3.2.5.4 Backside fluorescence

As additional evaluation method to confirm the different dye distribution inside the cross section, fluorescence spectra have been collected from the other side, respect to where particles or dye were pipetted, of paper samples. A higher fluorescence was expected from samples containing nanoparticles, in which dye was more distributed and, consequently, closer to the backside of such samples.

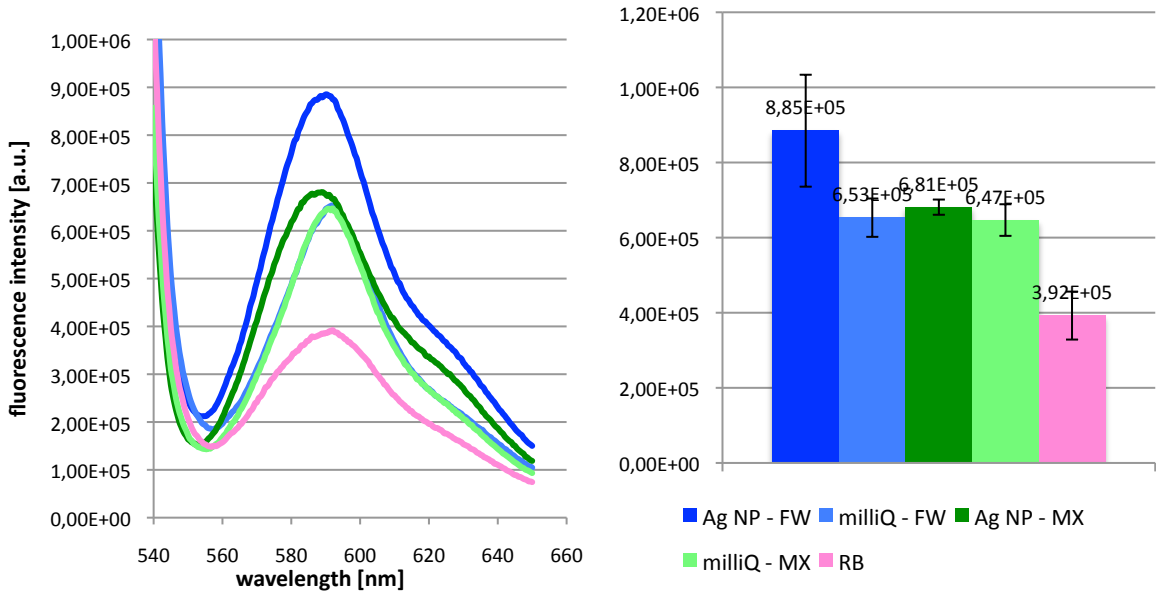

Fig. 67 Fluorescence intensisties measured from the backside of the paper samples, and detail of the peak value and error bars. FW stands for "forward", while MX stands for "mixing"

As expected, a relatively high fluorescence (2.6-fold) could still be observed from the sample where particles were present (Ag NP – FW). Lower enhancement (1.76-fold) was recorded from the sample in which particles and dye were mixed before the application on paper (Ag NP - MX): the difference respect to the previous one can be attributed to the already cited inhomogeneity that could be evidenced. The two samples with milliQ (milliQ - FW and milliQ - MX) still retained some fluorescence (1.6-fold), but they have the same value of emission, as a confirmation of the same distribution of dye in the cross section.

2.3.3 Solution measurements of Rose Bengal absorption and fluorescence

Finally, absorption and emission of Rose Bengal have been evaluated in solution. Rose Bengal has been dissolved at first in ethanol (as in the reference article[74]), and its absorbance and fluorescence spectra have been collected. The experiment has been repeated increasing at any step the quantity of water and decreasing that of ethanol, thus changing the EtOH:water ratio. The total volume (2 mL), as well as the concentration of Rose Bengal (10^{-4} M) have been kept constant.

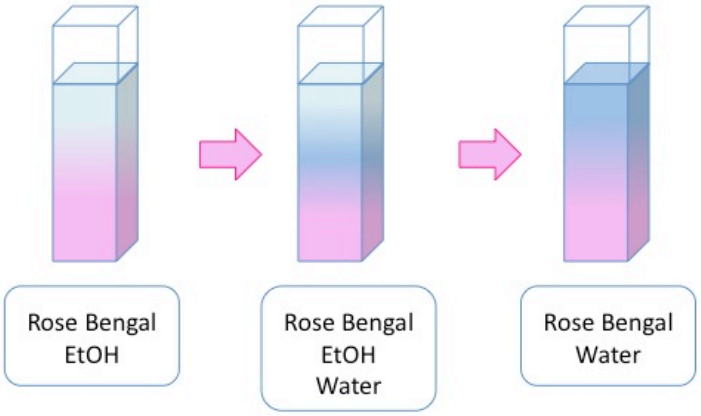

Scheme 13 Representation of the solvent composition used to evaluate changes in fluorescence intensity

Specifically, the ratio EtOH:water was varied from 10:0 to 0:10. In each case, the quantity of Rose Bengal was 100µL, having a concentration of 10^{-4}M, to allow a quantitative comparison of the spectra. Results of the absorbance and fluorescence measurements are provided below. The fluorescence spectra have been collected varying the excitation wavelength according to the absorption measurements: the value of wavelength at the peak in the absorption spectrum has been used as excitation λ for the fluorescence spectrum.

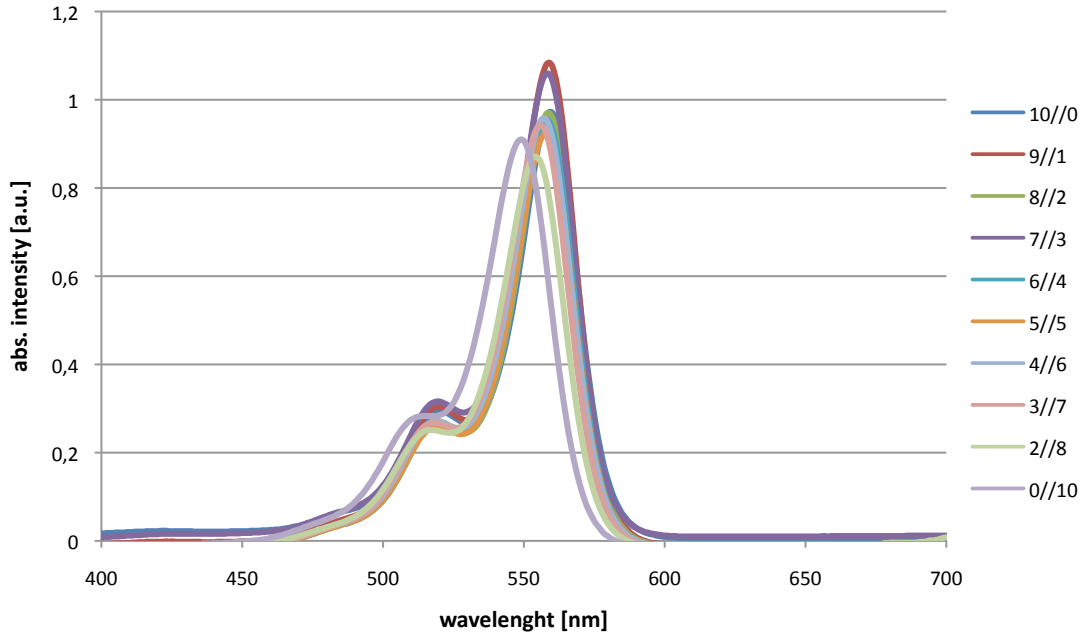

Fig. 68 Absorbance spectra of Rose Bengal dissolved in an ethanol/water mixture, in different proportions, from 10/0 (pure ethanol) to 0/10 (pure water)

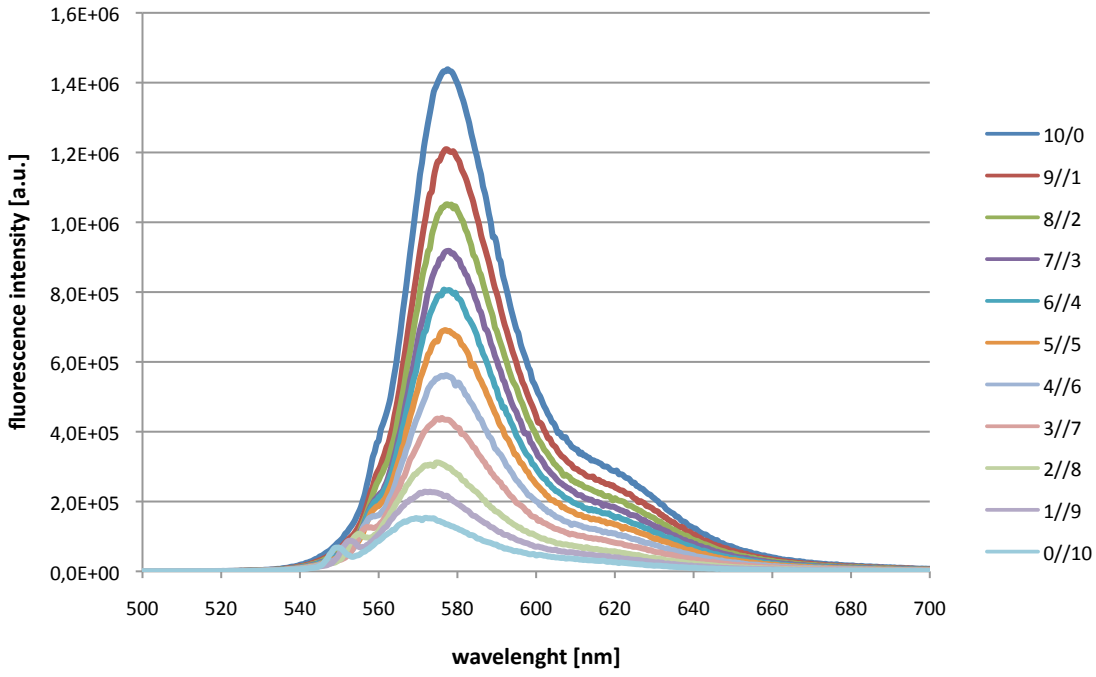

Fig. 69 Fluorescence spectra of Rose Bengal dissolved in an ethanol/water mixture, in different proportions, from 10/0 (pure ethanol) to 0/10 (pure water)

Going from pure ethanol to pure water solvent a blue-shift from 559 to 549 nm in the absorption spectra occurs, that corresponds also to a 7-fold decrease in fluorescence intensity. This is not surprising, as it has already been shown how fluorescence is affected by variations in the environment, particularly by solvent polarity. Nevertheless, it accounts for the decrease in fluorescence that is observed from paper samples when particles (dispersed in water) are mixed

with the dye before the application on paper ("mixing" type experiment), even though the distribution of particles and dye in the cross section is homogeneous (as in the "forward" type experiment). This experiment is not so explanatory in itself, but it may give a hint that a different aggregation of Rose Bengal occurs in different solvents.

2.3.4 Summary

In this chapter, many experiences and results have been presented. These experiments have been performed either using Ag NP or Ag@SiO_2 aiming, from one side, to maximize the fluorescence enhancement and, from the other side, to explain some unexpected phenomena (as the effect of water, in chapter 2.3.2.5). To explain anomalies in the results, measurements of the cross section of papers samples have been performed. The collection of results presented in this chapter indicates that fluorescence enhancement can be obtained from paper samples up to 4.36-fold the value for Rose Bengal only, when paper is functionalized with Ag@SiO_2 core@shell structures, having a 10nm shell. Such results can be achieved with a simple and inexpensive functionalization step of the paper surface. The following table summarizes the optimal condition for enhancement.

Assay	core@shell
Concentration [%wt]	0,1
Particles Volume [mL]	0,5
Dye volume [µL]	50
Particles:Dye (in volume)	10:1
Core/Shell ratio	0,97
Substrate	Filter paper #5C
Dep. method	Pipetting
Drying method	Naturally drying
Enh. factor	4.36-fold

Table 9 Summary of the best conditions to achieve fluorescence enhancement on paper

Bibliography

1. Lakowicz, Joseph R., ed. *Principles of fluorescence spectroscopy*. Springer, 2007.
2. Herschel, John Frederick William. "On a Case of Superficial Colour Presented by a Homogeneous Liquid Internally Colourless." *Philosophical Transactions of the Royal Society of London* 135 (1845): 143-145.
3. Cfr.1
4. Cfr.1
5. Stokes, George Gabriel. "On the change of refrangibility of light." *Philosophical Transactions of the Royal Society of London* (1852): 463-562.
6. Kasha, Michael. "Characterization of electronic transitions in complex molecules." *Discussions of the Faraday Society* 9 (1950): 14-19.
7. www.google.it,; last access 7.04.2014
8. Cfr.1
9. Cfr.1
10. Geddes, Chris D., and Joseph R. Lakowicz. "Editorial: Metal-enhanced fluorescence." *Journal of fluorescence* 12.2 (2002): 121-129.
11. Geddes, Chris D. "Metal-enhanced fluorescence." *Physical Chemistry Chemical Physics* 15.45 (2013): 19537-19537.
12. Drexhage, K. H. "Influence of a dielectric interface on fluorescence decay time." *Journal of Luminescence* 1 (1970): 693-701.
13. Drexhage, K. H., H. Kuhn, and F. P. Schäfer. "Variation of the fluorescence decay time of a molecule in front of a mirror." *Berichte der Bunsengesellschaft für physikalische Chemie* 72.2 (1968): 329-329.
14. Ford, G. W., and W. H. Weber. "Electromagnetic effects on a molecule at a metal surface: I. Effects of nonlocality and finite molecular size." *Surface Science* 109.2 (1981): 451-481.
15. Korzeniewski, Gregory E., Tsofar Maniv, and Horia Metiu. "Electrodynamics at metal surfaces. IV. The electric fields caused by the polarization of a metal surface by an oscillating dipole." *The Journal of Chemical Physics* 76.3 (1982): 1564-1573.
16. Barnes, W. L. "Fluorescence near interfaces: the role of photonic mode density." *journal of modern optics* 45.4 (1998): 661-699.
17. Persson, B. N. J. "Theory of the damping of excited molecules located above a metal surface." *Journal of Physics C: Solid State Physics* 11.20 (1978): 4251.
18. Ruppin, R. "Decay of an excited molecule near a small metal sphere." *The Journal of Chemical Physics* 76.4 (1982): 1681-1684.
19. Das, Purna C., and Ashok Puri. "Energy flow and fluorescence near a small metal particle." *Physical Review B* 65.15 (2002): 155416.
20. Lakowicz, Joseph R. "Radiative decay engineering: biophysical and biomedical applications." *Analytical biochemistry* 298.1 (2001): 1-24.
21. Cfr.10
22. Lakowicz, Joseph R., et al. "Radiative decay engineering: 2. Effects of silver island films on fluorescence intensity, lifetimes, and resonance energy transfer." *Analytical biochemistry* 301.2 (2002): 261-277.
23. Lakowicz, Joseph R. "Radiative decay engineering 3. Surface plasmon-coupled directional emission." *Analytical biochemistry* 324.2 (2004): 153-169.
24. Lakowicz, Joseph R. "Radiative decay engineering 5: metal-enhanced fluorescence and plasmon emission." *Analytical biochemistry* 337.2 (2005): 171-194.
25. Carminati, Rémi, et al. "Radiative and non-radiative decay of a single molecule close to a metallic nanoparticle." *Optics Communications* 261.2 (2006): 368-375.
26. Lakowicz, Joseph R., et al. "Plasmon-controlled fluorescence: a new paradigm in fluorescence spectroscopy." *Analyst* 133.10 (2008): 1308-1346.

27. Deng, Wei, et al. "Metal-enhanced fluorescence in the life sciences: here, now and beyond." *Physical Chemistry Chemical Physics* 15.38 (2013): 15695-15708.
28. Cfr.24
29. Cfr.25
30. Cfr.26
31. Aslan, Kadir, et al. "Annealed silver-island films for applications in metal-enhanced fluorescence: interpretation in terms of radiating plasmons." *Journal of fluorescence* 15.5 (2005): 643-654.
32. Cfr.24
33. Cfr.26
34. Cfr.10
35. Dragan, Anatoliy I., and Chris D. Geddes. "Metal-enhanced fluorescence: The role of quantum yield, Q0, in enhanced fluorescence." *Applied Physics Letters* 100.9 (2012): 093115.
36. Dragan, A. I., and C. D. Geddes. "Excitation volumetric effects (EVE) in metal-enhanced fluorescence." *Physical Chemistry Chemical Physics* 13.9 (2011): 3831-3838.
37. Cfr.36
38. Cfr.36
39. Cfr.36
40. Cfr.36
41. Cfr.36
42. Cfr.36
43. Dragan, Anatoliy I., et al. "Distance Dependence of Metal-Enhanced Fluorescence." *Plasmonics* 7.4 (2012): 739-744.
44. Zhang, Yongxia, Anatoliy Dragan, and Chris D. Geddes. "Wavelength dependence of metal-enhanced fluorescence." *The Journal of Physical Chemistry C* 113.28 (2009): 12095-12100.
45. Caires, Anderson RL, Luciano R. Costa, and Joelson Fernandes. "A close analysis of metal-enhanced fluorescence of tryptophan induced by silver nanoparticles: wavelength emission dependence." *Central European Journal of Chemistry* 11.1 (2013): 111-115.
46. Cfr.44
47. Cfr.45
48. Chen, Yeechi, Keiko Munechika, and David S. Ginger. "Dependence of fluorescence intensity on the spectral overlap between fluorophores and plasmon resonant single silver nanoparticles." *Nano letters* 7.3 (2007): 690-696.
49. Cfr.48
50. Kühn, Sergei, et al. "Enhancement of single-molecule fluorescence using a gold nanoparticle as an optical nanoantenna." *Physical review letters* 97.1 (2006): 017402.
51. Canesi, Eleonora V., et al. "Solution Processed, Versatile Multilayered Structures for the Generation of Metal-Enhanced Fluorescence." *The Journal of Physical Chemistry C* 117.25 (2013): 13197-13201.
52. Kim, Jongwook, et al. "Plasmon-induced modification of fluorescent thin film emission nearby gold nanoparticle monolayers." *Langmuir* 26.11 (2010): 8842-8849.
53. Renier, A., et al. "Gold/silica thin film for biosensors applications: Metal enhanced fluorescence." *Laser physics* 20.3 (2010): 591-595.
54. Zhang, Jian, and Joseph R. Lakowicz. "Metal-enhanced fluorescence of an organic fluorophore using gold particles." *Optics express* 15.5 (2007): 2598-2606.
55. Garoff, S., et al. "Electrodynamics at rough metal surfaces: Photochemistry and luminescence of adsorbates near metal-island films." *The Journal of chemical physics* 81.11 (1984): 5189-5200.
56. Ray, Krishanu, Mustafa H. Chowdhury, and Joseph R. Lakowicz. "Aluminum nanostructured films as substrates for enhanced fluorescence in the ultraviolet-blue spectral region." *Analytical chemistry* 79.17 (2007): 6480-6487.
57. Guzatov, Dmitry V., et al. "Plasmonic enhancement of molecular fluorescence near silver nanoparticles: theory, modeling, and experiment." *The Journal of Physical Chemistry C* 116.19 (2012): 10723-10733.
58. Cfr.57

59. Cfr.57
60. Deng, Wei, et al. "Metal-enhanced fluorescence in the life sciences: here, now and beyond." *Physical Chemistry Chemical Physics* 15.38 (2013): 15695-15708.
61. Cfr.20
62. Nooney, Robert, et al. "Enhancing the analytical performance of immunoassays that employ metal-enhanced fluorescence." *Analytical and bioanalytical chemistry* 396.3 (2010): 1127-1134.
63. Aslan, Kadir, et al. "Metal enhanced fluorescence solution-based sensing platform 2: fluorescent core-shell Ag@ SiO2 nanoballs." *Journal of fluorescence* 17.2 (2007): 127-131.
64. Tovmachenko, Oleg G., et al. "Fluorescence Enhancement by Metal-Core/Silica-Shell Nanoparticles." *Advanced materials* 18.1 (2006): 91-95.
65. Aslan, Kadir, et al. "Fluorescent core-shell Ag@ SiO2 nanocomposites for metal-enhanced fluorescence and single nanoparticle sensing platforms." *Journal of the American Chemical Society* 129.6 (2007): 1524-1525.
66. Viger, Mathieu L., et al. "Reduction of self-quenching in fluorescent silica-coated silver nanoparticles." *Plasmonics* 3.1 (2008): 33-40.
67. Deng, Wei, et al. "Ultrabright Eu–Doped Plasmonic Ag@ SiO2 Nanostructures: Time-gated Bioprobes with Single Particle Sensitivity and Negligible Background." *Advanced Materials* 23.40 (2011): 4649-4654.
68. Zhang, Yongxia, et al. "Metal-enhanced fluorescence from paper substrates: Modified spectral properties of dyes for potential high-throughput surface analysis and assays and as an anti-counterfeiting technology." *Dyes and Pigments* 77.3 (2008): 545-549.
69. Aslan, Kadir, et al. "Metal-enhanced fluorescence from plastic substrates." *Journal of fluorescence* 15.2 (2005): 99-104.
70. Aslan, Kadir, Patrick Holley, and Chris D. Geddes. "Metal-enhanced fluorescence from silver nanoparticle-deposited polycarbonate substrates." *Journal of Materials Chemistry* 16.27 (2006): 2846-2852.
71. Cfr.68
72. Cfr.68.
73. Cfr.68
74. Cfr.68

3. PATTERNING PAPER FOR SENSING DEVICES: μPADs AND INK-JET PRINTING TECHNOLOGY

3.1 An overview on microfluidics and paper-based sensing

Microfluidics is the science and technology of systems that process or manipulate small (10^{-9} to 10^{-18} litres) amount of fluids, using channels with dimensions of tens to hundreds of micrometers[1] Several research groups contributing in this field are those of G. Whitesides (Harvard University, USA)[2], P. Yager (University of Washington, USA)[3], A.W. Martinez (CalTech, USA)[4], S.T. Phillips (Penn State University, USA)[5], G. Garnier (Monash University, Australia)[6] and D. Citterio (Keio University, Japan)[7]. Moreover, an interesting web-based platform, created by Yager's group, is available for everyone who is interested in the topic[8].

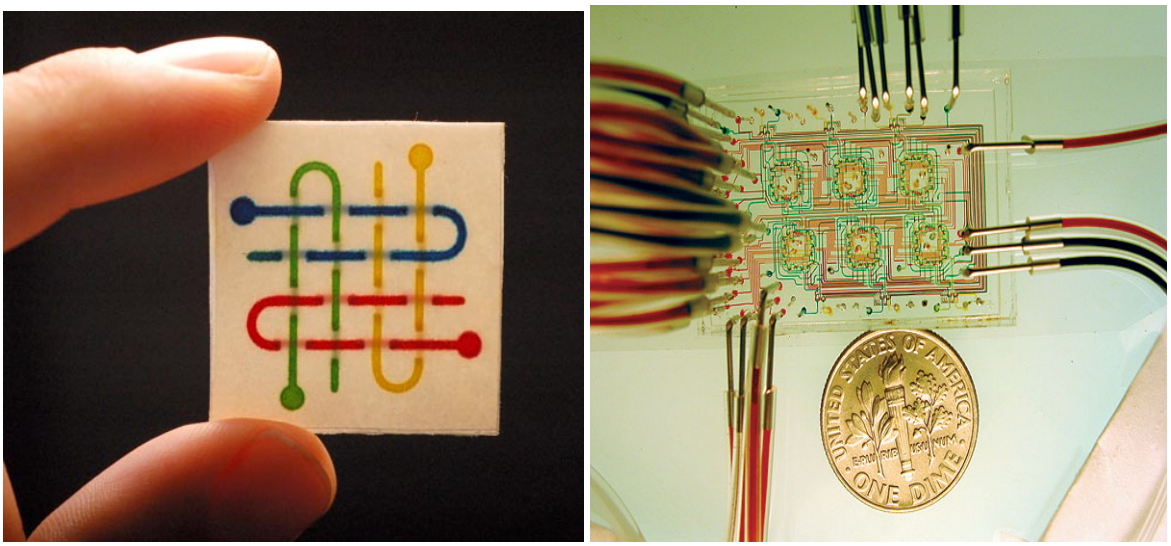

Fig. 70 a-b: Examples of microfluidic devices. a)3D Paper-based[9] and b)chemostat to control microbial growth[10]

Chemical analysis has been the first application of microfluidic platforms which allows detection and separation of small quantities of chemicals and reagents with high resolution and sensitivity, low cost, short time for analysis and small footprints for the analytical devices. An important difference of microfluidic systems, with respect to large-scale systems, is the absence of turbulence in the channels, leading to laminar flow. On large scales, fluids mix through convection, reflecting the fact that inertia is generally more important than viscosity. In microsystems, the opposite situation occurs: two fluid streams that together flow in parallel with

no turbulence, diffusion across the interface being the only cause of mixing. Examples of application of microfluidic devices are: screening conditions for protein crystallization[11], screening in drug development[12,13], bioanalysis[14-16], manipulation of multiphase flow, (creation and manipulation of bubbles in a liquid stream)[17], immunoassay[18].
Four different factors have contributed to the origin of microfluidics:

- The driving to scale down dimensions of Microanalytical methods, such as gas-phase chromatography (GPC), high-pressure liquid chromatography (HPLC) and capillary electrophoresis (CE), which allowed to obtain high sensitivity and resolution with small sample quantities.
- By the end of the *Cold War*, biological and chemical weapons seemed to be the biggest military and terrorists' threats; in the 1990s the Defence Advanced Research Project Agency (DARPA) of the US Department of Defence supported studies to develop microfluidic systems to be used on-site for the detection of potentially toxic weapons.
- In the 1980s the strong interest in genomics and related science also increased the demand for high sensitive platform able to operate with very small quantities of species.
- The same technologies of Microelectronics used to realize silicon wafers and MEMS, namely photolitography and related techniques, have been used to pattern substrates to be applied in microfluidics. Silicon and glass devices were first produced but, being not suitable for some types of samples (e.g. living mammalian cells), microfluidic science mainly started working on elastomers, as PDMS (polydimethylsiloxane).

3.1.1 POC – Point-of-care diagnostics

A major application of microfluidic devices is represented by point-of-care (POC) diagnostics. The ideal POC test would deal with small sample volumes (from hundreds of nanoliters to ≈1mL) of complex biological media with femtomolar to millimolar concentration of analytes. Other main features include:

i. Distribution of the sample solution in spatially segregated regions to enable multiplex assay
ii. Fluid flow only due to capillary action
iii. Fast, cost-effective and easily reproducible fabrication
iv. Disposability

The application of POC tests spreads over different fields, as summarized in fig.71. Besides medical diagnosis which, especially in developing Countries, represents the major application of POC, it worth to mention other opportunities. Veterinary diagnostics is particularly important since it is related to human health: in developing Countries, where there is a closer human-to-animal relationship in daily life, the identification of zoonoses (communicable diseases) is a crucial factor to avoid the spreading of serious conditions, including HIV, SARS, coronavirus and influenza. Food safety is also directly linked to human health: food adulteration may lead to bacterial infections or more serious conditions can occur when food is contaminated with toxic

substances (milk adulterated with melamine in China, in 2008, was an emblematic case). Finally, environmental monitoring can also profit by the implementation of POC testing.

Fig. 71 Possible application fields of POC testing[19]

In medicine, POC testing has been already successfully adopted for many years. The two main classes of POC tests are represented by the *lateral flow test*, which makes use of a membrane or paper strip to indicate the presence of protein markers such as pathogen antigens or host antibodies, widely applied in pregnancy or HIV tests, and dipstick test. *Lateral flow test* are often low-cost, lightweight, portable, and require minimum sample preparation, although they often lack of sensitivity. The most famous and successful example of POC that combines microfluidics and microfabrication is the i-STAT® device (fig.72), that consists of an array microfabricated thin-film electrodes on silicon chips for the detection of blood chemicals (sodium or potassium salts, chloride, glucose, haematocrit and gases).

Fig. 72 a-b: a)i-STAT® glucose-meter and b)i-STAT® wireless glucose-meter that combines POC and telemedicine[20]

One of the most important challenges in POC and microfluidics in general, is the integration of different functionalities in one device, like sample collection and pre-treatment, analyte-specific reaction and signal production. This is not trivial, especially in the case of multiplexed assays. In addition, a POC test has to offer concrete advantages over traditional centralized-lab testing, in quality of care, convenience and cost reduction. POC does not have to be "cheap", rather they have to be cost-effective in order to provide the desired clinical benefit. The cost of "discounting" is another important parameter: the availability of a good service today has the same or even grater value than the same good or service in the future. If available today, even an imperfect POC test would save millions of lifes per year, and that waiting for a perfect test that will not be available for the next years will still cost millions of lives in the meanwhile. Finally, real-time results would be the best achievement, but a POC test that provides results in a time as short as possible is another challenge of this developing technology. Several critical reviews, reporting details and concrete examples of POC applied in different cases, can be easily found on-line[21-24].

3.1.2 Sensing approaches on paper-based devices

Paper, as sensing substrate, is not a new entry: its origin dates back to the year 1979, when Pliny the Elder demonstrated a method for estimation of the quality of Tyrian purple dye by means of a technique similar to chromatography on papyrus, and a papyrus-based spot test for ferrous sulfate[25]. Actually, the earliest paper-based device has been realized in 1937 (fig.73), consisting in confined spaces, defined by paraffin wax, for qualitative spot testing. Paraffin wax has been chosen due to its chemical inertness and great availability.

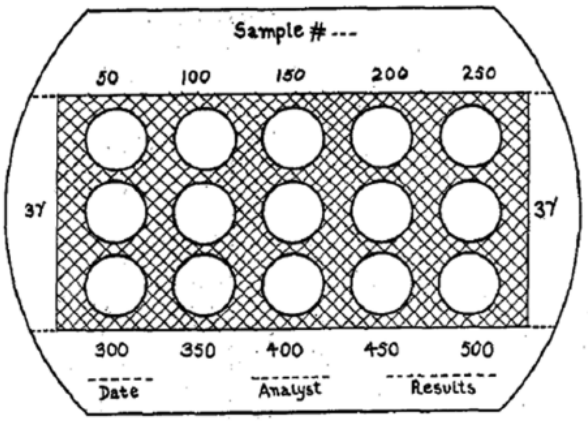

Fig. 73 The first paper-based device, dating 1937[26]

With the proceeding of years, paper has been extensively used, with the following milestones in the last century proposing paper as inexpensive substrate for commercial assays:

- In 1956, A.Keston presented the first colorimetric enzymatic glucose assay on filter paper based on the reaction of *o*-toluidine with hydrogen peroxide[27]
- In 1964, the first commercial paper test was introduced by Ames company, an enzymatic blood dipstick called Dextrostix[28]
- In 1988, the first commercial immunoassay was developed, when Unipath launched home pregnancy test kits[29]

Moreover, in 2007, Whitesides published the first paper describing a multichannel system with photoresist walls[30]. The invention of the paper-based microfluidics is attributed to the Whitesides group right due to this publication, although an earlier work reported by Müller et al. in 1949[31] may be considered as the origin of this technology. Müller and co-workers carried out a study on the preferential elution of a mixture of pigments within a channel on paper, impregnated by paraffin wax. The layout of their system, shown in figure 74, does not differ very much from modern microfluidic devices.

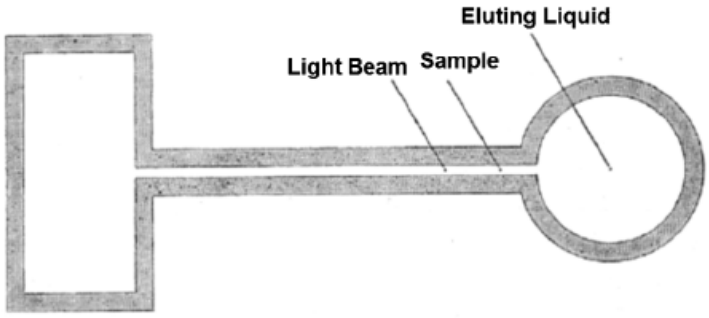

Fig. 74 Layout of the microfluidic paper-based device realized by Müller and co-workers in 1949

Microfluidic paper-based analytical devices (µPADs) are a relatively new class of analytical systems that has recently gained increasing attention due to the combination of advantages of both microfluidic systems and paper substrate. They have been mainly developed for use in developing Countries as point-of-care diagnostic techniques, as they are inexpensive, easy to use and disposable[32]. In developing Countries, indeed, basic infrastructures, like reliable power, refrigeration and trained personnel, are often not available: µPADs represent a valid solution, since they fulfil all the requirements that, according to the World Health Organization (WHO), a sensing device should have. Specifically, sensors should be "ASSURED", that is: Affordable, Sensitive, Specific, User-friendly, Rapid and robust, Equipment-free and Deliverable. µPADs are more functional than traditional dipstick-type paper tests, and often they allow for multiple tests on a single liquid sample. This is achieved by creating pathways or channels for liquid flow in the paper, shaping distinct regions that can be further functionalized with chemical indicators.

As substrate, paper has peculiar properties (summarized in table 10) that allows for easy fabrication, decrease of time required to analysis and, of course, low cost: compared to other microfluidic substrates, paper (0,1 cents/dm^2) is 200 times less expensive than PET and 1000 times less expensive than glass. Other features of paper compared to other substrates are given in table 11. Apart from the price, the development and introduction to the market of paper-based systems requires a relatively small investment and, moreover, these kind of device can not only spread among the scientific community, but, also, be easily applied in real-life situations (developing Countries, military field or emergency situations).

	Property	*Impact*
Mechanical properties	Flexibility High specific stiffness, lightness (≈10mg/cm^2)	Formation of complex 3D structures that will not tear when bent
	Thickness	Thickness of tens or hundreds of micrometers results in low (µL) total volume required for device preparation
	Soft texture	Good contact with solid objects, collection of traces of analytes by swabbing
Fibrous and porous structure	Absorbency	Storage and delivery of an exact volume of reagents inside the paper matrix, which frees the final user from handling chemicals; enrichment of the sample via multiple addition/drying steps; as the combined area of the channels is defined, there is no need for a constant sample volume
	Air permeability	Free diffusion of gas throughout the material removes problems usually associated with microfluidic systems-air bubbles
	Network structure	Filtration of the sample, e.g. contaminated with solids, separation of analytes by means of chromatography
	High surface-to-volume ratio	Increase in the number of enzyme molecules or colorimetric probes that can be immobilized
	Capillary action	Ability to wick fluids dispenses with the use of pumps and permits fluid flow in all directions
Natural origin	Compatible to biological samples, easy to sterilize, chemically and biologically inert, chirality (advantageous for immobilization of antibodies/proteins)	Increase in thermal stability of immobilized molecules, including enzymes and gold nanoparticles
	Disposability and biodegradability	Recyclable, rapidly degraded by microorganisms (≈50 days), and easily disposed of by incineration, eliminating the problem of contamination with biological material

Table 10Properties of paper[33]

Property	*Material*			
	Glass	*Silicon*	*PDMS*	*Paper*
Surface profile	Very low	Very low	Very Low	Moderate
Flexibility	✗	✗	✓	✓
Structure	Solid	Solid	Solid, gas-permeable	Fibrous
Surface-to-volume ratio	Low	Low	Low	High
Fluid flow	Forced	Forced	Forced	Capillary action
Sensitivity to moisture	✗	✗	✗	✓
Biocompatibility	✓	✓	✓	✓
Disposability	✗	✗	✗	✓
Biodegradability	✗	✗	To some extent	✓
High-throughput fabrication	✓	✓	✗	✓
Functionalization	Difficult	Moderate	Difficult	Easy
Spatial resolution	High	Very high	High	Low to moderate
Homogeneity of the material	✓	✓	✓	✗
Price	Moderate	High	Moderate	Low
Initial investment	Moderate	High	Moderate	Low

Table 11 Comparison among different substrates for sensing devices, with paper column evidenced in grey[34]

In terms of applications, paper-based microfluidic devices can be classified into two types[35]:

1. *On-demand* devices, which are blank microfluidic platforms that, depending on the samples to be tested, can be functionalized by the introduction of detection agents by the user prior to the test, either before or after the addition of the testing samples
2. *Ready-to-use* devices, which consist of complete sensors that integrate the indication reagents into the detection areas of the device. Based on the specific chemistry of such agents, specific analytes can be recognized by such devices

The majority of publications focuses on this latter type, with applications that include: the simultaneous detection of multiple analytes in a single sample solution (for example, glucose and proteins in urine[36]), the semi-quantitative analysis of multiple analytes by detecting the unknown sample and the standard solutions using a set of devices (for instance, the quantification of glucose, lactate and uric acid in urine[37]). Paper-based microplates have the potential to substitute the traditional plate for Enzyme-Linked ImmunoSorbent Assays (ELISA).

Paper-based sensing can be performed with a number of different approaches, that can be broadly classified in two main categories, depending on the detection system: optical or electrochemical.

Optical methods are the easiest to perform, as well as the most inexpensive. After performing a proper white-balance correction, subtraction of the background color from the output image or comparison of calibration curves with standards, the method is universal. A variety of detectors can be applied to optical sensors, from visual analysis, to common devices as cameras or scanners, to most sophisticated ones, like spectrophotometers and fluorimeters. Colorimetric paper-based sensors are the most prevalent, and they have been applied to many different fields. The cited work by Whitesides et al.[38] represents the breakthrough of paper-based diagnostics and consists of a colorimetric sensor for glucose and proteins. Other works focused on the detection of enzymes and their inhibitors[39], metals[40], temperature sensors[41], blood typing[42]. Fluorescence methods are also common, although the result has to be taken with much care since paper sometimes contains whitening additives that cause fluorescence and can affect the reliability of the measurement. Methods based on surface-enhanced Raman spectroscopy (SERS)[43-45], chemoluminescence[46], variations of transmittance (taking advantage of the tunable thickness of paper)[47] and various types of immunoassays[48-50] have also been developed. Figure 75 provides a collection of images of some of the cited devices. The newest perspective in colorimetric detection is represented by the implementation of phone cameras as sensing tools[51,52], especially considering that use of mobile phones is constantly increasing in among the population in developing countries (it was 30% in 2011 in Africa[53]). There are two advantages with this system: on-site readout with apps and telemedicine.

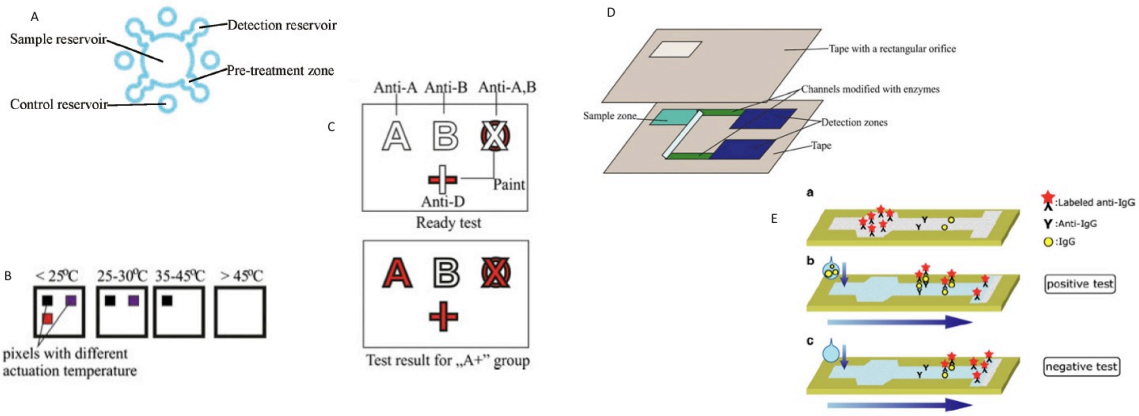

Fig. 75 a-e: Examples of paper-based sensing devices. A) for particulate metals[54]; B) temperature sensor[55]; C) blood typing[56]; D) chemoluminescence-based[57]; E) ink-jet printed immunoassay[58]

Electrochemical sensors are less diffused with respect to optical ones, although they are in principle more reliable, being insensitive to light, dust and insoluble compounds,. Detection systems are quite inexpensive, but the interpretation of results requires some degree of knowledge. Broadly speaking, they can be classified as voltammetric sensors, potentiometric sensors, and conductivity-based sensors. The description of such methods goes beyond the aim of the present work, but can be easily found elsewhere[59]. These systems differ from previous ones only for the detection method, but the analytes are basically the same. The first report dealing with electrochemical measurement on paper has been published in 2009 by Dungchai and co-workers[60], who fabricated the electrodes with photolithographic methods. In recent years, many other works have been published following the same trend[61-64].

In addition to analyte detection, paper-based devices have been used also for other applications:

- Template for the fabrication of thin film materials used for drug delivery, cell encapsulation and as sorbent for toxic metals in wound dressing[65,]
- Stamp for the contact printing of biochemicals onto planar substrates[66]
- Flexible substrate for prototyping PDMS devices[67]
- Platform for 3D cell culture or analysis[68,69]

Currently, there are still some limitations to the extensive production of microfluidic paper-based sensing devices:

i. Sample retention in the channels and sample evaporation during transport, leading to an inefficient delivery of the sample within the device. Usually, the fraction of the sample that effectively reaches the sensing area is less than 50%, which may be too small for a quantitative detection when the amount of sample is already very low.
ii. Some hydrophobic agents cannot actually build up hydrophobic barriers strong enough to prevent flow of samples with very low surface tension (like biological samples with surfactants). In such cases, the sample will leak out of the microfluidic channels, rendering the device ineffective.
iii. The limit of detection (LOD) is generally small, especially for colorimetric devices. Colorimetric detection is popular, for examples, in biologic scenarios where the concentration of analytes is in the milli-molar range, but becomes ineffective when sensing many environmental contaminants, as arsenic or mercury, that become hazardous already when their concentration is in the ppb (parts per billion) range.

3.1.3 Patterning paper: ink-jet printing

In the beginning, paper-based sensors were usually just of "YES/NO" logics: the most typical example is the pregnancy kit. In the case that they could provide quantitative information, they only allowed to detect one sample at a time. Nowadays, by properly engineering the paper surface it is possible to achieve many and different functionalities in one device. The easiest way is patterning the surface, which can be performed through several methods: cutting, drawing, dip-coating, plotting, via photolitography and by printing. When the formation of channels is not required, cutting allows for the design of complex shapes[70], fig 76.

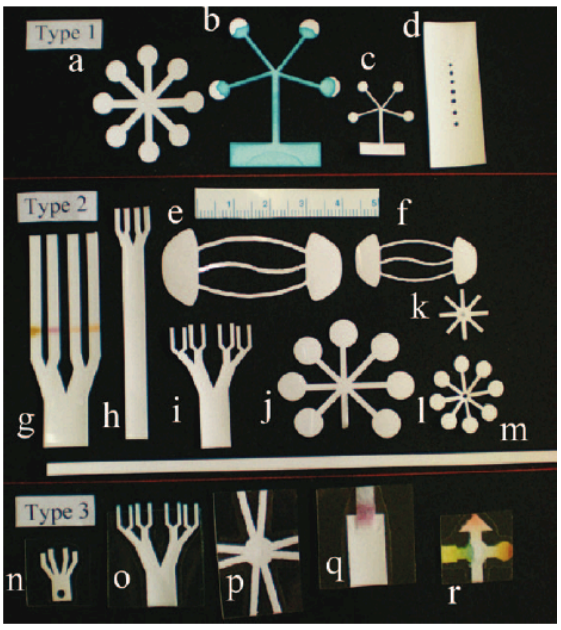

Fig. 76 Three types of devices cut into many different 2D shapes[71]

Except cutting, the fundamental idea of all these techniques is to pattern hydrophilic-hydrophobic regions on a sheet of paper in order to create micro-scale capillary channels on paper. A variety of chemicals have been used for patterning, from relatively expensive photoresist agents (SU-8, ≈$0.1 for patterning 100 cm^2 of filter paper) to the extremely cheap AKD (alkyl ketene dimer, ≈$0.00001 /100 cm^2)[72]. SU-8 is the photoresist used by Whitesides and co-workers print the pattern in their milestone paper (fig.77). A drawback of photolitograpy refers to damage of the photoresist that may occur during bending or folding.

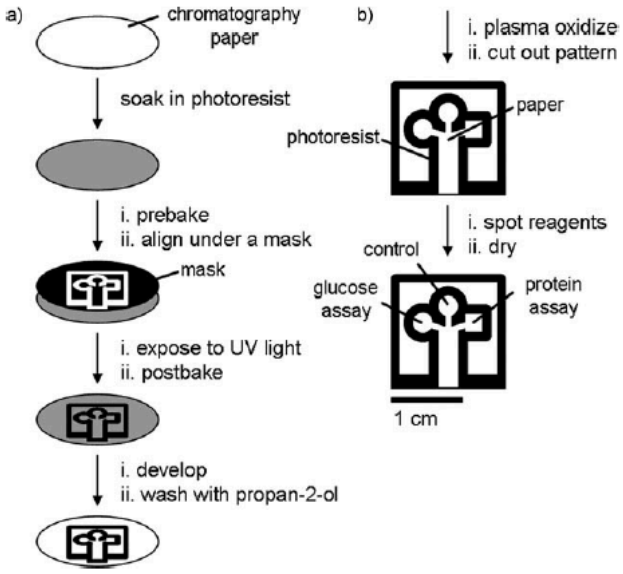

Fig. 77 a-b: a) photolitographic steps b) modification of patterned paper for bioassay (Whitesides et al., 2007)[73]

Wax printing[74] can be used to create microfluidic channels, as it is rapid, inexpensive and efficient, and can fabricate a prototyping device in less than 5 minutes. However, an important drawback is the different spreading of wax in the vertical and horizontal direction, as a consequence of the preferential orientation of cellulose fibers. Similarly, wax painting[75] and wax dipping[76] can also be performed.

The papers patterning principles are basically three:

1. Physically blocking the pores in paper (using agents such as photoresists or polydimethylsiloxane, PDMS)
2. Physical deposition of hydrophobizing agents, like polystyrene or wax
3. Chemical modification of the paper surface, via cellulose reactive agents, such as AKD

In the first and second approach, the chemicals impregnate the paper, without any chemical reaction with the cellulose fibers, enabling the formation of areas with modified wetting properties. On the contrary, the third route requires a chemical reaction typically with the –OH groups of the cellulose structure, as shown in fig 78.

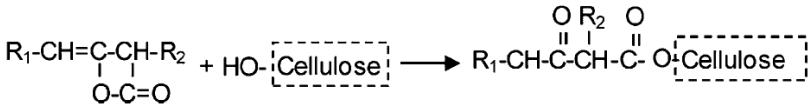

Fig. 78 Reaction of AKD and cellulose[77]

Generally, chemical modification cannot be removed by organic solvent extraction; on the contrary, if the hydrophobizing agent is only physically deposited, etching by means of organic solvent is possible to selectively dissolve it in some area and define the barriers of the microfluidic device.

Hence, the patterning approaches can be distinguished into two categories:

i. Selective hydrophobization (one-step fabrication)
ii. Entire hydrophobization followed by selective de-hydrophobization (two-steps fabrication)

A comparison of the patterning techniques mentioned above are summarized in Table 12 and details can be found elsewhere[78-81].

FABRICATION TECHNIQUE	ADVANTAGES	DRAWBACKS
Photolitography	High resolution of microfluidic channels (width is as narrow as 200µm; sharp barriers	Expensive equipment Washing step required to remove un-crosslinked polymer Vulnerable to bending
Plotting	Cheap patterning agents (PDMS) Flexible devices	Poor barrier definition High throughput production not possible
Ink jet etching	Single apparatus for etching/printing sensing reagents	10 times longer than printing Customized printing apparatus Not suitable for mass production
Plasma treatment	Very cheap patterning agent (AKD) Low materials cost	Different masks required for different patterns
Wax printing	Fast (5-10min) and simple production Suitable for mass production	Expensive wax printer Heating step after deposition
Ink jet printing	Very cheap printing agent (AKD) Fast production (<10min) Requires a single desktop printer to produce device/deposit reagents All-in-one fabrication	Heating step after deposition Modification of printer required (only for non VOC-free printing agent)
Flexography printing	Direct roll-to-roll production No post-treatments	PS must be printed twice Different printing plates Print quality depends on surface smoothness
Screen printing	Simple	Poor resolution of barriers Different screens are required for different patterns
Laser treatment	High resolution (min. feature 62µm)	Lateral flow not allowed Extra coating is required for fluid flow

Table 12 Main advantages and drawbacks of paper patterning techniques[82](adapted)

In the thesis work herein presented, the microfluidic devices have been fabricated *via* ink-jet printing. Printing is a well-established technique, used everyday by all kinds of users. Ink-jet printing can be successfully applied for paper patterning, since it enables the formation of microchannels via a single-step hydrophobization, by selective deposition of hydrophobic agents, making it a promising system for the fabrication of sensing devices[83]. Compared to other techniques, ink-jet printing is easier to perform, fast and cheap, as it requires only a desktop printer. It has the potential to be easily implemented for mass-production, with limited investment. Ink-jet printing allows the fabrication of microfluidic devices with outstanding resolution and complex designs (fig.79)[84,85].

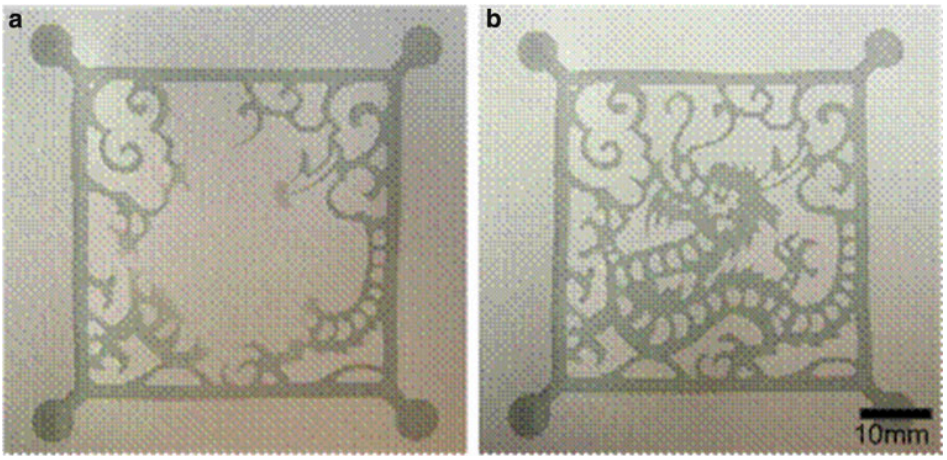

Fig. 79 a-b: Purely decorative µPAD illustrating the complex patterns achievable by ink-jet printing: a) water penetrating the channels b) fully-wetted pattern[86]

Probably, the main advantage given by ink-jet printing is that a final device can be realized with the same technology. A common desktop printer is sufficient to create the pattern on paper with the only required modification being the replacement of the ink cartridges with a cartridge containing the printing agent. Originally, a two-steps approach was performed, which requires the dissolution of unnecessary hydrophobic regions by soaking the paper in an organic solvent, generally toluene[87]. Major drawbacks consisted in i) the use of a volatile organic compound (VOC), with related environmental impact, as well as ii) the customization of the printer. Recently, a different approach, using VOC-free precursors has been proposed[88,89] to overcome both the environmental issues and the need for printer modification. This method has been proved to be effective for the successful fabrication of µPADs and implementation for real sample sensing[90].

In addition to the various techniques used to pattern paper, a second approach can be performed to enable specific and quantitative sensing, consisting in increasing the functionality of the substrate, obtaining, for example, sensors based on paper electronics[91] or paper-based piezoelectric sensors[92].

3.2 Ink-jet printing and fluorescence evaluation of μPADs: my work

The final step of the thesis work herein presented consisted in the fabrication of the micro-fluidic device on paper, by means of ink-jet printing. As mentioned in the introduction, both the fabrication step and the deposition of the nanoparticle solution have been accomplished via ink-jet printing. The fluorescent output has been evaluated to confirm the enhancement effect and prove the feasibility of the whole concept.

3.2.1 Set-up of the printing stage

The ink-jet printing stage of the microfluidic devices has been performed using two conventional desktop ink-jet printers, namely (PX-101 and PX-105) by Epson® and a more sophisticated Dimatix™ printer (DMP-2800) by Fujifilm (fig.80).

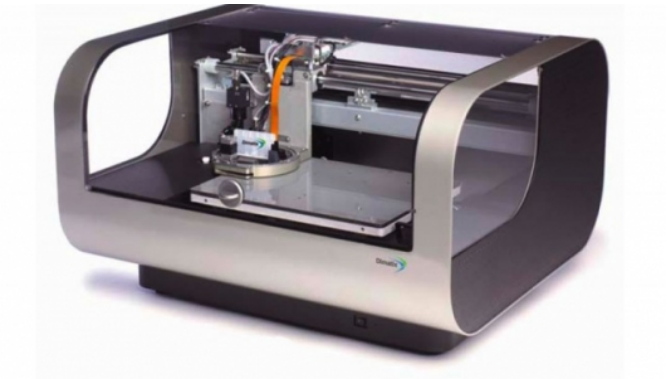

Fig. 80 Dimatix™ DMP-2800

The three printers are used in sequence to accomplish the following steps (scheme 14):

1. Print on a filter paper disk the frame of the area in which the final device will be printed
2. Print on the same sheet the layout of the μPADs by means of a UV-curable, hydrophobic ink
3. Print the solution of particles/dye in the dedicated areas of the device

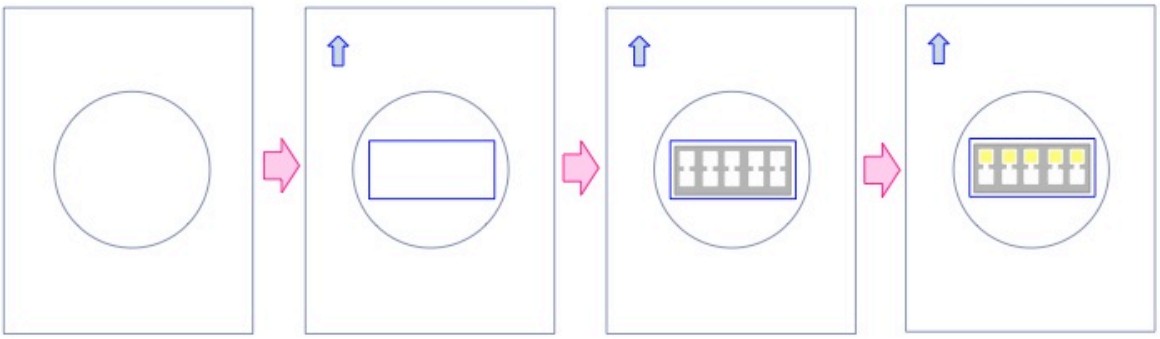

Scheme 14 Representation of the three printing steps for the fabrication of the µPAD

In the first step, the frame to define the printing area is required to properly align the nozzles of the Dimatix™, since the UV-curable ink used to draw the channels is uncolored. The Dimatix™ printer has a live-view camera system that allows micrometric precision in the alignment of the nozzles. 185mm in diameter of filter paper #5C by Advantec are used: to fit them in the Epson® printers, they are attached to A4 copy paper (scheme 15). The copy paper has been cut with a cutter in the central area to allow the access to both sides of the filter paper.

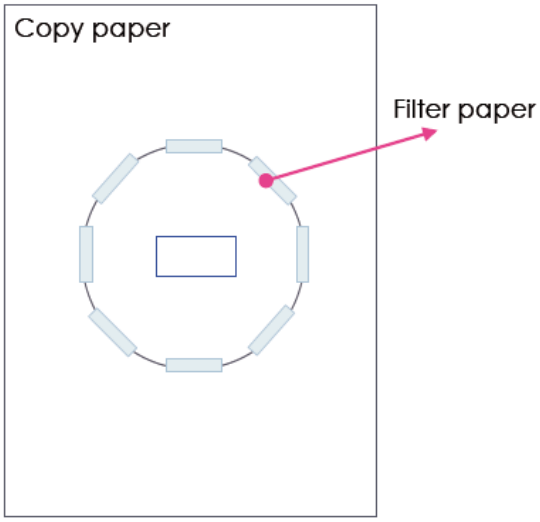

Scheme 15 The printing substrate for the µPADs. The blue rectangle defines the area in which the devices are printed.

Then, the sheet of paper is placed in the Epson® PX-105 printer, a conventional system in which the ink has been replaced with a UV-curable ink, consisting in a mixture of ODA (Octadecyl acrilate) and DDA (1,10-Decanediol diacrylate) 7:1 and BDK (Benzyldimetylketal) as photoinitiator. The UV ink is printed differently on the two sides of the paper sheet (scheme 16): on the front side, it defines the pattern of the µPAD, whereas on the other side it consists of a rectangle, with the same dimensions, to prevent leaking of the particle solution through the whole cross section of the filter paper. Each side is cured for 20 minutes under a UV lamp to promote reticolation, which is the reason for hydrophobicity. The printing parameters and the curing time have already been optimized in previous works[93].

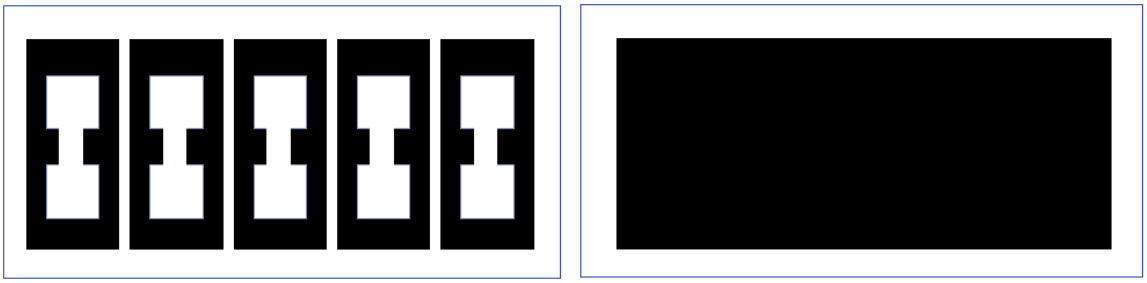

Scheme 16 Front side (L) and back side (R) of the ink.-jet printed devices. The area in black is printed with the UV-curable ink

In the third step, core@shells or the fluorescent dye are printed in the dedicated areas via the Dimatix™ ink-jet printer. With this printer, many parameters can be modified in order to have a personalized drop-on-demand system: not only any device can be realized in principle, but it is also possible to modify the number of nozzles active for each printing cycle, as well as the spacing between two drops, the frequency of dropping and the waveform that is used for the electrical impulse that activates the piezoelectric nozzles. Such parameters have been optimized to enable the printing of core@shells and Rose Bengal. Thanks to the live-view camera, it was possible to verify the correct functioning of the nozzles to ensure the effectiveness of printing. Figure 81 provides a summary of the three steps taken from the literature[94] which differs from the present work only for the curing time.

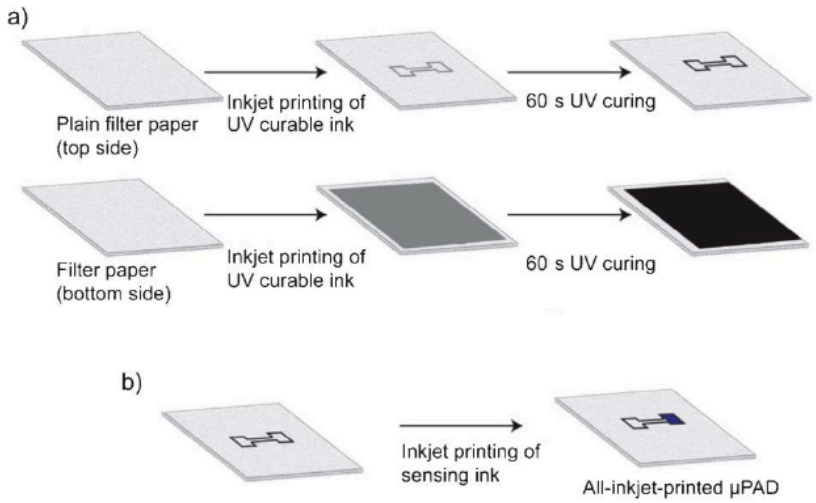

Fig. 81 Representation of the three steps for the device fabrication. a) UV-curable ink printing, with Epson® printer; b) deposition of sensing ink, with Dimatix™[95].The curing time in the picture is different from that adopted in the present work (set to 20 minutes)

3.2.1.1 Layouts of the printed designs

In the present work, several designs have been tested that aimed at resembling the conditions of the experiments previously performed by simply pipetting the core@shells onto paper, as described in chapter 2.3. Drawing the flow channels is particularly easy, because it is done using Microsoft® Power Point®. The basic layouts are reported in scheme 17.

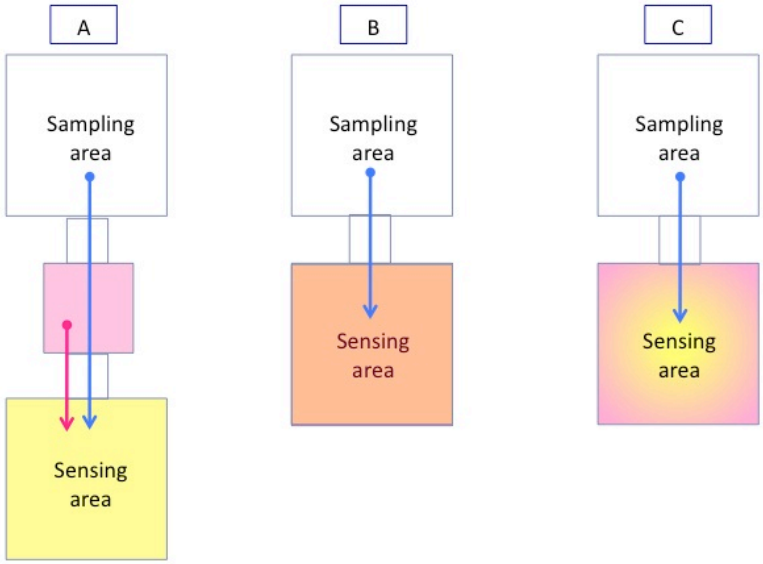

Scheme 17 Designs of the printed µPADs.

- Concept (A) consists of three separate areas: in the sensing area core@shells are printed, while Rose Bengal is printed in another dedicated area. The idea is that by pipetting a certain amount of sampling solution in the sampling area, this will flow in the microchannels towards the sensing area, dragging the Rose Bengal that will possibly mix with the core@shells, locally. The most critical aspect here is the flow of Rose Bengal, that is not trivial.
- In concept (B), Rose Bengal is printed directly on top of the core@shells, printed in the sensing area in a previous step. Here there is no drag, nevertheless it is important to evaluate how long particles and fluorescent dye are stable together and still provide enhancement.
- Finally, in concept (C) a mixed solution of core@shells and rose bengal is printed into the sensing area.

The as-prepared devices have been tested with HORIBA FluoroLog® spectrofluorimeter with the same parameters described in chapter 2.4.

3.2.2 Ink-jet printing and fluorescence evaluation

3.2.2.1 Dye flow

To evaluate the applicability of the concept to microfluidic device, a qualitative experiment has been performed in order to roughly check the capability of Rose Bengal to flow in the filter paper. This experiment should provide a hint for the feasibility of concept A. 36 filter paper #5C stripes (8,5 cm*2,5 cm) have been prepared, and 5 µL of a 10^{-4}M solution of Rose Bengal in ethanol has been pipetted at ≅2 cm from the bottom side. On half of such stripes, 50 µL of Ag@SiO_2 solution has been pipetted approximately in the middle of the sample. All stripes have been then placed vertically in some TLC plates, containing 2,5 mL of milliQ water. In this way, the water can flow through the filter paper and, trigger the Rose Bengal towards the area where the core@shells have been deposited.

The stripes have been kept in such position for 10 min, afterwards they were taken out and let dry naturally, before collecting the fluorescence spectra. This experiment aimed at mimicking the functioning of microfluidic devices, which would drag the fluorescent dye towards the sensing area, functionalized with core@shells. Figure82 and Scheme 18 illustrate the experimental set-up.

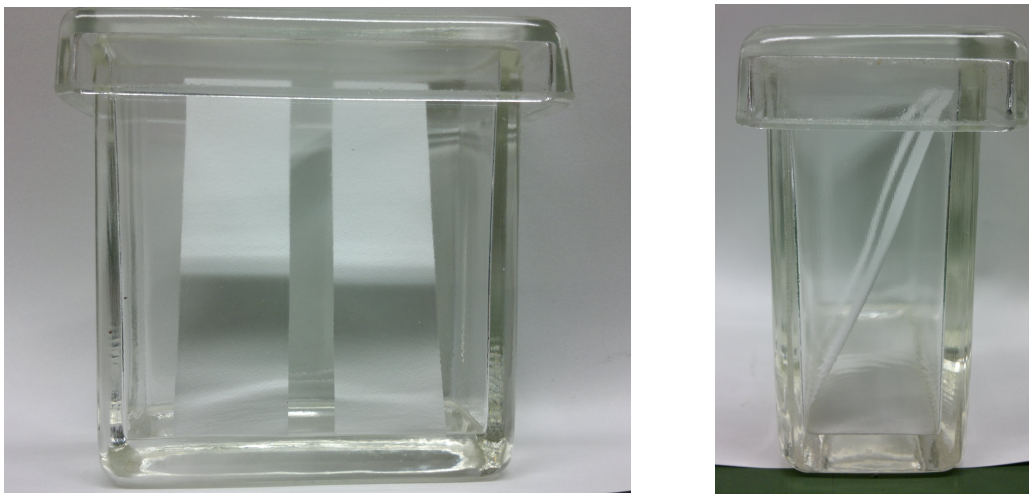

Fig. 82 a-b: a)Front and b)side view of the TLC plates containing the stripes of filter paper

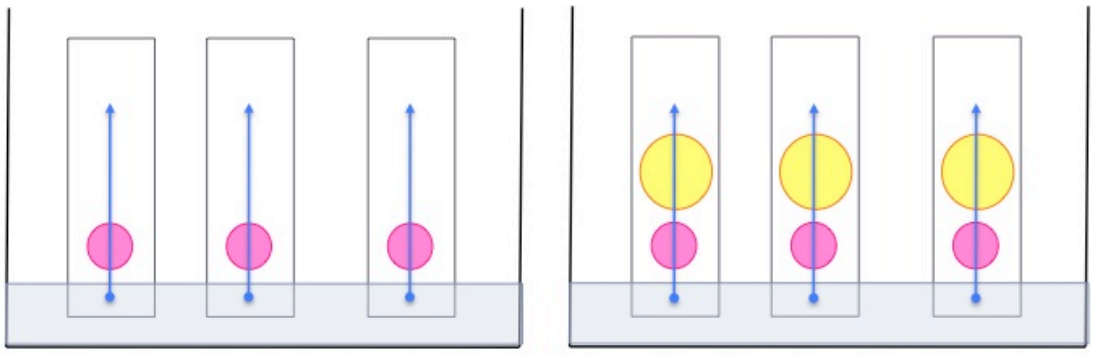

Scheme 18 Representation of the experimental set-up. Stripes contain Rose Bengal only (L) and core@shell particles and Rose Bengal (R). Both have the same amount of milliQ water

The fluorescence spectra after water elution represented in fig.83 is the average of 18 spectra of each type.

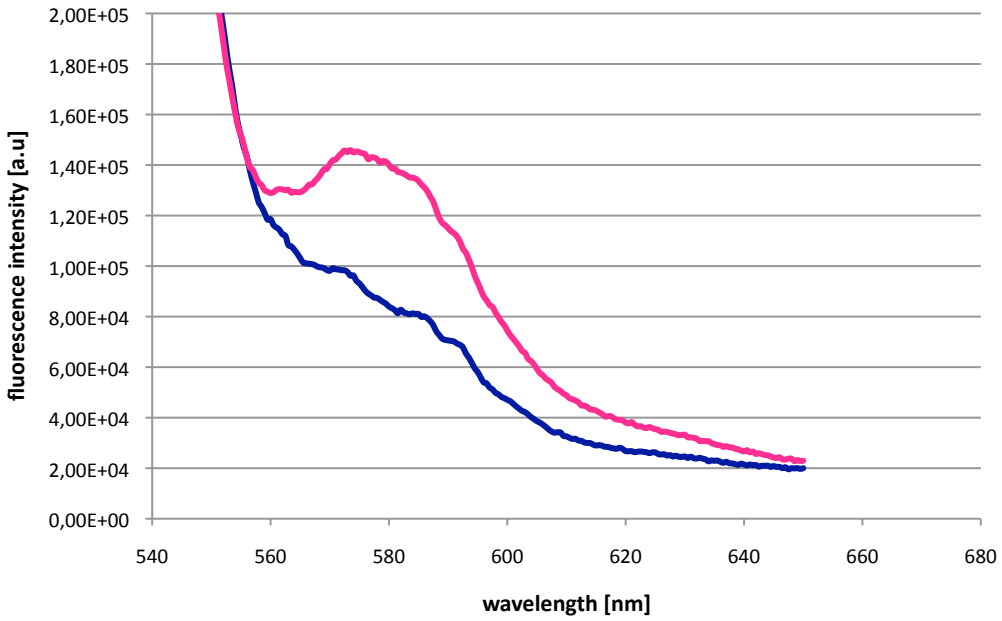

Fig. 83 Fluorescence spectra of the two situations: the blue line represents the fluorescence intensity after water elution of samples without deposited core@shell particles. Pink line represents the same quantity but from paper samples functionalized with core@shell particles

The idea behind this experiment is that if it an increased fluorescence from the stripes containing core@shells is detected with respect to the reference Rose Bengal samples, then the flowing capability of Rose Bengal, as a consequence of the dragging action of water, is confirmed. Despite the simple set-up and the possible water-dragging of the nanoparticles that alter the 10:1 (particle:dye) ratio that seems to be ideal from the previous findongs, a difference in fluorescence about 1.4-fold can be actually measured. This suggests that Rose Bengal can effectively be dragged by water into the filter paper and its fluorescence be enhanced by the metallic nanoparticles locally deposited.

3.2.2.2 Flow channels design – concept A

The first design tested to evaluate the feasibility of concept A, consisted of a pattern of two 6mm*6mm and one 3mm*3mm squares, connected by channels of 2mm*2mm (PATTERN #1, fig.84).

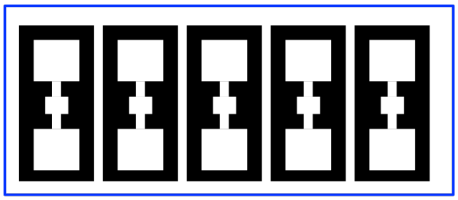

Fig. 84 Ink-jet printed PATTERN #1

For the optimization of the enhanced fluorescent intensity, the 10:1 -particles:dye ratio has to be maintained. With the Dimatix™ printer, it is possible to set the spacing between the droplets in the printing area. The droplets have a volume of 10 pL each. Hence, it is possible to calculate the total volume of solution that can be printed at a time (namely, in one layer). To determine the number of layers for each design, the following procedure has been adopted.

The round paper sample used so far, has a diameter of approximately 25 mm, corresponding to an area of 490,87 mm^2. For these samples, 500 µL of particles solution has been set as optimal value for the enhancement. In the case of PATTERN 1, the sensing area is 36 mm^2 wide. The ratio between the two areas is

$$\frac{490,87}{36} = 13,64$$

So, the total volume of particle solution that must be printed in the sensing area is

$$\frac{500\mu L}{13,64} = 36,65\mu L$$

The spacing between the droplets, which are deposited in the sensing area accordingly to the pattern in scheme 19, can be arbitrarily fixed; from previous works, the value of 10µm seems to be ideal to have a homogeneous coverage of the area. Hence, 601 droplets are printed in each line, resulting in a total of 601*601 droplets for each layer.

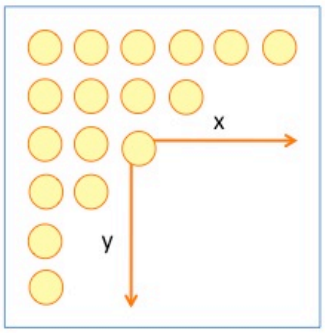

Scheme 19 Representation of how droplets are deposited on paper by Dimatix™

Being known the volume of each droplet, it is possible to calculate the total volume that can be printed for each layer.

$$601 * 601 * 10\,pL = 3612010\,pL$$

Finally, it is possible to calculate the number of layers, or printing stages

$$\frac{36{,}65\,\mu L}{3{,}612\,\mu L} = 10\,layers$$

The ratio particles:dye means that the total volume of Rose Bengal that has to be printed is 3,665 µL. The area contains 301*301 droplets, for a total volume of 906010 pL per each layer. Hence, the number of layers is

$$\frac{3{,}665\,\mu L}{0{,}906\,\mu L} = 4\,layers$$

The same calculation procedure has been adopted for all the designs to be printed.

Figure 85 shows the result of the printing stage. It is possible to see that there is a small misalignment of the printed Rose Bengal with respect to the frame of the dedicated area: this may derive from errors in the manual alignment of the nozzles, and also the machine itself sometimes leads to unpredictable misalignment with respect to the desired pattern.

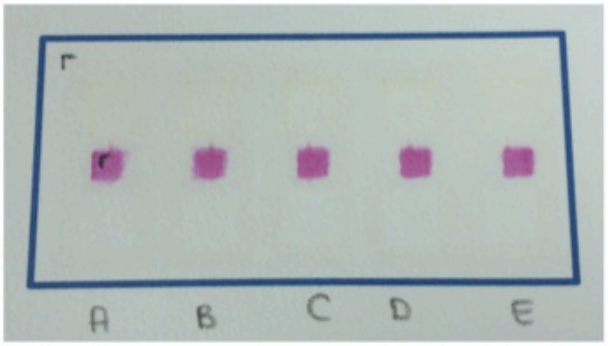

	Dye [µL]
A	35
B	30
C	15
D	20
E	25

Fig. 85 Five printed patterns, with both core@shell particles (yellow) and Rose Bengal (pink) printed by Dimatix™. The table provides the quantity of milliQ water used to make the dye flow

The different patterns have been marked with letters from A to E, and on each one a different quantity of milliQ water has been pipetted to drive the Rose Bengal flow. The fluorescence emission has then been measured considering three different areas for sample A (scheme 20).

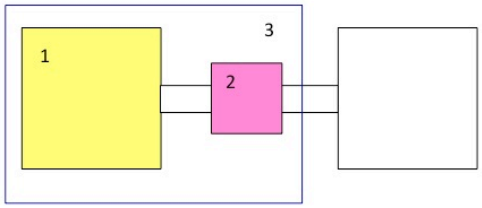

Scheme 20 Representation of the three areas from which fluorescence spectra has been collected for PATTERN #1

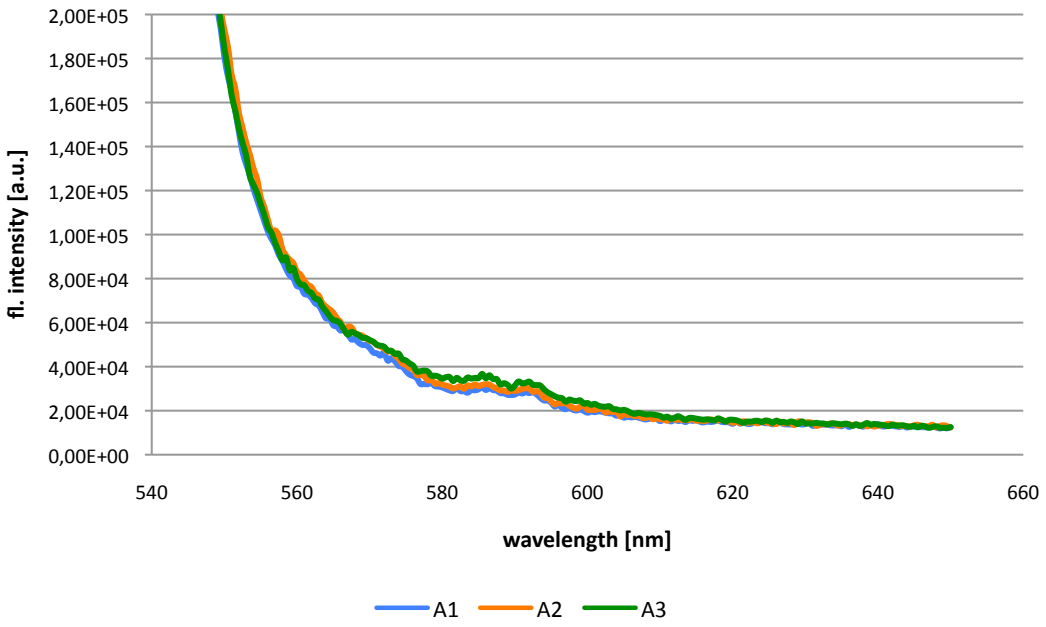

Fig. 86 Fluorescence spectra of PATTERN #1A. The three lines represent the fluorescence intensity from three different spots (see scheme 20) of the same device (in fig.85) λ_{exc}= 532 nm

Plot 2 shows basically no difference in the intensity from the three different areas. Hence, a different approach has been adopted. To facilitate the water-induced drag of Rose Bengal, the design of the µPAD has been slightly modified (fig.87), enlarging all areas, including the channels.

	AREA [mm]	TOTAL VOLUME [µL]	N° OF LAYERS
Sensing area (core@shell)	7*7	50	10
Rose bengal area	4*4	5	3
Channels	2*3		
Sampling area	7*7		

Fig. 87 PATTERN #2 and specifications of the size of the different areas

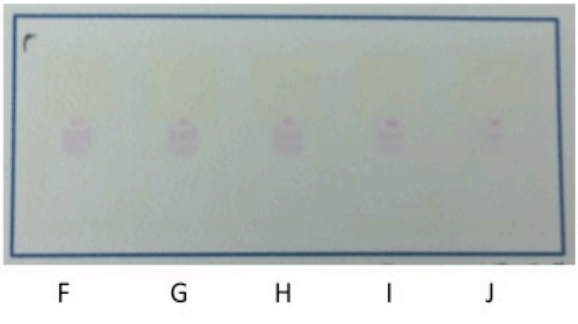

	milliQ [µL]
F	15
G	20
H	30
I	40
J	50

Fig. 88 Picture of the printed pattern and specification of the amount of milliQ to enable dye flow

Surprisingly, part of Rose Bengal leaked out from its area and spread in the channel, prior to the application of milliQ. Fluorescent intensity has been measured in zone 1 and in zone 3, according to scheme 20.

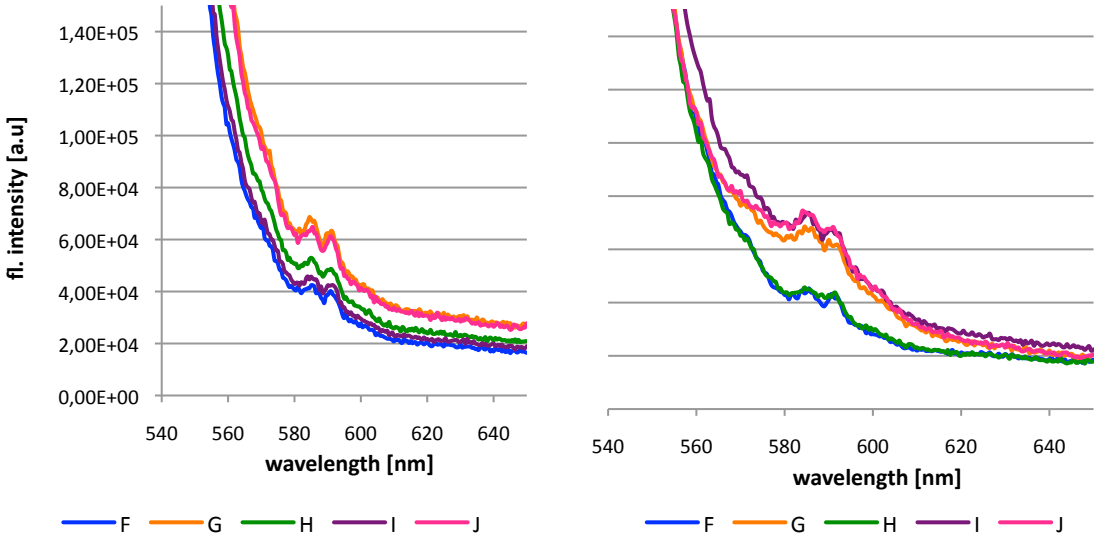

Fig. 89 a-b: Fluorescence intensity for PATTERN #2 in a)zone 1 and b)zone 3. For this latter one, consider the same values on the y-axis as the plot on the left to have direct comparison

There is only a little difference in the two results, with the fluorescent output slightly higher in the case of zone #3, that includes sensing and Rose Bengal areas. Moreover, this difference is bigger the higher the quantity of milliQ. Nevertheless, this is enough to state that there is no flow of dye towards the sensing area.

Given these results, it seemed that core@shell particles were not effectively printed in the sensing area, despite the paper turned yellow after the printing stage, thus suggesting that a correct deposition occurred. Alternatively, also the Rose Bengal could maybe be not effectively printed, due to the very small volume. Hence, the PATTERN #2 with printed and flowing Rose Bengal has been compared to pipetting the same amount of dye directly in the sensing area. Additionally, to prove the consistency with previous results, Rose Bengal was deposited either from an EtOH solution either from an aqueous one (fig.90).

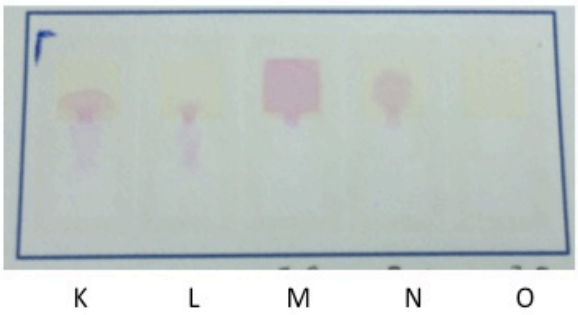

Fig. 90 PATTERN #2 with Rose Bengal either printed and flowed or pipetted

50 µL of core@shell particles have been printed for all the devices. Regarding the dye, here are the specifications of the five PADs:

K: printed 5 µL (EtOH) + flow with 30 µL milliQ
L: printed 5 µL (milliQ) + flow with 30 µL milliQ
M: pipetted 5 µL (EtOH)
N: pipetted 5 µL (milliQ)

In this case, the fluorescent spectra have been taken only from the sensing area. For PADs K and M the spectra have been collected before and after the wetting. As a comparison, Rose Bengal only from paper substrate has been considered.

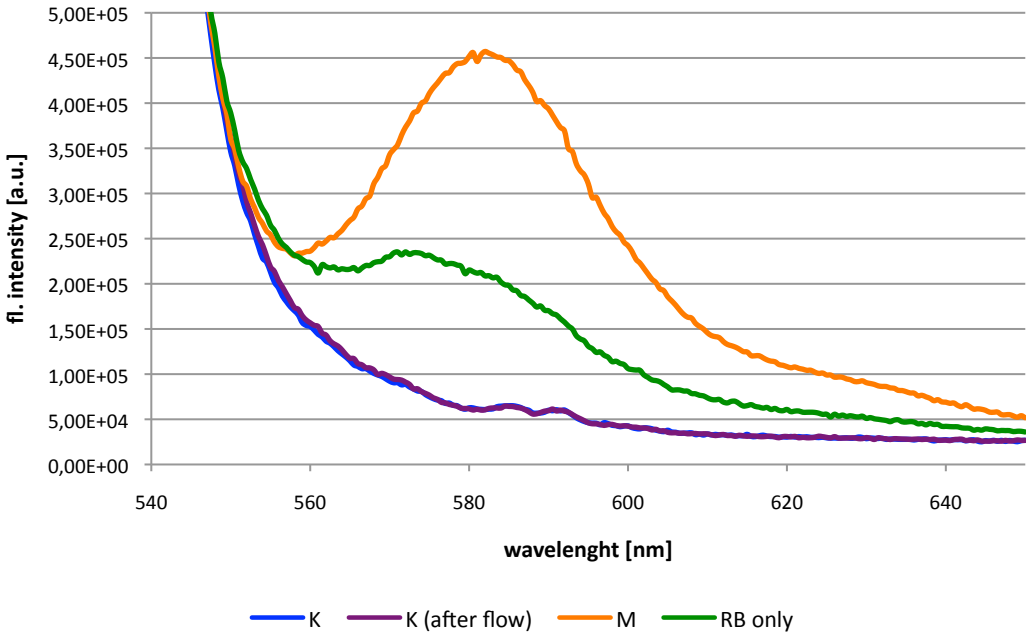

Fig. 91 Fluorescence spectra of PATTERN #2 flow vs. pipetting (rose bengal in EtOH)

Analysing fig. 91, some considerations can be derived:

- The fluorescence intensity of PAD K does not change after water deposition which, in principle, should drag the dye from its area towards the core@shell particles. This can be due, to two reasons:
  i. Inefficient flow, resulting in an insufficient drag of dye
  ii. Modification of the fluorescence yield of Rose Bengal, due to the contact with water
- PAD K is also less fluorescent than the control sample (no particles)
- On the contrary, a 2-fold enhancement can be recorded from PAD M. This result is consistent with previous results from the same batch of core@shell particles and, also, the wavelength value at the peak is the same of the results shown in chapter 2.3. This seems to be a confirmation of the validity of the application of core@shell particles as MEF substrate.

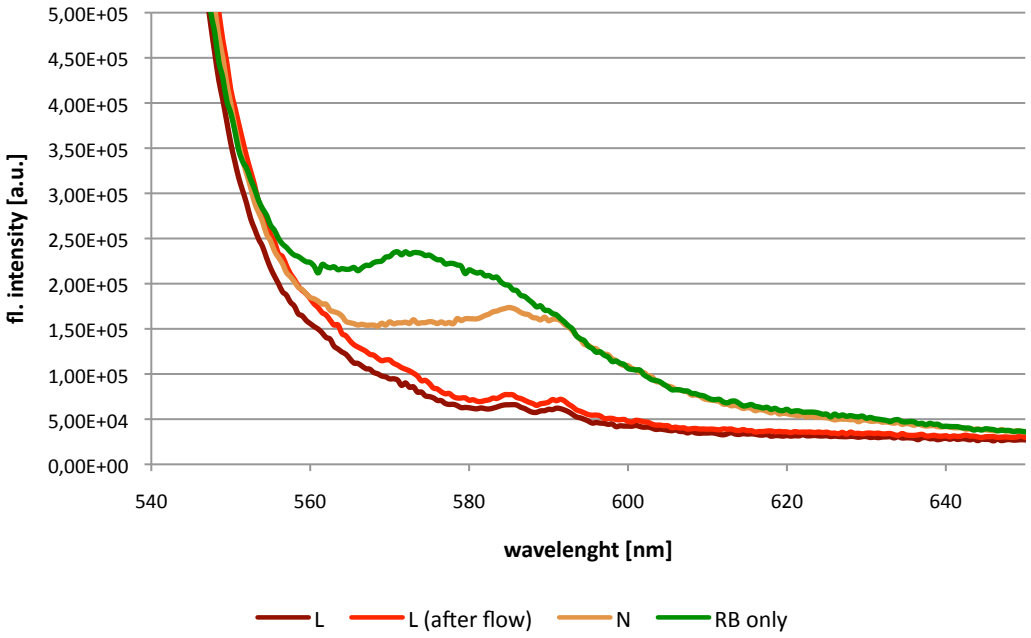

Fig. 92 Fluorescence spectra of PATTERN #2 flow vs. pipetting (Rose Bengal in milliQ)

Results are consistent with expectations regarding the lower fluorescence of Rose Bengal if dissolved in water. It is also shown that a correct flow is not accomplished, since the fluorescence from PAD L is basically the same before and after flow. PAD N, even though more fluorescent than L, is still less emissive than the control sample.

The result of PAD M is worth noting because it is, to best of our knowledge, the first example of MEF from paper substrate where the enhancing system (metal nanoparticles) has been deposited via ink-jet printing. However, enhancement occurred only with Rose Bengal pipetted onto the substrate and not printed. In addition, it was not possible to demonstrate the enhancement in the case of an aqueous sample which flows in the µPAD.

3.2.2.3 Flow channels design – concept B

As a second step, the feasibility of concept B was evaluated. As design, PATTERN #2 has been used to ensure a direct comparison with fluorescence values obtained from the experiment described by fig.91. Rose Bengal has been printed (5 µL, 1 layer) or pipetted (5 µL) directly into the sensing area, where core@shell particles have been previously printed (50 µL, 10 layers).

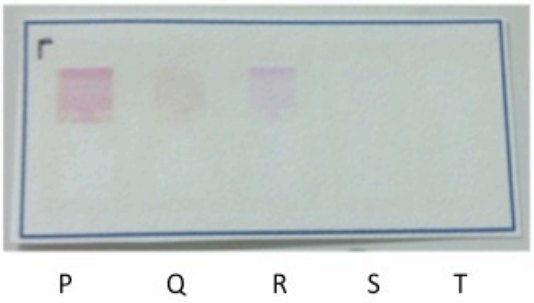

Fig. 93 Pictures of 4 µPADs based on PATTERN #2

The specifications are as follows:

P: Ag@SiO_2 printed; printed RB
Q: Ag@SiO_2 printed; pipetted RB
R: printed RB (control sample)
S: pipetted RB (control sample)

The graph in fig. 94 shows the results from fluorescence measurements.

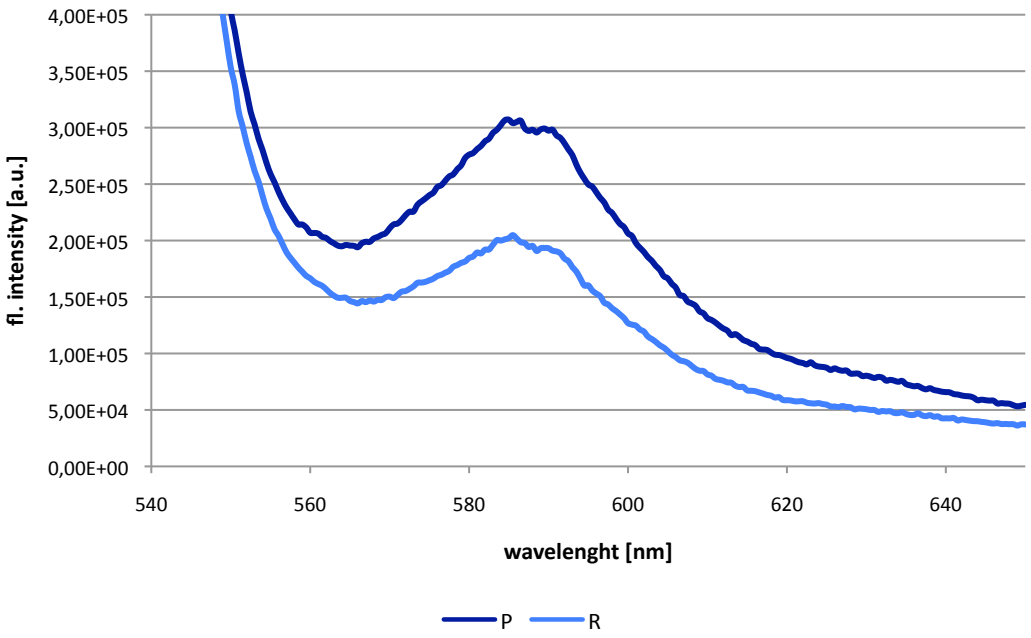

Fig. 94 Fluorescence intensity from µPAD where both Ag@SiO_2 and Rose Bengal are printed via Dimatix™

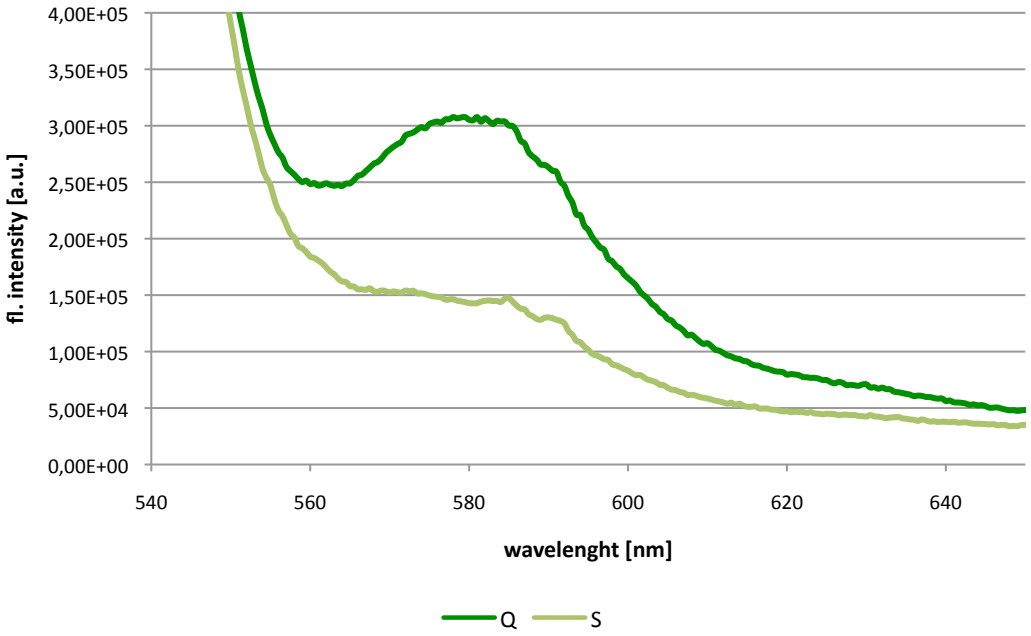

Fig. 95 Fluorescence intensity from µPAD where Ag@SiO_2 is printed and Rose Bengal pipetted

To evaluate the reproducibility of the data, fluorescence spectra have been collected in four different spots for each device, and then averaged. Data are summarized in fig.96.

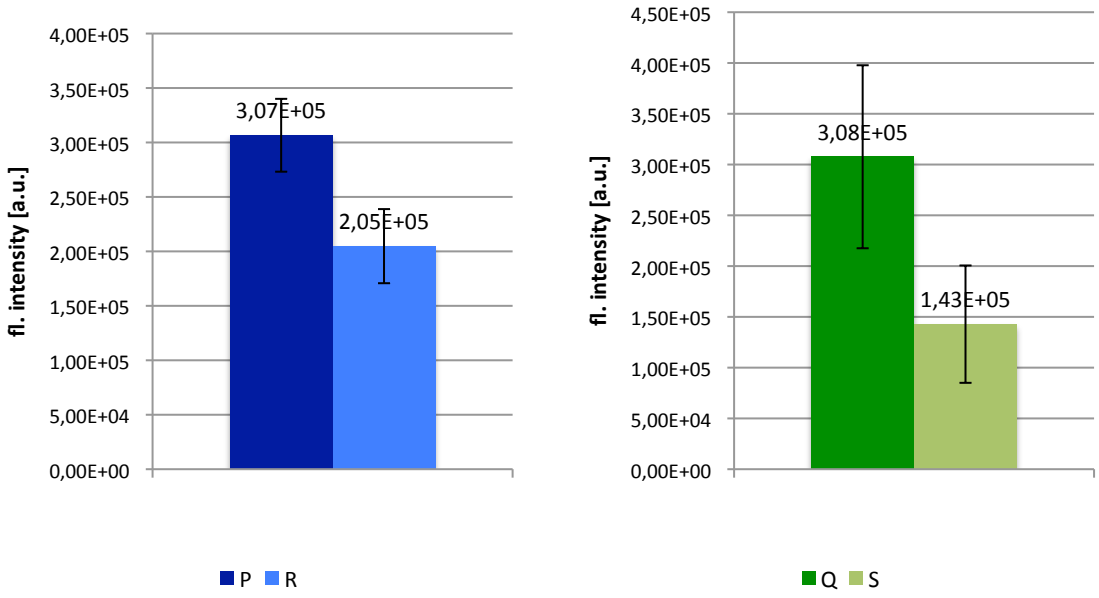

Fig. 96 a-b: Specification of fluorescence intensity from the 4 µPADs, comparing a)printing and b)pipetting

In this case, it was possible to record enhancement from both the experiments. In the case that both particles and dye have been printed (P), there is a 1.5-fold enhancement while, in the case that Rose Bengal is pipetted onto printed particles (Q), the enhancement is 2.2-fold. This is similar to the situation shown in fig.91 where the enhancement was 2-fold.

It is interesting to notice that even though the enhancement is larger in the case of pipetted dye, the wider error bars show a lower reproducibility in the data. Hence, the result from PAD P is

particularly important because not only enhancement occurs, but also the reliability of the data is good, thus confirming the feasibility of the whole concept.

To evaluate a possible source of errors in the measurement, the same experiment, comparing printing and pipetting dye, has been made using bigger PADs, approximately of the same dimension of the rounded filter paper samples used in chapter 2. The idea was to analyse if any difference could be observed when using bigger systems and larger quantities of reagents. The Dimatix™ printer, although generally accurate, may lead to dropping or alignment error that may (or not) become significant when the dimensions are very small. Hence, square PADs having 22 mm side (exactly the same area of the rounded filter paper samples) have been fabricated.

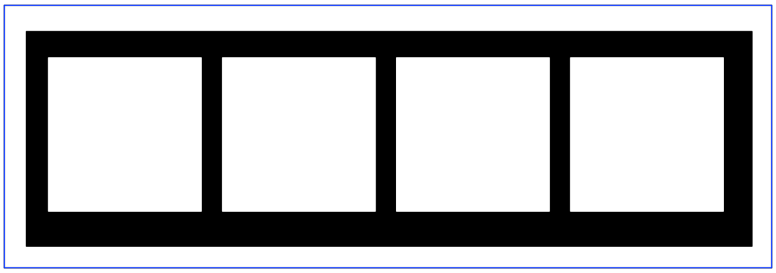

Fig. 97 Representation of big PADs (PATTERN #3)

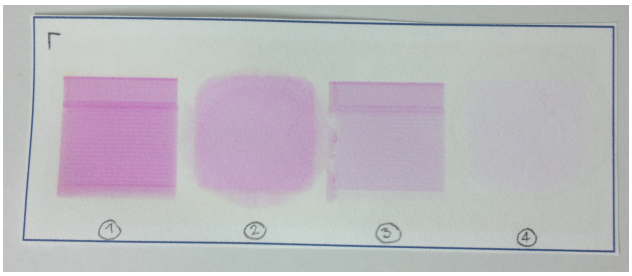

	AREA [mm]	TOTAL VOLUME [µL]	N° LAYERS
Core@shell	22*22	500	10
RB	22*22	50	1

Fig. 98 a-b: a)Picture of the four printed PADs (PATTERN #3) and b)specifications of dimensions, quantity of reagents and printing parameters

The functionalization of the four PADs is as follows (numbers refer to fig.98a):

1. Printed core@shell, printed RB
2. Printed core@shell, pipetted RB
3. Printed RB (control sample)
4. Pipetted RB (control sample)

It can be noticed that, in PADs 1 and 3, the printing of Rose Bengal was not perfectly accomplished, as one “line” of the passing nozzles is evident. Furthermore, the UV-curable ink was not perfectly hydrophobic against the dye, which leaked out a bit from the borders (cases 2 and 3). This is maybe due to the formulation of the dye itself, which is diluted in an organic solvent (EtOH).

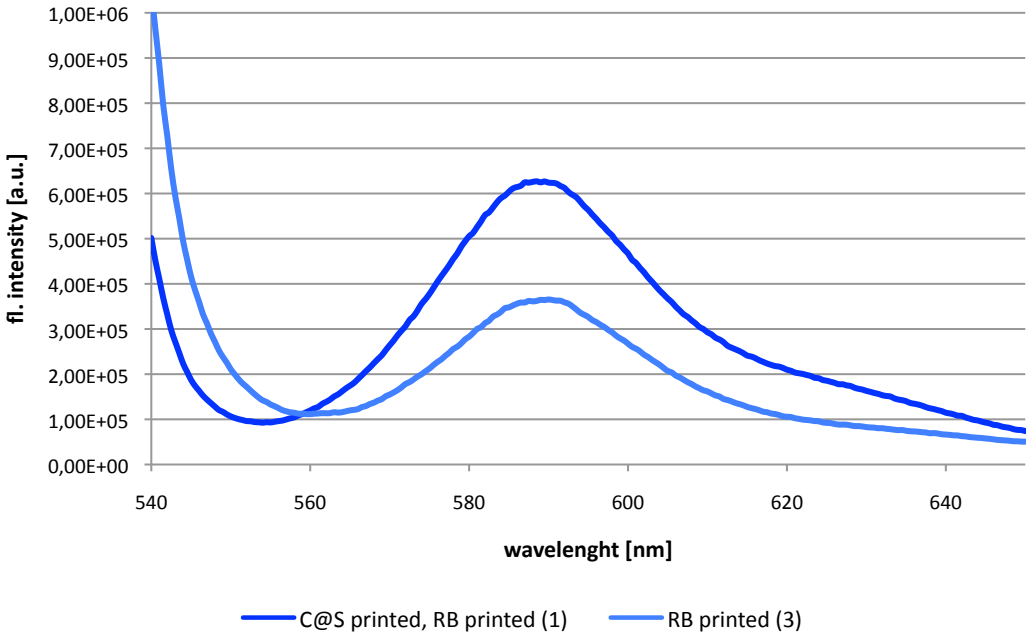

Fig. 99 Fluorescence intensity big from PAD with printed dye

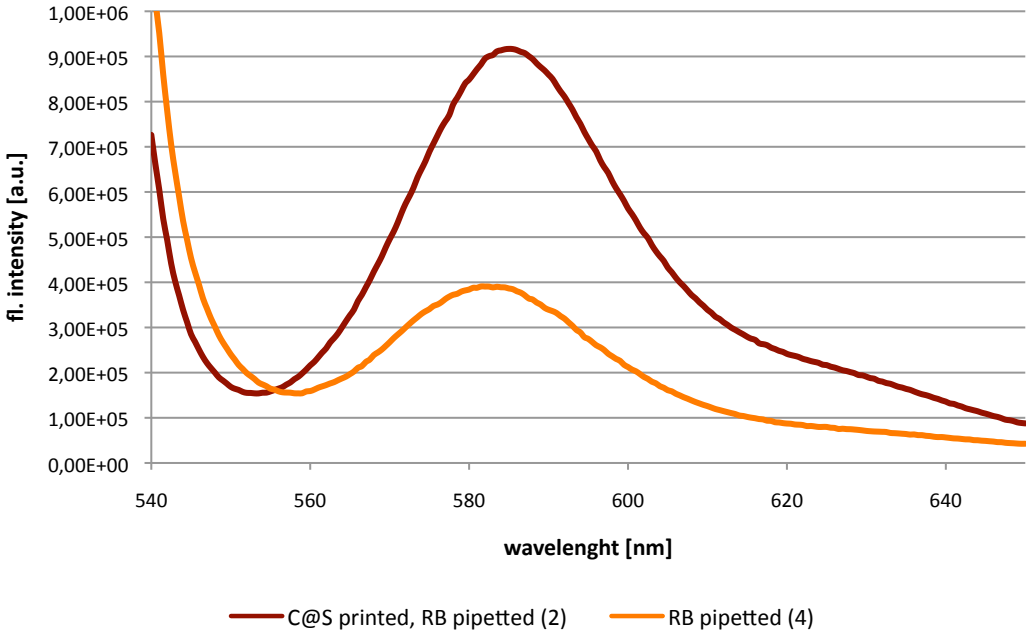

Fig. 100 Fluorescence intensity from PAD where core@shell particles have been printed and dye pipetted

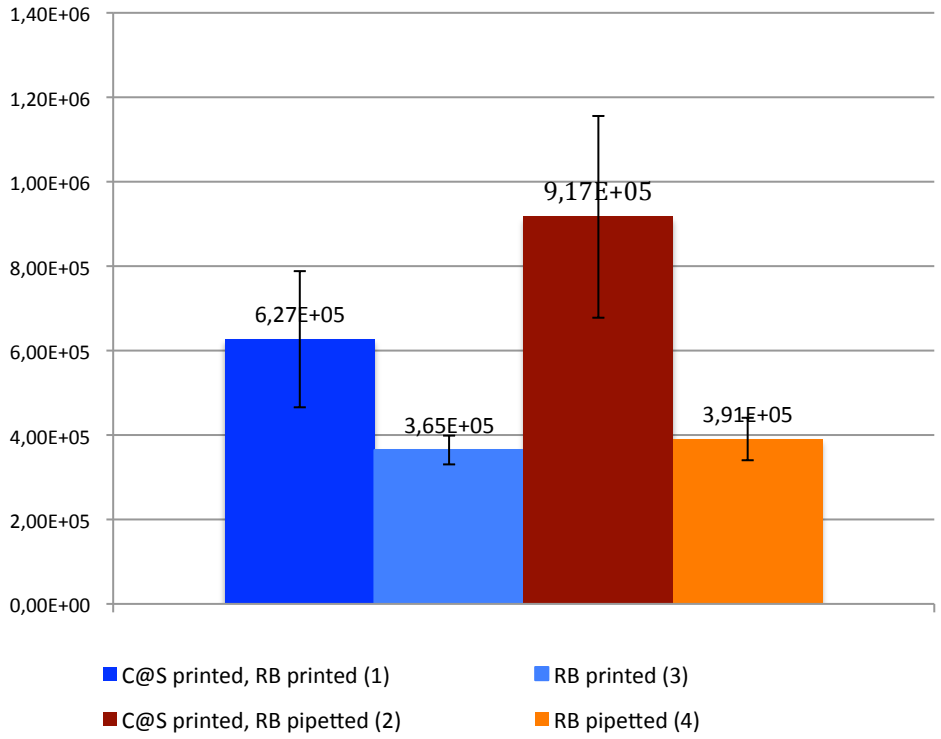

Fig. 101 Comparison of fluorescence intensity from PAD with printed or pipetted dye: specification of the peak value and its error

Again, both experiment lead to an enhancement, 1.7-fold in the case of printed dye and 2.3-fold in the case of pipetted dye. Additionally, the reproducibility in the case of pipetting the dye is still lower than the other case. The results of the scaling up confirmed what has been already noticed from the previous one.

As a conclusion, concept B successfully proved that is possible to have MEF from entirely printed microfluidic paper-based devices for the first time. Concept B consisted in the deposition, in the same area, of both the particles solution and subsequently, once the particle solution is dry, of the fluorescent dye.

3.2.2.4 Flow channels design – concept C

Finally, the concept C has been also tested (PATTERN #4, fig.102). The layout chosen consists only of two areas of the same size, namely a sampling area and a sensing area. In this latter one, a mixed solution of core@shell particles and Rose Bengal has been printed (11 layers, specifications in fig.102). Fluorescence has been evaluated in the same condition of the previous paragraphs, and compared to filter paper containing Rose Bengal only, wetted with different amounts of milliQ. Very small or no enhancement from these PADs were expected, as occurred from similar samples, shown in chapter 2.3.

	AREA [mm]	TOTAL VOLUME [µL]	N° OF LAYERS
Sensing area (core@shell + rose bengal)	6*6	40	11
Channels	2*3		
Sampling area	6*6		

Fig. 102 PATTERN #4 and specifications of size

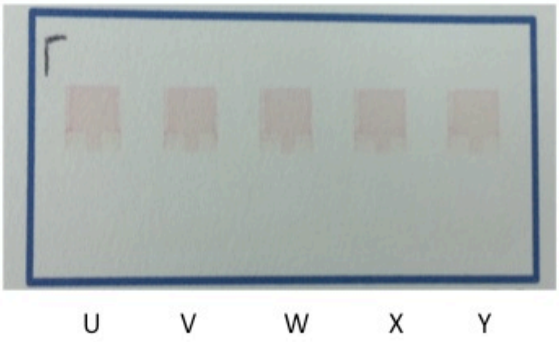

	Dye [µL]
U	15
V	20
W	30
X	40
Y	50

Fig. 103 Picture of the five µPADs and detail of the amount of sample solution (milliQ) let flow into the channels

It can be easily noticed that this PAD was not very nicely fabricated. The leaking out of the sensing area is quite significant, probably due either to nozzles misalignments either due to the formulation (mixing of an aqueous solution and EtOH).

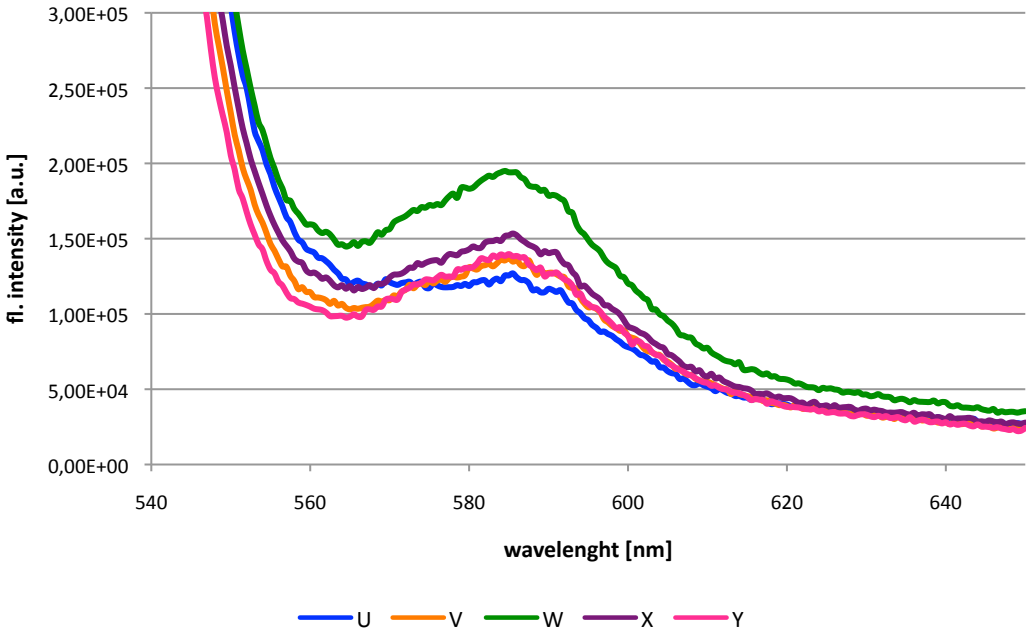

Fig. 104 Fluorescence intensity from µPADs with a printed solution of particles and dye pre-mixed

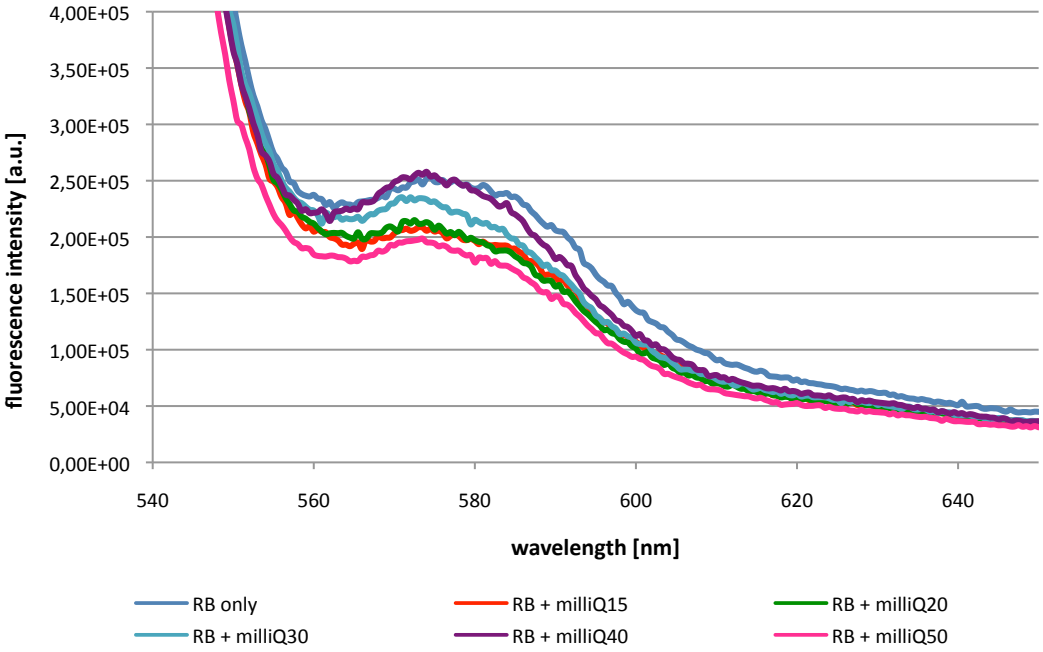

Fig. 105 Fluorescence intensity from rose bengal on paper, control samples. The different lines represent Rose Bengal mixed with different quantities of water

It is evident that there is no enhancement from these PADs, and, also leaving out the weak signals, it is not possible to identify a clear trend depending on the amount of sampling solution pipetted.

3.2.3 Summary

To summarize all the results of the experiments shown, the following conclusions can be drawn:

- ✓ Core@shell particles can be effectively ink-jet printed onto filter paper
- ✓ Rose bengal can also be effectively printed
- ✓ The complete fabrication of a µPAD (paper patterning to create the channels and functionalization with particles and dye) can be accomplished within 12 hours at maximum
- ✓ MEF can be obtained from µPADs, with a maximum value of 1.5-fold if both particles and dye are printed. Enhancement can be obtained also by simply pipetting dye onto fabricated µPADs (2.2-fold), but the reproducibility and reliability of data is generally lower

- × It was not possible to evidence enhancement in the case of devices where flow was expected

In conclusion, the applicability of the concept was demonstrated, with MEF from printed µPADs and, as far as we know, this is the first work proving this concept. As outlook, effort should be put to understand how to increase dye flow in microfluidic channels.

Bibliography

1. Whitesides, George M. "The origins and the future of microfluidics." *Nature* 442.7101 (2006): 368-373.
2. http://gmwgroup.harvard.edu/; last access 7.04.2014
3. http://faculty.washington.edu/yagerp/; last access 7.04.2014
4. http://chemweb.calpoly.edu/awmartin/; last access 7.04.2014
5. http://www.psu.edu/dept/phillipsgroup/index.html; last access 7.04.2014
6. http://eng.monash.edu.au/about/people/profile/garnier; last access 7.04.2014
7. http://suzuki-lab.applc.keio.ac.jp/index.html; last access 7.04.2014
8. http://www.mf20.org/; last access 7.04.2014
9. Martinez, Andres W., Scott T. Phillips, and George M. Whitesides. "Three-dimensional microfluidic devices fabricated in layered paper and tape." *Proceedings of the National Academy of Sciences* 105.50 (2008): 19606-19611.
10. Balagaddé, F. K., You, L., Hansen, C. L., Arnold, F. H. & Quake, S. R. Long-term monitoring of bacteria undergoing programmed population control in a microchemostat. *Science* 309, 137–140 (2005).
11. Zheng, B., Tice, J. D., Roach, L. S. & Ismagilov, R. F. A droplet-based, composite PDMS/ glass capillary microfluidic system for evaluating protein crystallization conditions by microbatch and vapor-diffusion methods with on-chip X-ray diffraction. *Angew. Chem. Int. Ed.* 43, 2508–2511 (2004).
12. Dittrich, P. S. & Manz, A. Lab-on-a-chip: microfluidics in drug discovery. *Nature Rev. Drug Discov.* 5, 210–218 (2006).
13. Pihl, J., Karlsson, M. & Chiu, D. T. Microfluidic technologies in drug discovery. *Drug Discov. Today* 10, 1377–1383 (2005).
14. Sia, S. K. & Whitesides, G. M. Microfluidic devices fabricated in poly(dimethylsiloxane) for biological studies. *Electrophoresis* 24, 3563–3576 (2003).
15. Breslauer, D. N., Lee, P. J. & Lee, L. P. Microfluidics-based systems biology. *Mol. Biosys.* 2, 97–112 (2006).
16. Huh, D., Gu, W., Kamotani, Y., Grotberg, J. B. & Takayama, S. Microfluidics for flow cytometric analysis of cells and particles. *Physiol. Meas.* 26, R73–R98 (2005).
17. Garstecki, P. *et al.* Formation of monodisperse bubbles in a microfluidic flow-focusing device. *Appl. Phys. Lett.* 85, 2649–2651 (2004).
18. Abe, Koji, et al. "Inkjet-printed paperfluidic immuno-chemical sensing device." *Analytical and bioanalytical chemistry* 398.2 (2010): 885-893.
19. Yetisen, Ali Kemal, Muhammad Safwan Akram, and Christopher R. Lowe. "Paper-based microfluidic point-of-care diagnostic devices." *Lab on a Chip* 13.12 (2013): 2210-2251.
20. http://www.abbottpointofcare.com/Products-and-Services; last access 7.04.2014
21. Chin, Curtis D., Vincent Linder, and Samuel K. Sia. "Commercialization of microfluidic point-of-care diagnostic devices." *Lab on a Chip* 12.12 (2012): 2118-2134.
22. Gubala, Vladimir, et al. "Point of care diagnostics: status and future." *Analytical chemistry* 84.2 (2011): 487-515.
23. Cfr.19
24. Rozand, C. "Paper-based analytical devices for point-of-care infectious disease testing." *European Journal of Clinical Microbiology & Infectious Diseases* 33.2 (2014): 147-156.

25. P. the Elder, *Natural History*, 1601st ed. 79AD
26. Yagoda, Herman. "Applications of confined spot tests in analytical chemistry: preliminary paper." *Industrial & Engineering Chemistry Analytical Edition* 9.2 (1937): 79-82.
27. Rocco, Richard M., ed. *Landmark papers in clinical chemistry*. Elsevier, 2005.
28. Cfr.27
29. Liu, Hong, et al. "Aptamer-based origami paper analytical device for electrochemical detection of adenosine." *Angewandte Chemie* 124.28 (2012): 7031-7034
30. Martinez, Andres W., et al. "Patterned paper as a platform for inexpensive, low-volume, portable bioassays." *Angewandte Chemie International Edition* 46.8 (2007): 1318-1320.
31. Müller, R. H., and DORIS L. Clegg. "Automatic paper chromatography." *Analytical Chemistry* 21.9 (1949): 1123-1125.
32. Martinez, Andres W., et al. "Diagnostics for the developing world: microfluidic paper-based analytical devices." *Analytical chemistry* 82.1 (2009): 3-10.
33. Nery, Emilia W., and Lauro T. Kubota. "Sensing approaches on paper-based devices: a review." *Analytical and bioanalytical chemistry* 405.24 (2013): 7573-7595.
34. Cfr.33
35. Li, Xu, David R. Ballerini, and Wei Shen. "A perspective on paper-based microfluidics: current status and future trends." *Biomicrofluidics* 6.1 (2012): 011301.
36. Martinez, Andres W., et al. "Simple telemedicine for developing regions: camera phones and paper-based microfluidic devices for real-time, off-site diagnosis." *Analytical Chemistry* 80.10 (2008): 3699-3707.
37. Dungchai, Wijitar, Orawon Chailapakul, and Charles S. Henry. "Use of multiple colorimetric indicators for paper-based microfluidic devices." *Analytica chimica acta* 674.2 (2010): 227-233.
38. Cfr.30
39. Zhao, Weian, et al. "Paper-based bioassays using gold nanoparticle colorimetric probes." *Analytical chemistry* 80.22 (2008): 8431-8437
40. Mentele, Mallory M., et al. "Microfluidic paper-based analytical device for particulate metals." *Analytical chemistry* 84.10 (2012): 4474-4480.
41. Peiris, Roshan Lalintha, Owen Noel Newton Fernando, and Adrian David Cheok. "A dynamic AR marker for a paper based temperature sensor." *Ambient Intelligence*. Springer Berlin Heidelberg, 2011. 195-199.
42. Li, Miaosi, et al. "Paper-Based Blood Typing Device That Reports Patient's Blood Type "in Writing"." *Angewandte Chemie International Edition* 51.22 (2012): 5497-5501.
43. Cheng, Min-Liang, Bo-Chan Tsai, and Jyisy Yang. "Silver nanoparticle-treated filter paper as a highly sensitive surface-enhanced Raman scattering (SERS) substrate for detection of tyrosine in aqueous solution." *Analytica chimica acta* 708.1 (2011): 89-96.
44. Yu, Wei W., and Ian M. White. "Inkjet printed surface enhanced Raman spectroscopy array on cellulose paper." *Analytical chemistry* 82.23 (2010): 9626-9630.
45. Wei, W. Yu, and Ian M. White. "Inkjet-printed paper-based SERS dipsticks and swabs for trace chemical detection." *Analyst* 138.4 (2013): 1020-1025.
46. Yu, Jinghua, et al. "Microfluidic paper-based chemiluminescence biosensor for simultaneous determination of glucose and uric acid." *Lab on a Chip* 11.7 (2011): 1286-1291.
47. Ellerbee, Audrey K., et al. "Quantifying colorimetric assays in paper-based microfluidic devices by measuring the transmission of light through paper." *Analytical chemistry* 81.20 (2009): 8447-8452
48. Cheng, Chao-Min, et al. "Paper-Based ELISA." *Angewandte Chemie International Edition* 49.28 (2010): 4771-4774.
49. Liu, X. Y., et al. "A portable microfluidic paper-based device for ELISA." *Micro Electro Mechanical*

Systems (MEMS), 2011 IEEE 24th International Conference on. IEEE, 2011.

50. Cfr.18
51. Shen, Li, Joshua A. Hagen, and Ian Papautsky. "Point-of-care colorimetric detection with a smartphone." *Lab on a Chip* 12.21 (2012): 4240-4243.
52. Cfr.36
53. Kearney, AT. "African mobile observatory: driving economic and social development through mobile services." *London: GSMA* (2011).
54. Mentele, Mallory M., et al. "Microfluidic paper-based analytical device for particulate metals." *Analytical chemistry* 84.10 (2012): 4474-4480
55. Peiris, Roshan Lalintha, Owen Noel Newton Fernando, and Adrian David Cheok. "A dynamic AR marker for a paper based temperature sensor." *Ambient Intelligence*. Springer Berlin Heidelberg, 2011. 195-199.
56. Li, Miaosi, et al. "Paper-Based Blood Typing Device That Reports Patient's Blood Type "in Writing"." *Angewandte Chemie International Edition* 51.22 (2012): 5497-5501.
57. Yu, Jinghua, et al. "Microfluidic paper-based chemiluminescence biosensor for simultaneous determination of glucose and uric acid." *Lab on a Chip* 11.7 (2011): 1286-1291.
58. Cfr.18
59. Cfr.33
60. Dungchai, Wijitar, Orawon Chailapakul, and Charles S. Henry. "Electrochemical detection for paper-based microfluidics." *Analytical chemistry* 81.14 (2009): 5821-5826.
61. Apilux, Amara, et al. "Lab-on-paper with dual electrochemical/colorimetric detection for simultaneous determination of gold and iron." *Analytical chemistry* 82.5 (2010): 1727-1732.
62. Nie, Zhihong, et al. "Electrochemical sensing in paper-based microfluidic devices." *Lab on a Chip* 10.4 (2010): 477-483.
63. Liu, Hong, and Richard M. Crooks. "Paper-based electrochemical sensing platform with integral battery and electrochromic read-out." *Analytical chemistry* 84.5 (2012): 2528-2532.
64. Zang, Dejin, et al. "Electrochemical immunoassay on a 3D microfluidic paper-based device." *Chemical Communications* 48.39 (2012): 4683-4685.
65. Bracher, Paul J., et al. "Heterogeneous films of ionotropic hydrogels fabricated from delivery templates of patterned paper." *ACS applied materials & interfaces* 1.8 (2009): 1807-1812.
66. Cheng, Chao-Min, et al. "Millimeter-scale contact printing of aqueous solutions using a stamp made out of paper and tape." *Lab on a Chip* 10.23 (2010): 3201-3205.
67. Lu, Yao, Bingcheng Lin, and Jianhua Qin. "Patterned paper as a low-cost, flexible substrate for rapid prototyping of PDMS microdevices via "liquid molding"." *Analytical chemistry* 83.5 (2011): 1830-1835.
68. Thuo, M. M., et al. "Multizone Paper Platform for 3D Cell Cultures." (2011).
69. Derda, Ratmir, et al. "Multizone paper platform for 3D cell cultures." *PLoS One* 6.5 (2011): e18940.
70. Fenton, Erin M., et al. "Multiplex lateral-flow test strips fabricated by two-dimensional shaping." *ACS applied materials & interfaces* 1.1 (2008): 124-129.
71. Cfr.70
72. Cfr.35
73. Cfr.30
74. Lu, Yao, et al. "Fabrication and characterization of paper-based microfluidics prepared in nitrocellulose membrane by wax printing." *Analytical chemistry* 82.1 (2009): 329-335.
75. Cfr.74
76. Songjaroen, Temsiri, et al. "Novel, simple and low-cost alternative method for fabrication of paper-based microfluidics by wax dipping." *Talanta* 85.5 (2011): 2587-2593.

77. Cfr.19
78. Cfr.33
79. Cfr.32
80. Cfr.19.
81. Liana, Devi D., et al. "Recent advances in paper-based sensors." *Sensors* 12.9 (2012): 11505-11526.
82. Cfr.35
83. Komuro, Nobutoshi, et al. "Inkjet printed (bio) chemical sensing devices." *Analytical and bioanalytical chemistry* 405.17 (2013): 5785-5805.
84. Li, Xu, et al. "Fabrication of paper-based microfluidic sensors by printing." *Colloids and Surfaces B: Biointerfaces* 76.2 (2010): 564-570.
85. Li, Xu, Junfei Tian, and Wei Shen. "Quantitative biomarker assay with microfluidic paper-based analytical devices." *Analytical and bioanalytical chemistry* 396.1 (2010): 495-501.
86. Cfr.84
87. Abe, Koji, Koji Suzuki, and Daniel Citterio. "Inkjet-printed microfluidic multianalyte chemical sensing paper." *Analytical chemistry* 80.18 (2008): 6928-6934
88. Citterio, D., K. Maejima, and K. Suzuki. "VOC-free inkjet patterning method for the fabrication of" paperfluidic" sensing devices." *15th International Conference on Miniaturized Systems for Chemistry and Life Sciences, Seattle, Washington, USA*. 2011.
89. Maejima, Kento, et al. "Inkjet printing: An integrated and green chemical approach to microfluidic paper-based analytical devices." *RSC Advances* 3.24 (2013): 9258-9263.
90. Yamada, Kentaro, et al. "Antibody-Free Microfluidic Paper-Based Analytical Device for the Determination of Tear Fluid Lactoferrin by Fluorescence Sensitization of Tb 3+." *Analyst* (2014).
91. Tobjörk, Daniel, and Ronald Österbacka. "Paper electronics." *Advanced Materials* 23.17 (2011): 1935-1961
92. Liu, Xinyu, et al. "Paper-based piezoresistive MEMS sensors." *Lab on a Chip* 11.13 (2011): 2189-2196.
93. Cfr.88
94. Cfr.89
95. Cfr.89

CONCLUSIONS

The present work aimed at developing a strategy to enhance the luminescent signal of fluorophores, suitable to be applied for ink-jet printed microfluidic paper-based analytical devices (μPADs). Such strategy was based on a peculiar effect, called metal enhanced fluorescence (MEF), arising when fluorophores are placed in close proximity to nanoscopic metal structures. MEF represents a field which has been still relatively little studied and, to the best of our knowledge, the results coming from this work are the first demonstration of MEF from ink-jet printed sensors.

Specifically, the experimental activity consisted in a series of consequential steps. At first, silver nanoparticles have been synthesized *via* reduction of silver salts. The particles have been characterized with TEM (Transmission Electron Microscope) and DLS (Dynamic Light Scattering), to assess their size and morphology. Homogeneous, quasi-spherical silver nanoparticles, having average diameter of 50 nm, have been successfully prepared. Subsequently, the surface of the silver particles has been modified by the deposition of a silica shell, in order to obtain a so-called "core@shell" nanostructure. Such surface modification was intended as a substrate for a future functionalization with chemical species, able to specifically bind to analytes for a quantitative chemical sensing. The coating procedure implemented and optimized in the present work leads to an easy fabrication of a silica shell of tuneable thickness, down to 10 nm. An investigation of whether it was possible to observe MEF from paper substrate, functionalized by the deposition of the synthesized silver@silica nanoparticles, has been then performed. At this stage, it was particularly important to identify the most influential parameters to maximize the fluorescent enhancement. It was found that a 10:1 ratio in volume (particles:dye) is the optimal ratio to achieve up to 4.36-fold enhancement, using Rose Bengal as fluorescent dye and core@shell particles with a ≈ 10 nm thick shell. The reproducibility of the measurement is also particularly high, thus definitely confirming MEF from paper. As a substrate, hydrophilic filter paper has been used. It was also possible to prove that fluorescence enhancement can be obtained from various types of filter paper differing mainly for roughness, porosity and particles retention ability, almost regardless of the specific type. Filter paper represents the ideal substrate for the production of ink-jet printed microfluidic devices. Additionally, several supporting experiences have been carried out, investigating the penetration of dye and particles in the paper cross section and the comparison of fluorescence enhancement with core@shell particles and other types of particles (silica, polymeric particles). A deep penetration and a uniform distribution of the core@shell particles and the fluorescent dye inside the cross section of the paper were observed, thus leading to the hypothesis that the plasmonic interaction between silver nanoparticles and the Rose Bengal, which generates MEF, makes up for the lack in fluorescence due to the penetration of the dye. Strong enhancement factors have been observed only when using the silica-coated silver nanoparticles, thus suggesting that the enhancement is indeed due to a plasmonic coupling. In addition to Rose Bengal, several other common dyes have been tested: Rhodamine B, Fluorescein, Coumarin 343, Calcein and Acridine Orange. However, significant enhancement has been obtained only from Rose Bengal, no enhancement from Coumarin 343 and Acridine Orange,

and limited enhancement for the other ones. Analysing the chemical structure of these dyes, it was hypothesised that enhancement was possible when in presence of polar, protic groups, while no enhancement can be detected from dyes with non polar groups (Coumarin 343 and Acridine Orange). Nevertheless, a homologous series of dyes belonging to the same main family and differing for specific functional groups should be investigated to confirm this hypothesis. Finally, core@shell nanoparticles and Rose Bengal have been successfully ink-jet printed into the channels of a simple μPAD, which has been designed and also fabricated via ink-jet printing. Different designs have been proposed and fluorescence enhancement was detected. However, the enhancement was weak, that is 1.5-fold. It is worth noting that enhancement has been measured only in the case that the fluorescent dye has been printed directly on top of the previously printed nanoparticles, and not when it was dragged by a sampling solution. The latter would be ideal for the implementation of the whole concept for microfluidic devices. Nevertheless, these results are particularly satisfying since, to the best of our knowledge, this is the first time that MEF was measured from fully ink-jet printed devices. It is believed that this work could be the starting point for the complete implementation of a more sensitive ink-jet printed chemical sensor.

ACKNOWLEDGEMENTS

First of all, I would like to thank Prof.ssa Chiara Bertarelli, for her willingness to supervise the present work, for the valuable suggestions and the availability shown not only on this occasion, but throughout my academic career.

A huge thank to Prof. Koji Suzuki and Prof. Daniel Citterio, for the warm welcome in their laboratory, from the very first day. For me, being a "SuCi" Lab member this year was an amazing and enriching experience, both from a professional and from a personal point of view. Especially, I want to thank Prof. Citterio for the continuous support during my everyday work, and for being such a nice person inside and outside the laboratory.

To all my lovely "SuCi" laboratory mates: ありがとう. You have been the best example to follow, I learned a lot by watching how much you were working and I tried to do my best everyday, just as you. Also, thank you for all the precious moments and all the best memories that I collected during this year. I was glad to have the chance to meet some of you in Italy, and I can't wait to see you again. You all deserve my gratitude, but I have a few special mentions. First, my senpai, King-san: for the patience showed everyday, solving my doubts and answering my stupid questions, and for the nice talks. I wish you all the best. My girls Mochiko and Mikako: you belong to my best memories of Japan, from special occasions (sooo many! Hanabi, camping, onsen, Disneysea, Hakone, climbing, kamaboko (?) making, my birthday…) to everyday life (especially lunch time!). Thank you to the others "yon-maru-hachi" members: Hitomi (perfect cake maker!), Kame-chan (for teaching me wrong japanese), Rina (most beautiful girl at Keio) and Tsucchi (Disneysea best shot!), for making everyday a little mor fun. Sweet Emi I love you so much you are so pretty! I loved everyday "girls talking" with you, and I had so much fun going on trip together. Ken-chan, sorry for invading your space on the desk! Thank you for being soooo kind, I enjoyed talking with you and going on a trip together. You are so clever and such a nice guy, you really deserve all the best that life has to offer. Nissy, "faccia rossa", I should have taught you some more useful italian than what I did, at least you have a collection of funny words (paperino, topolino, pipa, squirtlesquirtlesquirtle, bevi di più!, cinque) that will always making you "felice" when thinking of me. Thank you for all the precious moments together! Shunchi, I can't forget how nice were you the first day, when I arrived to laboratory a little shy and confused. You wanted me to have nice memories of Japan, and I definitely have. Thank you sooo much for you help and suggestions and polymer particles (and for being so good looking!). Etsuko, Hikaru, Komu-pyon, Moe-chan and William-american you also owe a piece of my heart.

Thank also to the friends with whom I shared this "Japanese experience": Angelos, Hamza, Lorenzo, Marco, Mario, Nicolò and Nouha. It would not have been the same without you.

Thank you to my PoliMi friends, especially Davide, Luca and Roberto. We made a great team, and all my best university memories include you. I want to thank "Mom" in particular, for having been

close even if when I was far away, for the infine talks (especially in class…and on various topics) and for synchronized tv series watching (and comments on most important scenes).

Thank you, my beautiful Socie: Francesca, Gaia, Giorgia and Serena. How nice to wake up in the morning to find 347 whatsapp messages, most of them totally useless. I love you! We reached the goal of knowing each other for 8 years, so we will be friends forever.

A huge thank to my parents, for the sacrifices, for believing in me and for letting me have the incredible japanese experience. You are my best example in life, thank you for teaching me how to go trough difficulties and to always give the best. Thank you also to my sweet “little” brother, Mattia.

Finally, thank you, Marco, for making life just wonderful.

APPENDIX: absorbance spectra and chemical structures of fluorescent dyes

Rose bengal

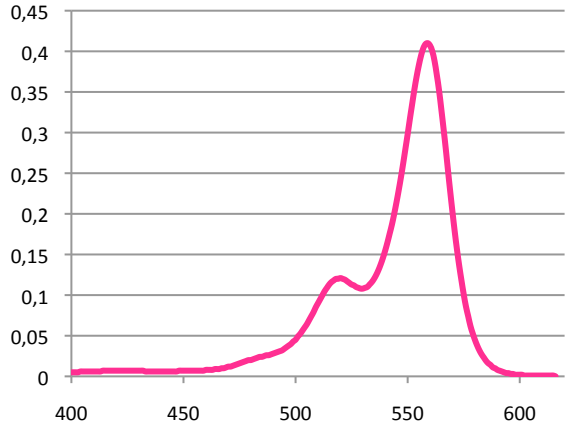

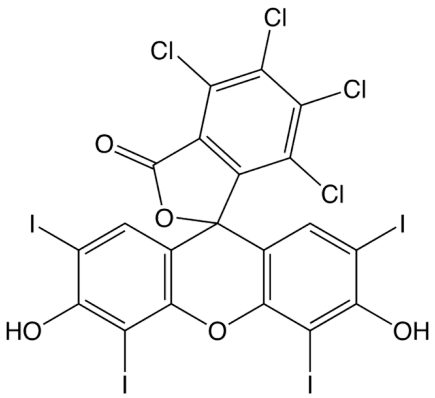

- **Peak value 558 nm**

Acridine Orange

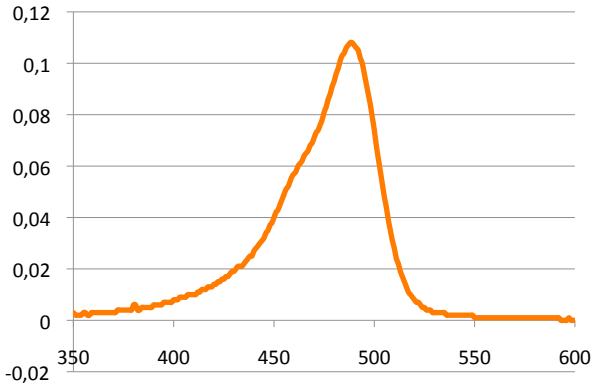

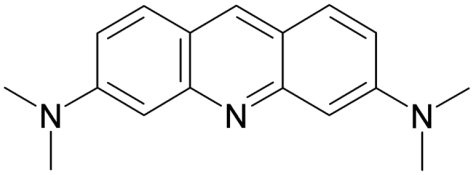

- **Peak value 488 nm**

Calcein

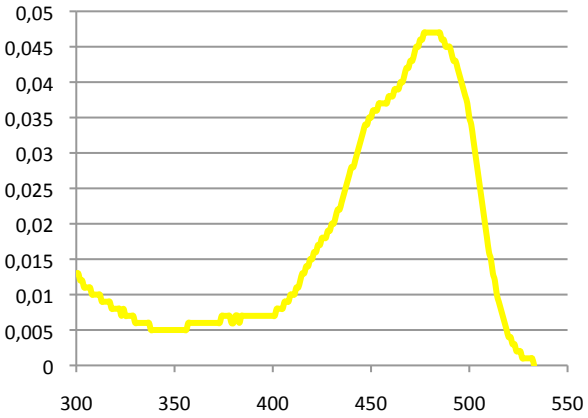

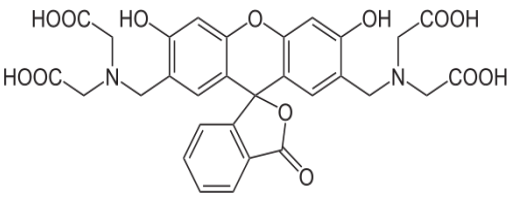

- **Peak value 477 nm**

Fluorescein

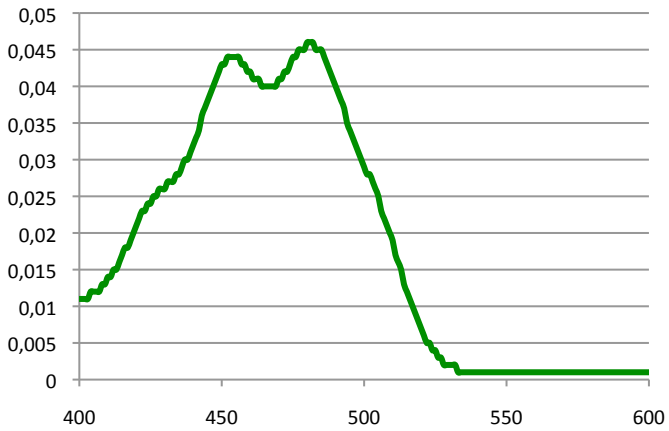

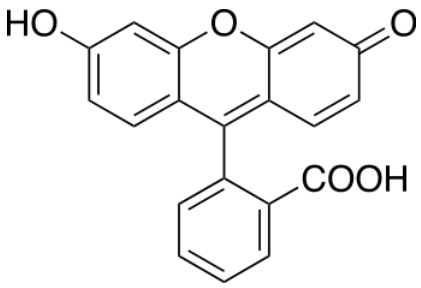

- **Peak value 480 nm**

Rhodamine B

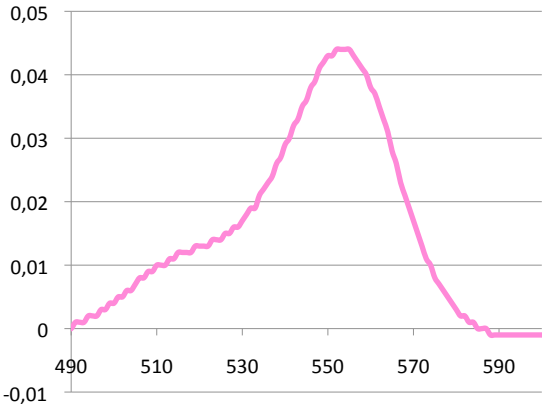

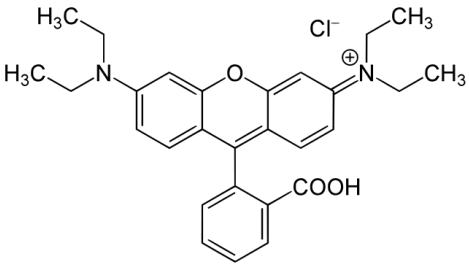

- **Peak value 545 nm**

Coumarin 343

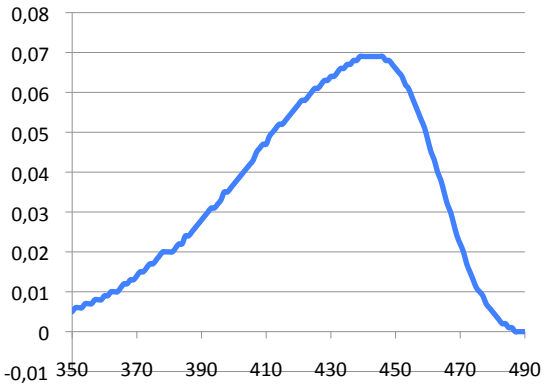

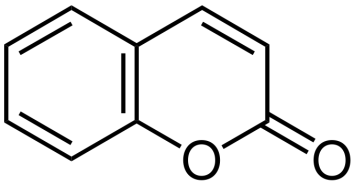

- **Peak value 445 nm**